Università degli Studi di Torino

Department of Veterinary Sciences

PhD in VETERINARY SCIENCES FOR ANIMAL HEALTH AND FOOD SAFETY

XXXV cycle

MEASURING KINEMATIC VARIABLES OF HIGH MOTION JOINTS IN ADULT HORSES USING WEARABLE INERTIAL SENSOR: VALIDATION STUDY AND APPLICATION TO VIRTUAL ENVIRONMENT

PhD candidate: Dr. Eleonora Pagliara

Supervisor: Prof. Andrea Bertuglia

PhD Coordinator: Prof. Maria Teresa Capucchio

Scientific Disciplinary Sector: VET/09 – Surgery

Academic years 2019- 2022

A Federica,

fonte di ispirazione quotidiana grazie al tuo supporto e alla tua preziosa amicizia

INDEX

1. INTRODUCTION AND AIMS OF THE THESIS

Horses are kept as domestic animals due to their outstanding locomotor skills, which have been employed for military use transportation and sport. Thus, there has always been great interest in the locomotor system of the horse either in a physiological sense or in pathological [1].

The horse, for its close proximity to the man, became a primary focus of veterinary science in the ancient societies and not surprisingly, first clinical comments were made on gaits.

It has been Aristotle (384-322 BC) who gives first attention to the principles of quadrupedal locomotion [2] but the first extensive work on equine conformation was performed years earlier by Xenophon (430-354 BC)[3]. These were mainly theoretical considerations not supported by experimental data. This was mainly due to the limitation of the human eye when observing faster gaits.

The first breakthrough in equine gait analysis was seen in the 19th century when the introduction of photography started a revolution for experimentation in the field of equine locomotion contemporary at the foundation of veterinary schools. The French physiologist Etienne Marey and the American photographer Eadweard Muybridge are considered the pioneer of modern gait analysis. Muybridge [4] was able in the 1870s trough the "photographic gun" to accurately visualize the various phases of the principal equine gaits The serial photography were a forunner of cine films. Marey [5] in the same time in France developed mechanical devices to record movement of the saddle, sacrum and all four limbs describing footfall pattern of horses in great details for the first time.

After the industrial revolution and the world wars the horse lost his role in the military completely and in the agriculture and transport to a large extent, the research in equine gait analysis slowed down reflecting this decline in societal relevance.

The booming economy of 1960's has seen an explosion in the popularity of equestrian sports and a concomitant revival locomotion research facilitated by the various new techniques developed such as high-speed film [6] and computer calculating power. The techniques allowed the quantification of equine gaits both in a kinematic either in kinetic way. The publications in the field of equine locomotion has increasing exponentially in two main areas [7]: general biomechanics related to performance [8] and locomotion changes due to lameness [9]. Due to technical and economic constraints, the experimentation remained largely limited to laboratory setting.

Only recently, in the past 10 years, quantitative analysis gained widespread use in the clinical setting for two main reasons:

- The introduction of portable gait analysis systems based on accelerometric devices attached to the horse body with wireless transmission of data [10,11]
- The cost of this instruments become cheaper and affordable

The concept of body mounted sensors has been developed further into more advanced inertial measurements units (IMUs) that often contain additional tools like gyrometers magnetometers and often also gps devices [1].

The currents gaits analysis systems are largely limited measuring parameters in the sagittal plane primarily at the croup and at the poll which are used to provide information on left to right asymmetry during movement. A next logical step is expansion to other parts of the body including the distal limb in order to gain a complete assessment of temporal and spatial parameters related to the movement [1,12]

Aim and scope of the thesis

1. Describe and review the state of the art in distal limb kinematics and relation to lameness
2. Application of inertial measurements units' systems (IMUs) in order to quantify joint kinematics.
    a. Technical application of IMUs on general locomotion and natural occurring lameness: validation study on metacarpus/metatarsophalangeal joint
    b. Studying joint loading during specific locomotion condition using inverse dynamic analysis and multibody modelling

1.1. LIST OF ABBREVIATIONS

IMU= inertial measurement unit

OMC= optical motion capture

GRF= ground reaction forces

ROM=range of motion

MSI= musculo-skeletal injuries

DOF=degree of freedom

TB=thoroughbred

ST=standarbred

WB= warmblood

IS=Italian Saddle Horse

M=mare

G=gelding

LF= left forelimb

RF= right forelimb

LH= left hindlimb

RH=right hindlimb

SDFT= superficial digital flexor tendon

DDFT= deep digital flexor tendon

NV= navicular disease

OA=osteoarthritis

FJA=fetlock joint angle

FJROM= fetlock joint range of motion

PCC= Pearson Correlation Coefficient

RMSE= Root Mean Square Error

CV= coefficient of variation

Cr= radial carpal bone

Ci= intermediate carpal bone

Cu= ulnar carpal bone

C2= second carpal bone

C3=third carpal bone

C4= fourth carpal bone

l-MCL = long medial collateral ligament

s-MCL= short medial collateral ligament

l-LCL= long lateral collateral ligament

s-LCL=short lateral collateral ligament

l-LR=long lateral retinaculum

s-LR= short lateral retinaculum

C.Th= cartilage thickness

VOI=volumes of interest

BV/TV=bone volume fraction

Tb.Th=trabecular thickness

Tb.Sp=trabecular separation)

Tb.N= trabecular number

Tb.Pf= trabecular pattern factor

SMI= structure model index

Da= degree of anisotropy

SBC= subchondral bone

H&E= hematoxylin and eosin

SOFG= safranin O fast green

CoC= centre of contact

MPG=medial parasagittal groove

FEA= Finite element analysis

MB= multibody analysis

1.2 LIST OF TABLES

1.3 LIST OF SUPPLEMENT MATERIALS

1. Detailed custom-made Mathlab Script used for comparison of FJAP
2. Mathematical functions of the model
   a. Spring element implementation
   b. Bushing element implementation
   c. Contact implementation
3. QR Code video
   a. Video 1- Tomographic examination of the fracture
   b. Video 2- Model: entire simulated stride
   c. Video 3- Model: Migration of contact forces along the radius within the simulated stride
   d. Video 4- Qualitative µCT analysis with false colors

2. MOVEMENT

Gait is defined as the speed and the characteristic of a horse in motion. Biomechanically locomotion involves moving all the body and limb segments in a coordinated rhythmic and automatic pattern which define the various gaits. The natural gaits are walk, trot and gallop exhibited when a horse is free in a field [13] but a great diversity exist in equine gait parameters because quadrupedal locomotion allows many combination of inter-limbs coordination [14].

Two types of gait can be distinguished by the symmetry or asymmetry of the limb movement sequence with respect to time and the median plane of the horse: symmetric gaits (walk, tölt, pace,trot) and asymmetric gaits (canter, gallop)[15]. In symmetric gaits the limb pattern on one side is repeated on the other side (left-right side). The stride is defined as a full cycle of limb motion. A complete limb cycle includes a stance phase when the limb is in contact with the ground and swing phase when the limb is airborne. During the suspension phase at trot, pace, canter or gallop, there is no hoof contact with the ground. The duration of the stride is equal to the sum of the stance and swing phase durations (fig.1)

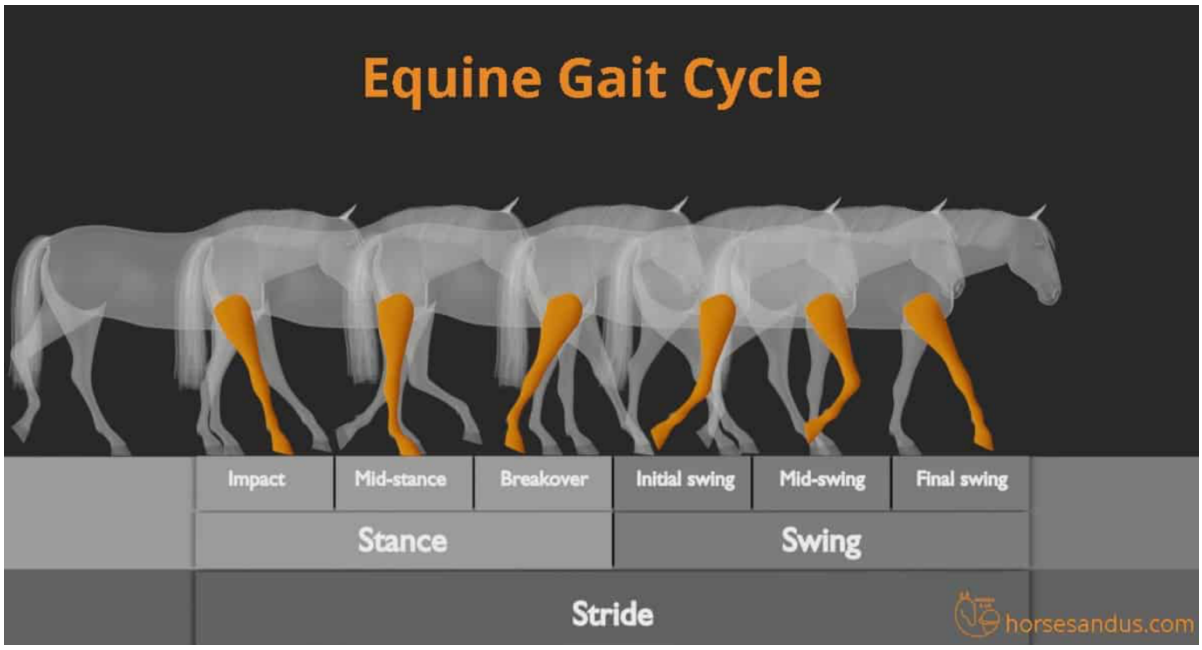

Fig 1. *Equine gait cycle at walk (figure from [16])*

Throughout all of the gaits the forelimb swing similar to a pendulum with the muscles of the scapula and humerus moving the proximal limb and the segment of the distal limb follows [17].
The stance phase is divided into more stages: primary impact, secondary impact, support and break over [18].

Primary and secondary impact
The impact stage of the stride involves the hoof contacting the surface and the force encountered depends strongly on the mechanical properties of the surface. The hoof works to dampen the shock in phase. The stage where the hoof travels in a downward motion and strikes the ground almost in a vertical position, represent the primary stage of impact [19]. As the horse move forward the force produced by itself causes the hoof to slide forward before stopping again causing additional collision and is termed secondary impact [19].
Support (mid stance)
This phase overlap with secondary impact and extend to heel lift. In this phase the limb experience peak vertical loads and there is a transition from breaking to propulsion [19]
The break over occurs as the hoof lifts at the heels during propulsion [18]. Vertical and horizontal forces fall towards zero and the limb is gradually unloaded.
The beginning of the swing phase occurs immediately after where the hoof and the digit flex rapidly [18]

At any gait, each limb performs the same action, slowing or increasing its relative motion according to speed [20]. The difference between gaits depends primarily on the sequence in which the limbs are placed on the ground.
The walk is a four-beat gait with large overlap times between stance phases of the limbs and no period of suspension. The entire forelimb shows a net absorption of energy in both stance and swing phases [21]. The elbow provides most of the positive work and is the only joint that shows net generation of energy over the entire stride.
As speed at the walk increases, the limbs move faster until the animal changes from a walk to a trot. This gait consists of alternating support by diagonally opposite fore and hind limbs moving in phase with one another. Each diagonal support phase is separated by an aerial phase [20].
Forelimb mechanics in the stance phase at trot are described in terms of a spring-mass system in which limb loading by the body mass stretches elastic springs that subsequently recoil as the limb is unloaded thus increasing the efficiency of gait [14]. The shoulder, elbow, carpal

and metacarpophalangeal (MCP) joints show elastic behavior with the MCP joint being the main site of elastic energy storage and release primarily due to the actions of the superficial digital flexor (SDF) tendon and the suspensory ligament [14].

Canter and gallop refer to the same gait performed at different speeds: the canter is a slow speed, three-beat gait and the gallop is a four-beat gait performed at a higher speed [14]. During the canter, the footfall pattern is changed so that the legs of one diagonally opposite pair move out of phase with each other while those of the other pair remain 'in-phase'. A single stride of the canter begins with the lead ('out-of-phase') forelimb, which throws the animal into the aerial phase. The animal lands on the diagonally opposite (out-of-phase) hind limb. The contralateral hind limb and its diagonally opposite (in-phase) forelimb make ground contact simultaneously in the same way that they did in the trot. As the stance phase of these diagonally opposite in-phase limbs ends, the out-of-phase lead forelimb is placed to the ground and provides the animal's sole support before it is propelled into the aerial phase of the next stride[20].

As the animal's speed increases it will change gait from a canter to a transverse gallop. The difference in limb sequencing between these two gaits specifically concerns the relationship between the in-phase fore and hind limb which at the trot and center had been working synchronously. During a transverse gallop the previously in-phase hind leg makes contact before the previously in-phase foreleg. A total four independent limb contacts are thus made with the ground, and in some animals the relationship of the previously synchronous (in-phase) pair of limbs becomes so extended that there is a second aerial phase between them [20].

2.1 Study methods of equine locomotion

Gait analysis has always been recognized as a key element in understanding equine athletic performance [22]. Human movement research has evolved rapidly with advances in wearable technologies, enabling comprehensive, 'real- world' monitoring and assessment of locomotor performance [7]. The same trends happened in the field of equine gait analysis, where science and technology applied to movement analyses have advanced significantly since the frame-by-frame photographic analysis of the 1870s, pioneered by Muybridge and Marey. The use of quantitative gait analysis has becoming more practical thanks to the use of portable technologies. The need to collect real world data and assist the veterinarian in the decision making process has pursued the validation of wearable sensor technologies and modelling approaches in the last decades [7].

Systems to objectively quantify equine locomotion can be divided into either force measuring (kinetics) or motion measuring (kinematics).

2.1.1 Kinetics analysis methods

Kinetics concerned with the study of the acting forces created by the movement. Kinetic gait analysis measures the ground reaction forces that are the results of a step. The most common method of kinetic gait analysis in horses in the stationary force plate [9,23] that was one of the first instrument used for objective lameness assessment [14–16]. A metal plate is mounted on the floor or a walkway and, as force is applied to the plate, the piezoelectric sensors distort thereby causing measurable voltage changes that are proportional to the applied force. During the stance phase of the stride the hoof exerts a reaction force against the ground and the ground exerts a reaction force against the hoof that is equal in magnitude and acts in the opposite direction (ground reaction force GRF). Placing the sensors in different orientations enables to obtained the direction and magnitude of forces in three dimensional (3D) resolving GRF into three components (vertical, longitudinal (craniocaudal) and transverse (mediolateral) (Fig.2). These forces are presented graphically with the peak forces as the maximum forces generated in the described phase of gait, reproducing a force-time curve.
Variables measured by a force plate include: stance duration, magnitude of vertical, longitudinal and transverse forces, time when the peak force occur, the impulses and the point of application of the force (zero moment).

The peak vertical force (PVF) is a single and largest force during the stance phase of the stride and represent a single data point on the force-time curve. Vertical impulse (VI) can be derived by calculating the area under the vertical force curve using time.

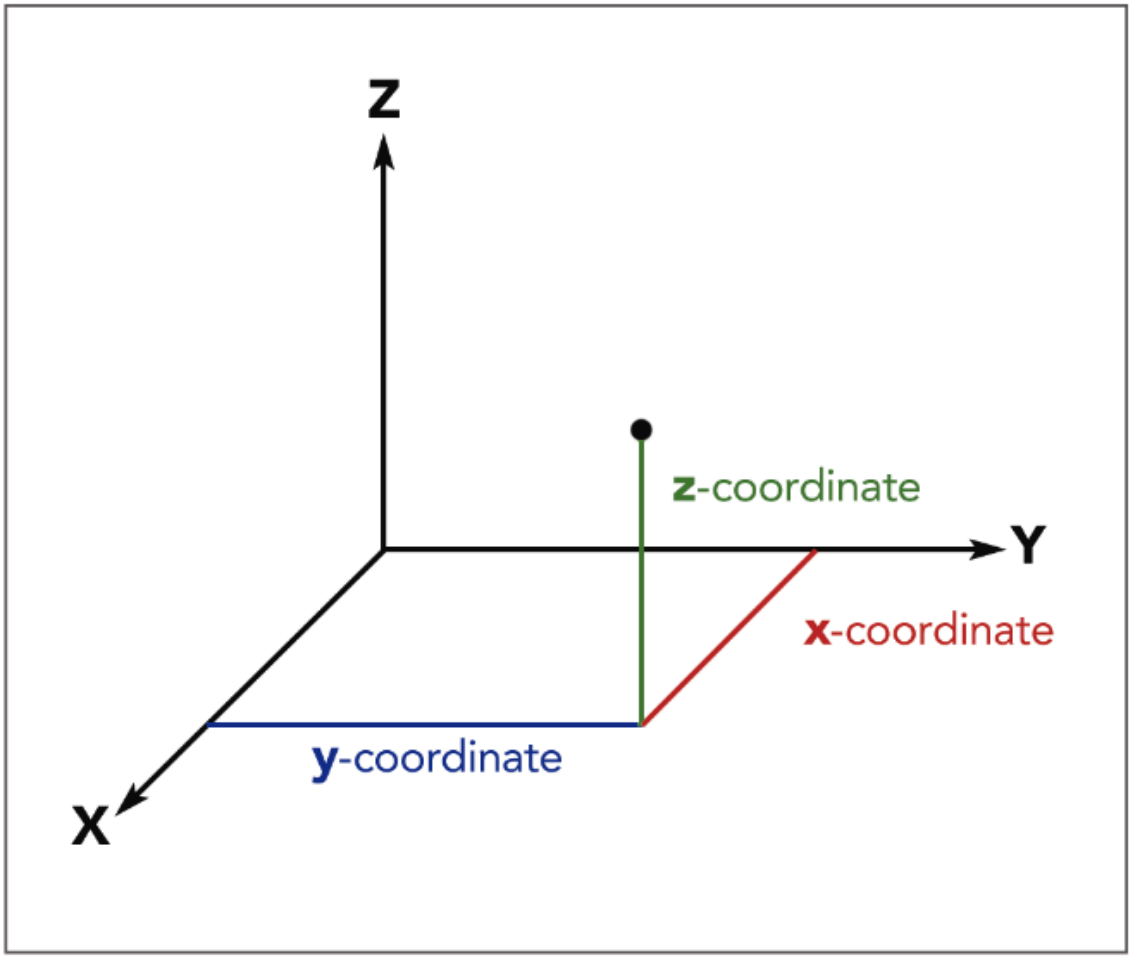

Fig 2. *Diagram showing the forces measured during force plate analysis (from [24])*

In a single limb lameness at the trot the most commonly reported changes measured in the limb affected are a reduction of PVF, VI and decreased swing duration [23]. In particular for unilateral forelimb lameness a decrease in mean PVF in the lame forelimb is accompanied by increase in mean PVF in the contralateral forelimb and in both hindlimbs at walk [25] and in the contralateral forelimb and hindlimb at trot [26] (Fig.3). For unilateral hindlimb lameness, a decrease in mean PVF in the lame hindlimb is accompanied by increase in mean PVF in both front limbs at the walk [25] but little change in the other limbs at trot [27].

Those two parameters (PVF and VI) in lame horses shown to have the lowest between and within-horse coefficient of variation and the highest correlation within subjective assessment of lameness grade. PVF also has high sensitivity and specificity for lameness classification [28].

Is also reported a reduction of peak breaking force (horizontal) as a consistent altered parameter due to lameness [28–31].

The use of PVF as a sole objective measure of lameness detection and quantification in horses has to be taken with caution as some lameness condition have caused not a decrease in mean PVF but a change in the shape of PVF signal [9]. In horses with mild lameness (less than grade 1 on AAEP scale) at trot mean forelimb PVF did not differentiate soundness from lameness but there was present a change in the shape of the PVF corresponding to different sources of lameness (tendonitis vs navicular disease) [32].

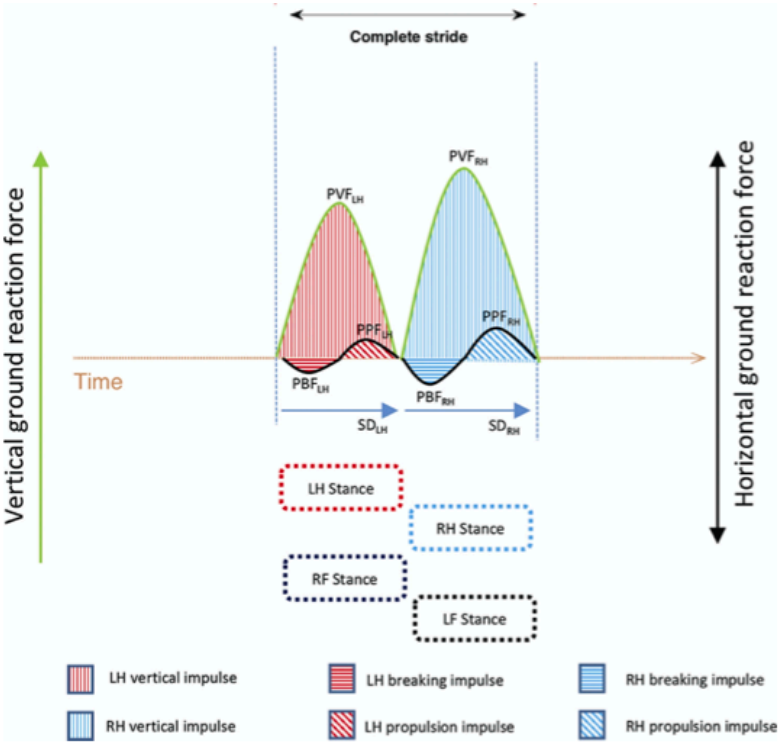

Fig 3. *Representation of vertical/horizontal ground reaction forces during a complete stride at the trot. The graph illustrates a left hindlimb lameness. The vertical ground reaction force and the horizontal ground reaction force are presented in green and black respectively. (LH: left hind, RH: right hind, LF: left front, RF: right front, PVF: peak vertical force, PBF: peak breaking force, PPF: peak propulsive force, SD: stance duration, asterisk: approximate timing of hoof-on). From* [23]

Although force place analysis represents the gold standard of kinetic evaluation in the horse, there are several limitation limiting its use including:

- inability to measure stride length
- need for consistent velocity, (small range of accepted velocity for a horse) so need of long dedicated walkways and multiple trials
- capturing enough valid and pure strikes of the limb of interest
- complexity of software data analysis that makes the use difficult and time consuming
- cost and impracticality for clinical use [9,23,24]

To overcome the need of long walkaways and the need of constant velocity, a force plate suitable for equine use has been embedded in a treadmill at the University of Zurich [33] (Fig. 4). It incorporates multiple piezo-electric sensitive sensors in the treadmill platform to determine the force application point enabling measurement of vertical forces of all four limbs over an unlimited number of steps at any gait. The treadmill has been used to generate some important information on the relation between GRF and lameness particularly on compensatory patterns in nonaffected limbs [26,27,34,35] and on correlation with subjective assessment of lameness [36]. Obviously, the instrumented treadmill is a custom-made device, is expensive and requires considerable expertise to use.

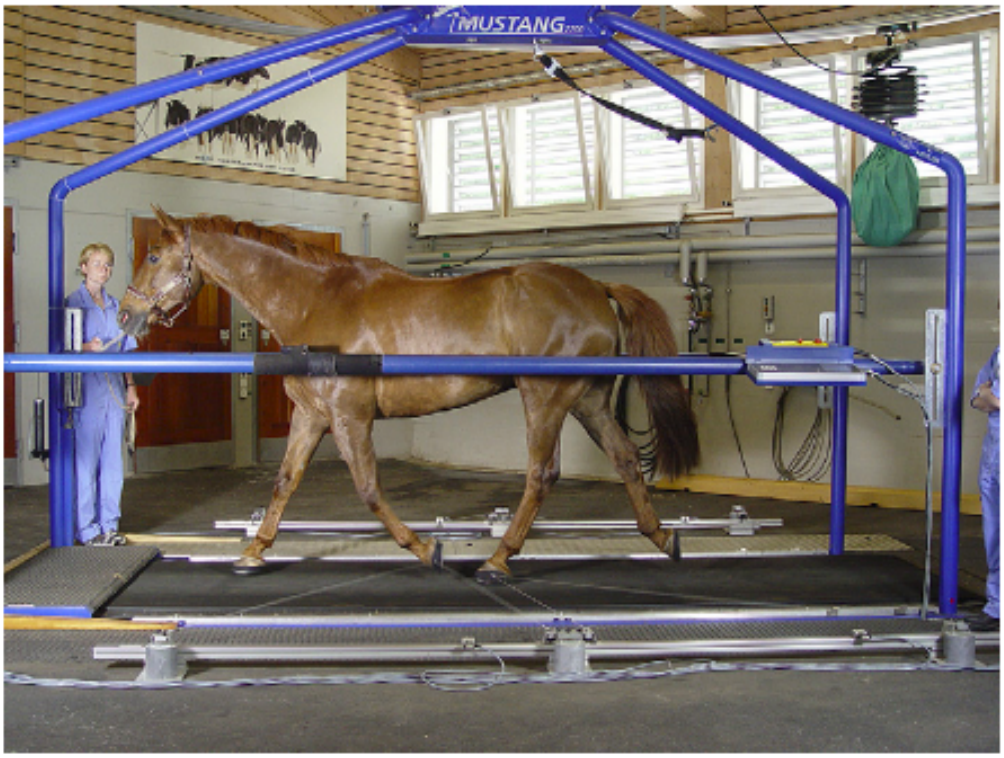

Fig 4. *Force-measuring treadmill, University of Zurich (Zurich, Switzerland)*

Another potential method of measuring PVF is the force shoe. A force shoe is a portable device that measures one or more component of the ground reaction force during a large number of successive stance phases overcoming the limitations of stationary force plates. The force measuring device may be attached directly to the hoof, sandwiched between a base plate (Fig.5) and a shoe or placed inside a boot attached to the hoof. Unfortunately, although many attempts [37–42] have been made to construct force measuring shoe that was small enough such as the normal limb kinematics was not altered, there are significant technical difficulties in manufacturing one that is accurate and reliable throughout the entire equine stance phase so none is currently marketed commercially. More recently a lighter version of a force shoe has been used successfully during athletic activity but the technology is not yet available [43].

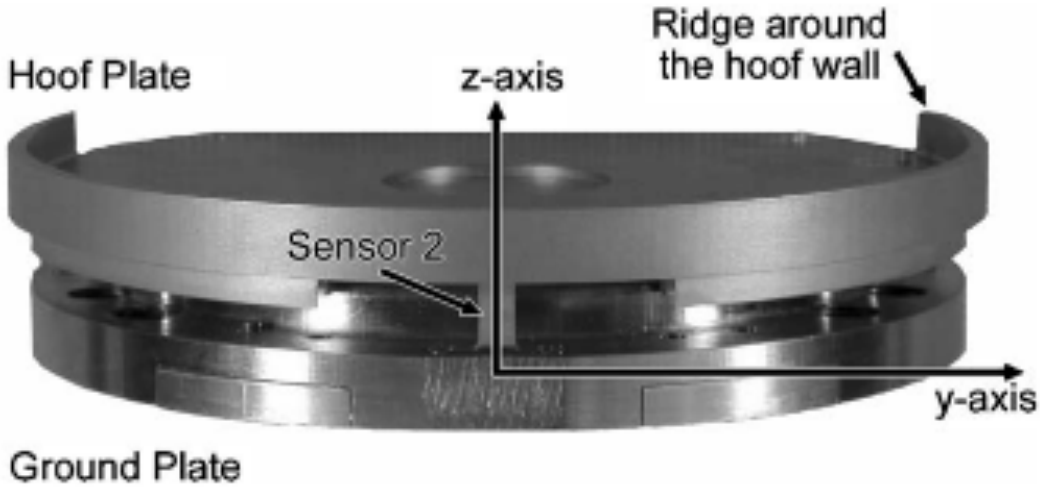

Fig 5. *Dynamometric horseshoe viewed from the toe with coordinate axes superimposed. From [41]*

Force can also be measured by strain gauges mounted on hoof walls [44–47]. These strain transducers measure the amount of strain based on changing of the electrical resistance in response to a deformation in a certain direction; the change in resistance is converted to a voltage output that is proportional to the strain. Despite these systems are promising for a clinical application since they are small, they collect data from a limited area that is not necessarily representative of the total strain or load in an entire structure [48]. These systems would also likely to be subject to a large variation with different types of foot shapes, state of trimming, presence or absence of shoe and overground surface conditions [11].

Overall, the currently available kinetic methods for assessment of lameness are not ready for widespread clinical application but the existing methods remain highly valued tools for researcher in the field of equine gait analysis.

2.1.2 Kinematics analysis methods

Kinematics is concerns with the study of the description of motion. Motion can be described spatially (height, displacement velocity/ acceleration as a function of time, of a body segment relative to a reference coordinate system or it can represent the relation (angle) between body segment.

High speed film was the first technique used for recording equine locomotion using reflective skin markers based on two-dimensional (2D) analysis [6]. Further technology developments allowed higher speeds recording in three dimensions (3D). The most common method for motion analysis nowadays involves optical motion capture (OMC) which can be accomplished using passive markers, active markers or marker-less methods [48]. Optical technology is limited by its use of cameras to record the activity and markers are tracked automatically based on the emission and detection of infrared or visible lights. Tracking the position of parts of the body using stationary cameras and markers suffers from limited resolution from large field of view; acquisition of proper data sets required that the horse be filmed when moving on a treadmill [9].

The sequence of events for motion analysis involves attaching markers to subject, setting up and calibrating the recording space, recording the subject in motion, tracking the subject to obtain digital coordinates and data analysis that might include smoothing, normalization, transformation and interpretation of the results [48]. OMC using skin markers is affected by skin displacement artefacts due to the displacement of the skin over skeletal structure [23]. The location of the marker on the body affects the artifact being almost negligible for the distal limb [49] but important for the proximal limb where for example the skin moves by as much as 12 cm relative to the bone in the sagittal plane [50]. However skin displacement correction algorithms have been developed [51].

Nowadays the most widely used system for 3D OMC in the horse with the purpose of lameness detection in the horse is Oqus/Qhorse (Qualisys AB) system [a]. This system uses 12 cameras to cover the volume where the horse trot in a straight line and another 8 cameras cover a circular volume (Fig.6) to record the position of several reflective markers simultaneously.

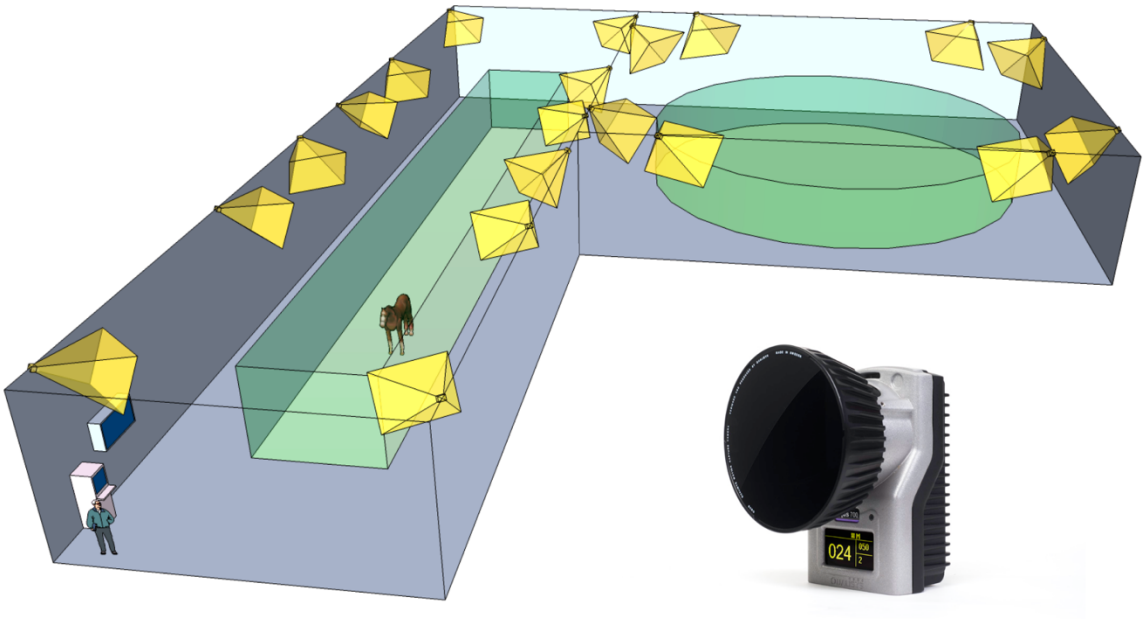

Fig 6. *System set up of Qualisys system (from https://www.qualisys.com/life-sciences/equine-lameness-detection/)*

The equipment is expensive and time consuming to operate, to the best author knowledge only 8 facilities have this equipment available in Europe.

Around the same time the use of OMC became more common in equine gait analysis, another method of kinematic analysis based on body mounted accelerometers was reported. Although the first reports on symmetry parameters to quantify lameness were based on acceleration measurements [52] research in the last two decades has focused more on measurements of vertical displacement. The technology relies on sensors attached to body segments and recording data during locomotion. This type of sensor measures the instantaneous change of velocity of a body during a given interval which corresponds to the acceleration applied to this body. The acceleration vector is proportional to the resultant force applied to the body where the sensor is attached [15]. The technique is very user-friendly, as it does not need a calibrated space and can be used everywhere and under many conditions. IMU sensors are composed of a gyroscope, accelerometer and magnetometer, measuring acceleration, angular velocity and the earth's magnetic field in all three dimensions. Using attitude estimation algorithms, specific data processing routines such as double-integration of acceleration and assumptions of cyclicity in the movement [12,53] relevant parameters can be calculated.

Detection of lameness using IMU sensors is based on the detection of differences in vertical displacement of maximum and minimum position of head/withers and pelvis between affected limb and contra-lateral. In fact, change in the amplitude of the vertical displacement in the stance phase of a lame limb, the head/withers and pelvis reach a minimum position that is higher when compared with the contralateral non-lame limb, resulting in a difference between minimum positions of either the head/withers or the pelvis in case of fore or hindlimb lameness (fig.7) respectively. The maximum positions of the head and pelvis at the end of the stance phase of the lame limb are also lower when compared to the non-lame limb, resulting in a difference between maximum positions (of the head/withers or pelvis in case of fore or hindlimb lameness (fig.7) respectively.

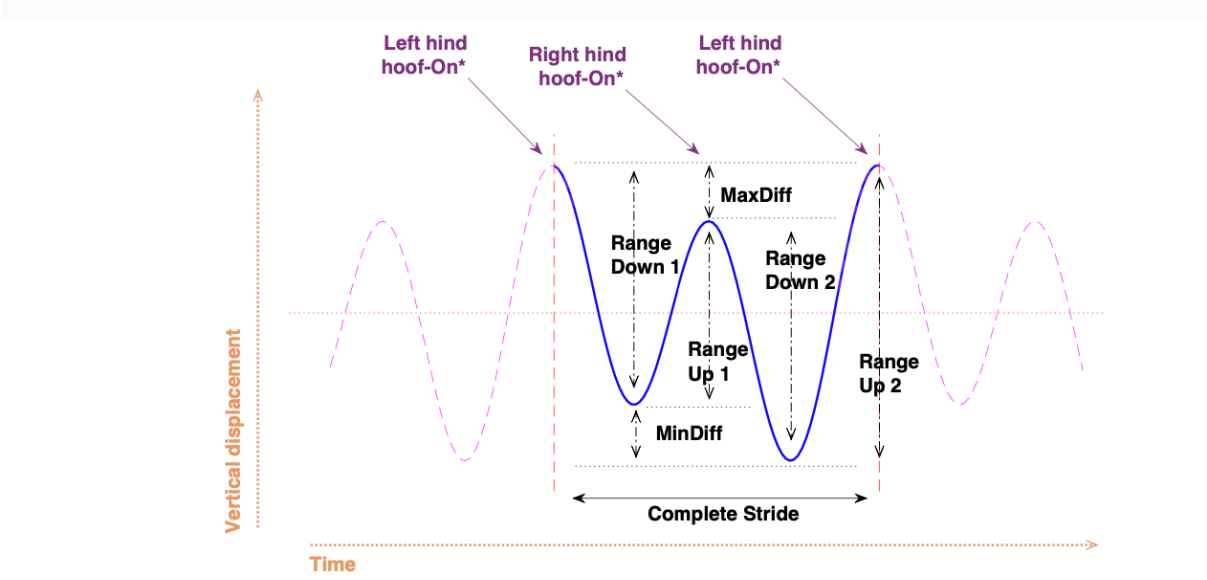

Fig 7 *.Graphical presentation of the vertical displacement of the pelvis during a complete stride at the trot of a horse showing left hind lameness. The vertical displacement of the pelvis is presented in blue (LH: left hind, RH: right hind, LF: left front, RF: right front, asterisk: approximate timing of hoof-on). From [12]*

Most research has focused on the kinematic analysis of head and pelvis movement, back motion and temporal and angular changes in limb motion [23]. IMU sensors are prone to integration errors that may accumulate making these instruments to be less accurate in calculating a position estimate as the recording progresses [23] Nevertheless modern IMU sensors can reach high levels of accuracy in the quantification of equine kinematics [12,53].

OMC and IMU technology can successfully measure overground locomotion (limitations and advantages are listed in table n. 1)

	OMC	IMU
pros	accurate	Portable (wearable) wireless unexpensive data collection under any range of distance and condition
cons	Expensive Collecting several strides is limited Requires special training for use and interpretation of results	Less accurate Prone to accumulation errors and discalibration

Table 1.

2.1.3 Inverse dynamic analysis and modelling

Inverse dynamic analysis calculates forces within the limb that cannot be measured directly. Input into the inverse dynamic model comes from synchronized kinematic and GRF data, which are combined with morphometric information and segment inertial parameters [48]. Using these data, the net joint torques and net joint reaction forces are calculated using Newton's equations of motion applied to a model containing a rigid segment. Net joint power is a measure of the mechanical work done across the joint and it is the product of net joint moment and joint angular velocity. The moment at the center of rotation of a joint is directly related to the combination of muscle forces acting across the joint. Inverse dynamic analysis treats the locomotor system as a system of rigid segments, with hypothetical moment motors at each joint representing the action of muscles. The analysis combines kinematic and force plate data to derive this joint moment trough the movement cycle.

Since Elftman [54] introduced the inverse dynamics analysis in biomechanics (1939) it has been applied successfully in human movement research and has been applied in horses to evaluate forelimb net joint moment and power at walk [21,55] and trot[56,57] and during jumping [58]. The effect of lameness on net joint moments and power also has been evaluated [31,59].

Computer modeling is the process of creating a representation of an object or system within the computer [14].

To date, computational methods have been widely used in biomechanical studies, with finite element analysis (FEA) and multibody (MB) analysis representing the two mostly used approaches for musculoskeletal research topics [60].

FEA mainly aims at predicting stress and strain distribution within hard and soft biological tissue but, due to high computational cost, is generally applied to small scale systems under static loading conditions [60]. MB, based on the dynamic equation of motion, allow to investigate the kinematical and dynamical behavior of a system consisting of multiple rigid or flexible bodies interconnected by joints [60]. All involve using 3D data of internal anatomy (obtained from CT and μCT scanning of preserved specimens) and material properties (obtained from literature or measured on a fresh specimen). Computer models then simulate strain and stress during mechanical loading (FEA) and how muscles transfer contraction force onto skeletal elements, and how they interact with each other (MB).

Computation modelling using finite element method has been previously applied to the distal portion of the third metacarpal bone and proximal phalanx in racehorses to study deformation of the trabecular bone and gain information on stress fracture pathogenesis [61–63]. Finite element simulation is informative of the stress and strain properties of the material. In contrast to FEA, traditional MB analyses are not able to provide information about stress or strain distributions, but they offer the possibility to deal with small as well large-scale systems considerably reducing computational costs [60]. In the light of mentioned advantages, MB simulations are valuable tools in basic research on functional anatomy and aetiology of injuries [64]. This explain the growing popularity of the methodology in biomechanics, starting from the first application in 1906, when it was employed to study human locomotion [65]. Numerical multibody models have proven to be a valuable tool for addressing open issues related to the musculoskeletal system as well as improving the understanding of complex anatomical structures, such as those constituting diarthrodial joints [66–68]. By exploiting these models, internal forces that cannot be measured in vivo directly (e.g., intra-articular contact forces) can be estimated to enable the identification of detrimental biomechanical conditions and allow the prediction of injuries [69,70].

2.2 **Lameness and Gait Adaptations**

The disciplines in which horses are involved are various including pacing, trotting and galloping races, eventing, show jumping, dressage, endurance and western performances. The musculoskeletal system of the horse is subjected to strong mechanical stresses during sports exercise. Disorders of that system become clinically manifest as lameness. Lameness is arguably the most important medical problem in horses [1] and can be defined as a deviation from the normal gait due to functional or structural disorder in the locomotor system [23]. To the horse owner and the horse trainer, lameness is the most important equine health issue they face and, for that reason, lameness is one of the main reasons for equine veterinary consultation [71].

Degradation of symmetry in the movement is a marker of lameness [72,73]. Lameness that results from the efforts of the horse to avoid pain during loading is defined supporting limb lameness.

The simplest and most sensitive indicator for clinical diagnosis of lameness is the characteristic movement of the head and trunk. Because of Newton's second law and the fact that trunk contains most body mass, asymmetries in head and trunk movements allow lame horses to reduce the vertical ground reaction force in their painful limb [74]. Movement asymmetry of head and trunk in the sagittal plane of horse (left-right) is obviously best evaluated in symmetric gaits (walk and trot).

Regarding temporal variables of the gait cycle, shortening of the swing duration in the lame limb is a consistent feature [75,76] during supporting limb lameness.

2.2.1 Subjective evaluation of lameness and limitation

Visual examination of equine gait has been the main clinical tool for diagnosis of lameness in horses during the past millennia. The clinical examination involves particular attention to the straightness and symmetry of the horse in the gait, its attitude, head and pelvic vertical displacement, the mobility of the back, the mobility of the limb including the protraction and retraction angles and range of movement of the metacarpus/metatarsophalangeal joint [77,78]. Many of these gait events can be and has been assessed effectively trough subjective visual lameness evaluation by an experienced clinician [79] but any observer is hampered by the limitations of the maximal temporal resolution of the human eye [80]. It has been proven that low agreement exists between clinicians for subjective scoring mild to moderate lameness

[81] and repeatability of subjective evaluation between veterinarians is only marginally acceptable [82]. Difficulty exist also in a consistent documentation of gait alteration which is mainly due to the lack of uniformity in lameness rating scales [9].

These issues complicate lameness examinations and form confounding factors affecting clinical decision-making and hampering clinical orthopaedic research on the evaluation of diagnostic procedures, treatments and rehabilitation protocols [23]. The importance of lameness in everyday practice justifies the great efforts now put in locomotion research.

2.2.2 Modern system of lameness detection

At the moment of writing this dissertation, five IMU based sensors systems for lameness detection are currently available on the market. The characteristic and the kinematics parameters used by each system are resumed in table n.2.

	Sensors number	position	parameters	limitations
Lameness Locator® (Equinosis, 104 E Brodway, Columbia)	3	-head-sacrum single axsis accelerometer Right forelimb single axis gyroscope	Vertical displacement of head and pelvis	Use only at trot Results related only to the upper body
Equigait® (Equigait Ltd, 167 Turners hill, Cheshunt, UK)	3-9*	Pool-withers-left tuber coxae-right tuber coxae-sacrum		Not used to assess limb-related parameters
Equimoves® (Inertia Technology B.V., Enschede, The Netherlands)	8	Pool-withers-sacrum-sternum-one each limb (lateral aspect of metacarpus-metatarsus	Limb angle parameters (protraction-retraction and adduction-abduction)	
Gait smart Pegasus® (Dynamic Metrics Limited, St Albans Road Codicote, Hertfordshire, UK)	6	Lateral surface of the distal tibia-lateral aspect of the metacarpus-metatarsus	Stride pattern (stride duration, speed, temporal limb phasing) Angular range of motion of the hock (sagittal-coronal)	Not fully validated Biological significance of parameters

Equisym® (Arioneo- Ile de France,Paris)	7	Head-withers-pelvis- 4 cannon bones	Stride pattern (stride duration, speed, temporal limb phasing) Vertical displacement of head withers and pelvis	

*Table 2. * Number of sensors according to type of assessment (gait and symmetry, back movement, horse-rider interaction).*

There is an ongoing interest on quantification of limb kinematics and spatial and temporal stride variables that could provide extra information related to specific gait changes due to lameness. Methods to accurately detect gait events are valuable in various applications including performance analysis and lameness quantification. The gold standard of equine gait event detection remains the force place measurement but its use is unsuitable for real-world scenarios as mentioned before. The detection of spatiotemporal events, i.e., Foot on and Foot off timings, is an essential step for data preprocessing in order to segment the data and then calculate the locomotor parameters. This step is the keystone for the analysis of the locomotion of the horse [83], especially for the next detection of lameness.

The accuracy to detect gait events from IMU systems placed on metacarpus and metatarsus has been already proved from both front limbs and hindlimbs compared to the gold standard (force plate) measurements [84,85] and OMC [86,87]. The methods for stance detection derived from gyroscopic data showed more precision than those developed from accelerometer data [86,88]. Briggs and Mazzà [88] compared gait event detection using different processing methods applied to data collected by IMUs attached to the fore and hindlimb pasterns and cannons and proved that pastern-based methods were superior to the current state of the art cannon-based alternatives.

In the last years IMU have been placed on distal extremities to assess distal limb displacement, translation of the metacarpus as a rigid segment, protraction and retraction angles and as well as for temporal and spatial variables detection of the strides during different gaits and conditions. A summary of publications using IMU's at distal extremity and outcome measurement are listed in table n 3. To the best author knowledge there are no reports of

placement IMU on distal limb to assess relative angle of two adjacent bone segment (joint angle).

Parameter studied	IMU specific placement	Comparison/validation	outcome	reference
Gait event detection	1 per limb-Distal end of the 4th metacarpal/tarsal bone	Force plate and OMC (Qualisys)	Good accuracy and precision for toe on and off-less precise in stance phase duration	[84]
Stride detection and quantification	1 per limb-lateral aspect of cannon	Force plate and OMC (Qualisys)	Good precision and accuracy	[26]
Limb sagittal segment angles at walk and trot	1 IMU per limb Lateral side of metatarsal/metacarpal bones	OMC (Qualisys)	No bias and high precision	[89]
Speed estimation	1 per limb-lateral aspect of cannon	Gps signal	High speed estimation accuracy	[90]
Trotting stance detection	Dorsal aspect of the cannon	OMC	Methods derived from gyroscope more precise	[86]
Repeatability of gait variables at trot	Six IMUs metacarpal/metatarsal region and distal tibial regions	IMU controlled exercise (treadmill)	High repeatability of gait variables of non-lame horses at trot	[91]

Automatic hoof on-hoof off detection on different surfaces	6 IMUs Lateral aspect of cannons-pasterns and hooves (front and hindlimbs)	Different processing methods	Pastern based methods superior	[88]
Protraction and retraction angles of limbs	1 IMU per limb- dorsal aspect of the cannon	OMC	Estimating protraction and retraction angle with a single IMU is feasible	[78]
Assessing horse behavior to early detection of MSI	1 IMU per limb (only forelimbs) Lateral aspect of the cannon	Video observation	IMU displayed high sensitivity to movement	[92]

Table 3.

3. IMU SYSTEM UNDER INVESTIGATION

3.1 Technical characteristics

The inertial system (MOVIT System G1[b]) is a wearable motion capture system previously validated in humans [93].

The system is composed by IMUs (MOVIT G1) and a receiver (Dongle G1) that connects to the computer through an usb (fig.8). This system is modular and allows to use from 1 to 16 IMUs simultaneously.

Each IMU measures 48 × 39 × 18 mm and weighs 40 g (fig.9). Each IMU hosts different sensors, in particular a 3-axis ±2g accelerometer and a 3-axis ±2000dps gyroscope [c] plus a 3-axis compass and a barometer (the latter two not used for the experiments).

In general, IMU-based systems rely on signals from the accelerometer and the gyroscope to gather roll and pitch information, and signals from the compass to gather yaw data. Advantageously, a patented calibration procedure (U.S. Patent 102016000041519, 14 November) allows obtaining roll, pitch and yaw without compass data, with the further advantage of overcoming limits due to magnetic interferences.

Since the heading components of the sensors will slowly drift away from each other, accurate measurements are limited in time after the calibration [94]. However, the system allows easy re-zeroing at any-time. By using the quaternion (6 degrees of freedom), sensors measure changes in orientation of the part of the body to which it is applied. In detail, sensors detect changes in rotation along the sagittal axis (backward/forward and rolling, respectively), frontal axis (up/down and yawing), and transverse axis (right/left and pitching).

Each sensor is provided with an internal flash memory card for data storage. Although the system also allows real time data recording with a dedicated software (Motion Studio[c]-fig.10) in this case the sampling rate is lower (100 Hz) than acquiring data into the internal storage (200 Hz). To obtain the maximum sampling rate and to avoid data loss due to wireless communication, internal storage was opted for the experiments in this thesis.

Fig 8. *Components of the MOVIT G1 System*

Fig 9. *Imu sensors and docking base*

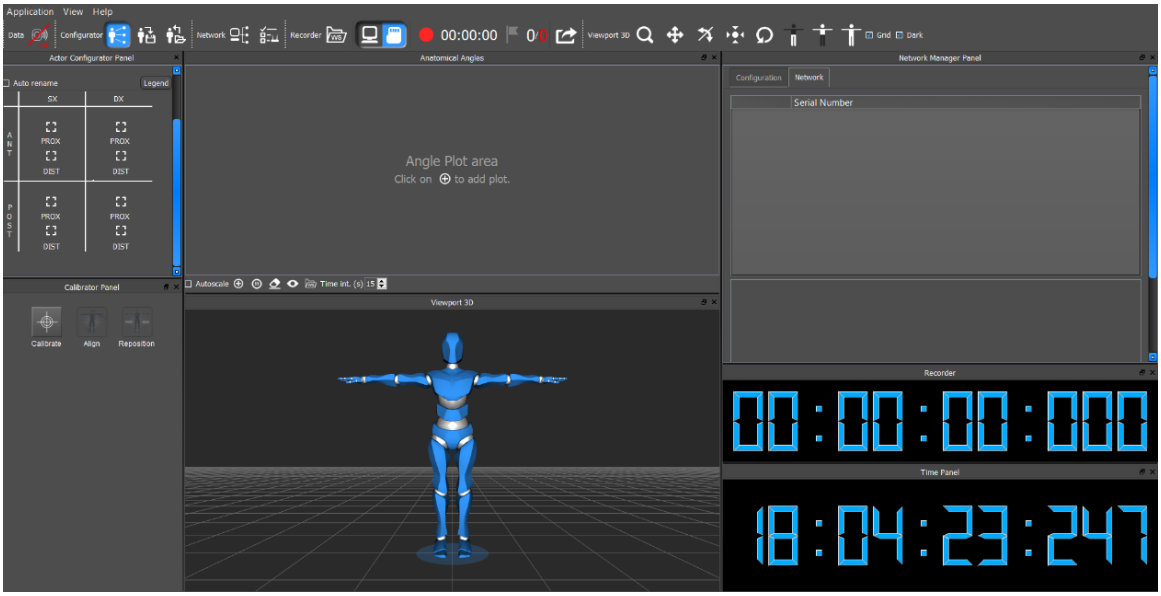

Fig 10. *Motion studio software*

The system also features a patented calibration that allows the sensors to have the same global reference system, via three orthogonal positions assumed by a baseplate (U.S. Patent 102016000041519, 14 November 2018). Starting from the same global reference system, it is possible to consider two sensors and measure relative orientation data.

Before each test, IMUs are calibrated following the steps described in the U.S. Patent

The steps are the follow:

-perform three 90° rotation with the calibration base holding the 8 sensors (fig. 11).

- put the IMU sensors over the joint of interest in couples (proximal and distal dorsal aspect of two adjacent segments on the horse limb). Each sensor has a docking base which makes positioning of the sensors over the body easy. Each docking base is indeed provided with Velcro, which allows the adhesion on an elastic band provided by the manufacturer (fig. 12).

-maintain a static position of all couples of IMU for few seconds with the horse standing with the limbs squarely positioned to finish the calibration phase (fig.13).

The angles are generated from the quaternion (6 DOF): from the proximal quaternion and the distal quaternion of each couple of sensors, the relative quaternion is calculated and, using a Euler decomposition, the relative angles are calculated (sagittal-frontal and transversal plane).

With this patented system of calibration of sensors, the problem of saturation of the accelerometer (max set to full-scale range of ±16g) to measure relative angles during movement is overcome because the generation of the quaternion in dynamic derives mainly from the gyroscope (measuring angular velocity within range of ±2000 dps). The accelerometer is used to make corrections to the roll and pitch components of the quaternions during the static phase of calibration. By doing this, the system can measure the dynamic relative angle of the joint of interest as the outcome unit.

The Motion Studio software provided by the IMU sensor manufacturer allows starting and ending data acquisition, as well as data visualization in real time. So, from raw data of each sensor, the MOVIT G1 software can retrieve joint angles over time in all three dimensions:

- sagittal plane range of motion of the joint as flexion (+) and extension (-) angles
- frontal plane range of motion of the joint as abduction (+) and adduction (-) angles

- transverse plane range of motion of the joint as internal (+) and external (-) rotation angles

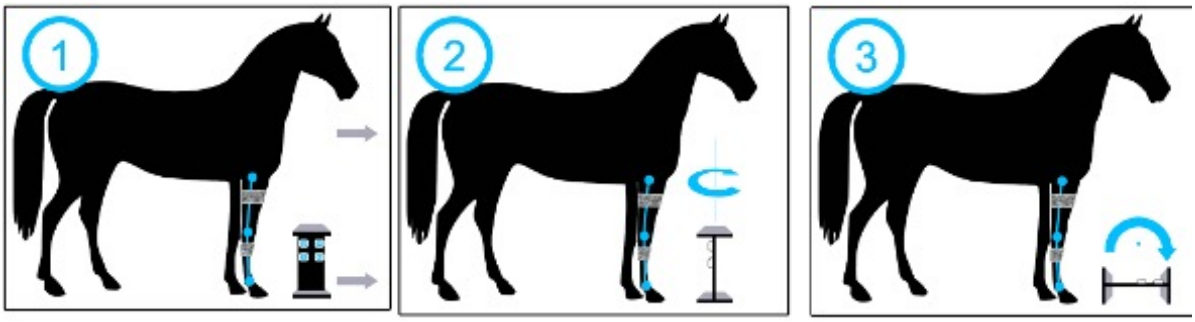

***Fig 11**. Calibration on the baseplate*

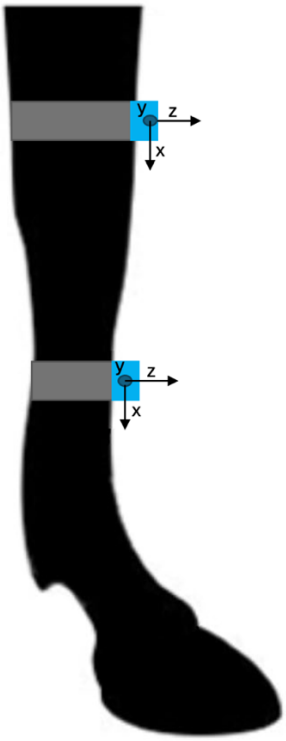

***Fig 12.** Placement of the IMUs over the joint of interest*

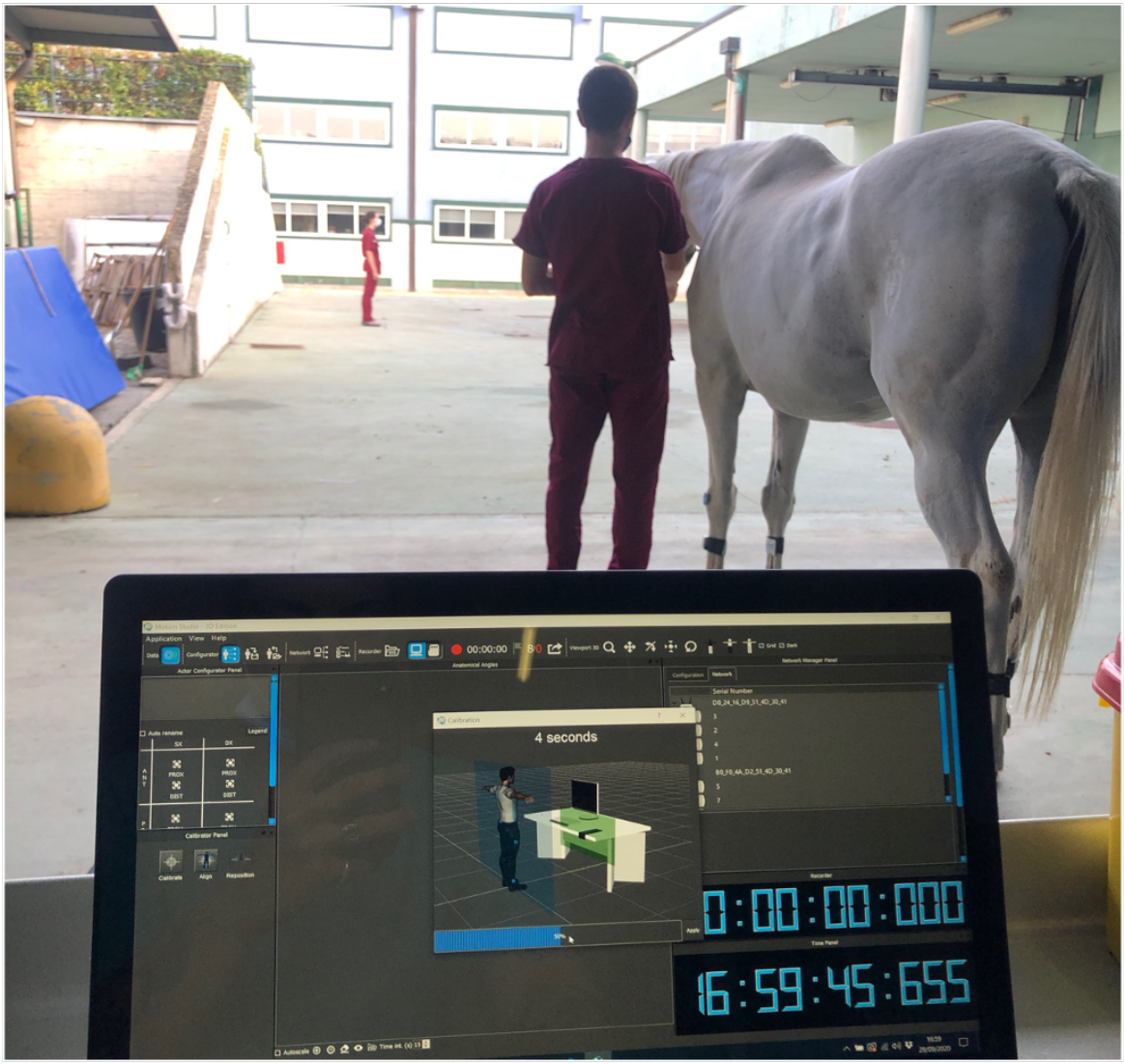

Fig. 13 *Alignment phase on the horse*

Conventionally, joint angles are set at 0° during calibration. Thus, positive and negative sagittal joint angles indicate flexion and extension of the joint, respectively, compared to the initial calibration point.

The Motion Studio software provided by the IMU sensor manufacturer allows starting and ending data acquisition, as well as data visualization in real time. As output data, the Motion Analyser software provides synchronized raw data (from the accelerometer, gyroscope, magnetometer and barometer of each sensor) with video and animation (fig. 14). Form raw data, an of angle/time diagram of joint motion in the sagittal, frontal and transverse plane is generated in the Motion Analyser software. An excel file is contemporarily generated with joint angle values at each timestamp.

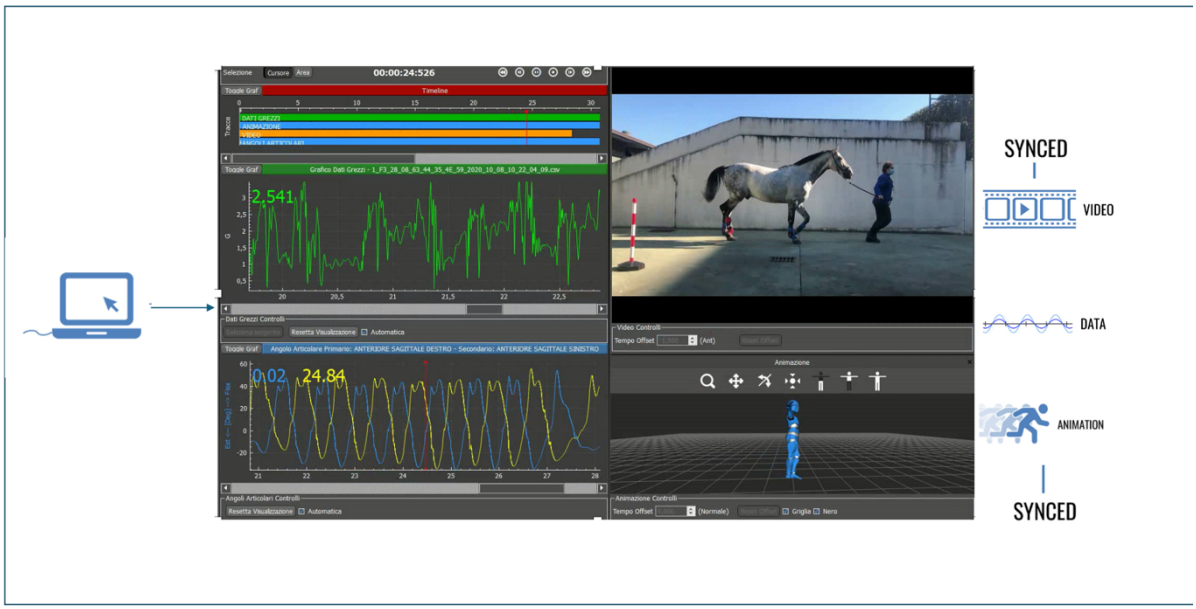

***Fig 14**. Motion analysis software. Top left of the picture showing raw data from a sensor; bottom left angle/time diagram of sagittal plane motion of metacarpo phalangeal joint of a right front limb (blue) and left front limb (yellow) simultaneously*

4. EXPERIMENTAL PART-FETLOCK JOINT

4.1 Introduction

The fetlock joint is the essential joint to the performance horse. The fetlock joint is a high motion joint that consists of two long bones (third metacarpus/metatarsus and first phalanx) and two sesamoid bones [95]. The joint accommodates rotation in the sagittal plane around the center of the distal aspect of the MC/T3. Internal/external movement is defined as a rotation around the first phalanx adduction/abduction movement of the joint runs cranio-caudally, perpendicular to the plane formed by the flexion/extension axis (fig.15).

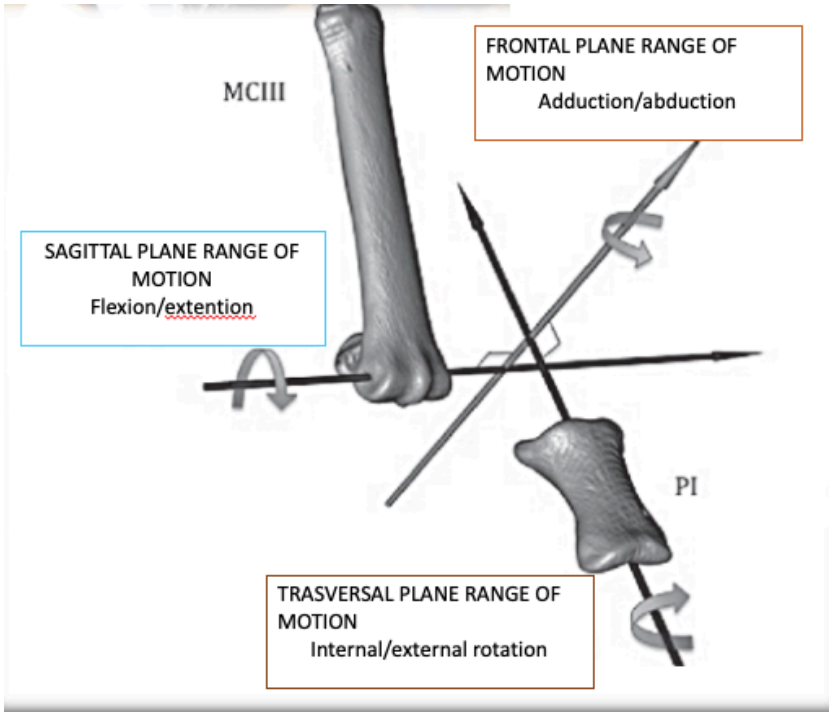

***Fig 15**. Planes of motion of the metacarpal/metatarsal phalangeal joint. Modified from [96]*

The fetlock experiences the largest load during locomotion and exhibit the greatest range of motion (ROM) in the sagittal plane (from 120° to 120°) of any equine joint. The MCP joint and its supporting structures are frequently injured in athletic horses, especially those that perform

at high speed [97]. The predominant plan of motion is the sagittal and the variability in flexion-extension pattern between horses is reported to be low [98]

The fetlock joint flexes during limb protraction, which is accomplished by muscle contraction and passive energy return from elastic structures, largely tendons and ligaments [99]. This moment is represented in an angle-time graph of the fetlock joint angle during the swing phase as a first peak, the second peak occurs soon after and represent the active muscle contraction [17,57] (Fig.). The joint extends in early stance reaching the maximal angle value during mid-stance (fig.16).

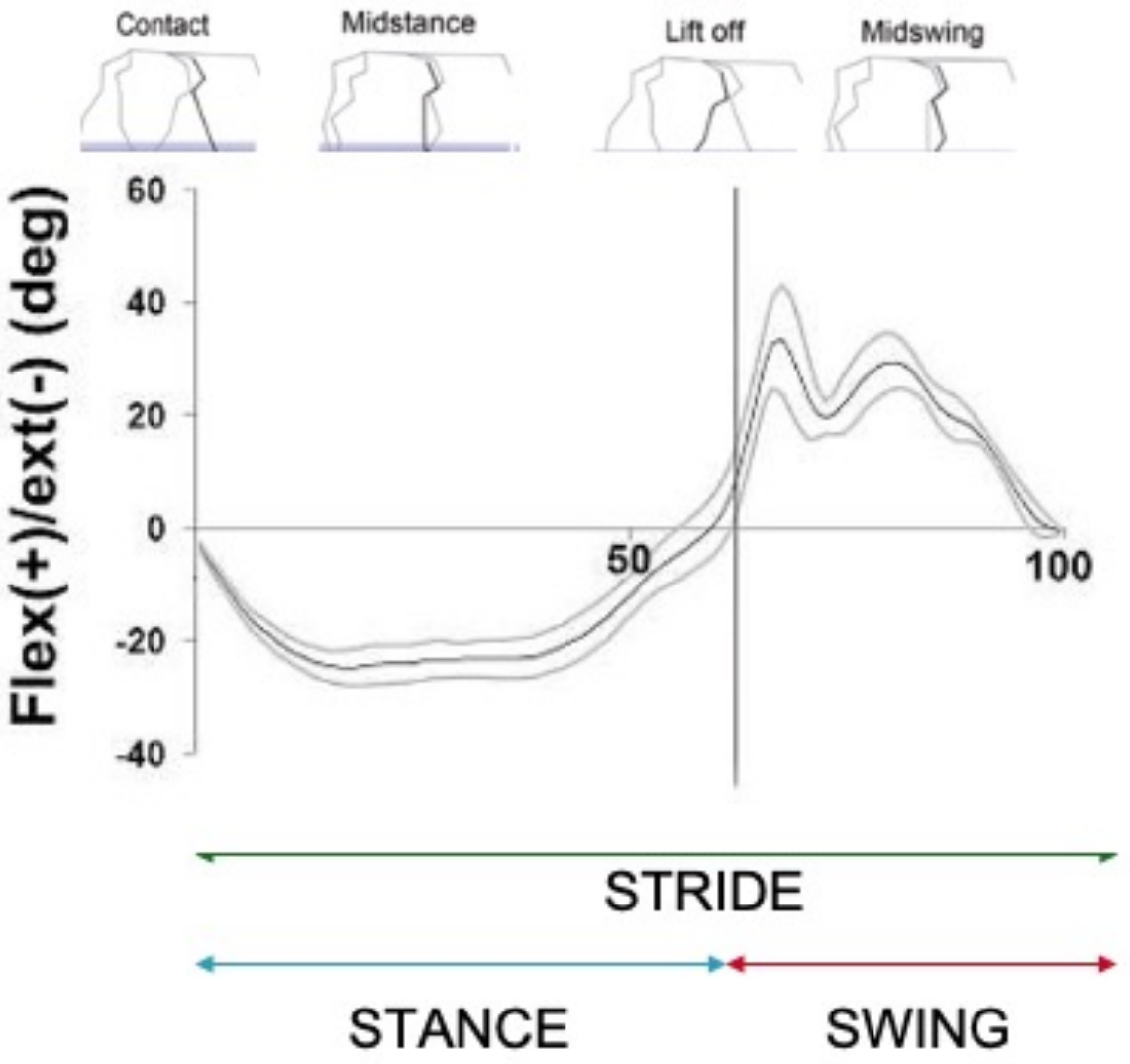

Fig 16. *Image shows the angle time diagram of fetlock joint angle in relation to the various phases of the stride at walk. Modified from [96]. Fetlock joint angle is quantified with 3-d OMC.*

The fetlock joint angle during stance is determined by and resemble the pattern of vertical GRF as demonstrated in sound horses with a force plate [100,101]. For this reason, the amount of hyperextension of the fetlock joint is one of the parameters that correlates well with subjective judgment of gait quality [102] and on the opposite, deficit in extension is an indicator of supporting limb lameness. In fact, the most consistently described changes in case of lameness induced in joints are reductions in stride duration, fetlock extension and in joint ROM [23] .

During supporting limb lameness, the horse tries to reduce the load on the painful limb and the amount of loading can be measured indirectly from distal joint angle patterns during the stance phase. In the lame limb, fetlock hyperextension at the middle of the stance phase is reduced proportionally to the grade of lameness [103] (Fig. 17-A). In contrast, fetlock hyperextension in the contra-lateral sound limb shows increased in the maximal values (Fig.17-B). This asymmetry indicates a compensation of the reduced loading of the lame limb by the contra-lateral sound [104].

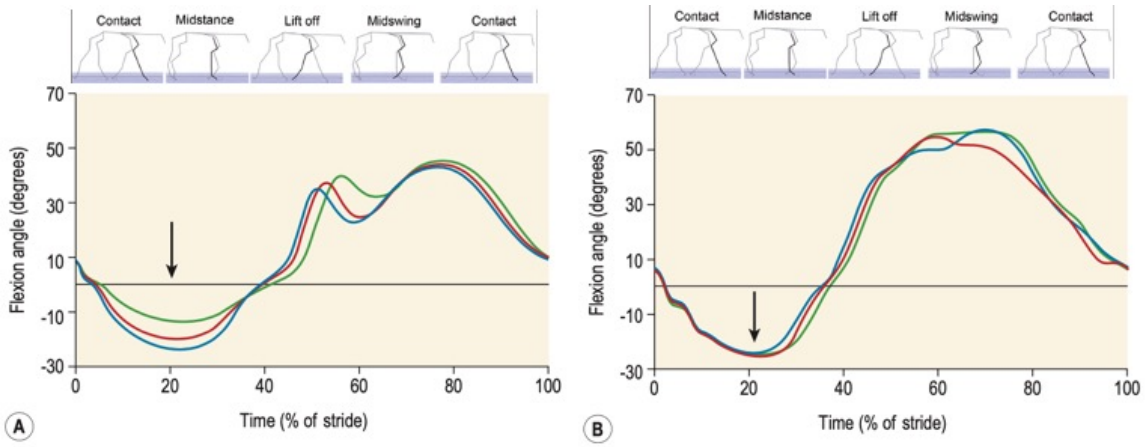

Fig.17 *Entire stride angle pattern of the fetlock joint during different degrees of forelimb lameness. A. affected B. contralateral sound. Modified from [105]*

To date fetlock joint angle and fetlock joint range of motion in normal and lame horses has been quantified using variety of methods that are resumed in table n 4.

Parameter	Method	Purpose	Treadmill/overground	Reference
Fetlock joint angle-time	OMC (2d kinematics	Descriptive (sound horses)	treadmill	[17,106]
Fetlock angle extension	OMC (2d kinematics)	Lameness (induced)	treadmill	[103]
Maximal angle of fetlock (extension)	OMC (2d kinematics)	Lameness (induced)	20 mt runway over force plate	[31]
Maximal angle of fetlock (extension)-time of maximum fetlock joint extension	OMC (2d kinematics)	Lameness (induced)	treadmill	[107]
Min-max fetlock joint extension	OMC (2d kinematics)	Lameness (natural occurring)	treadmill	[76]
Angle at impact-max extension-max flexion-range of movement	OMC (2d kinematics)	Gait quality Sound horses	treadmill	[102]
Angle of flexion and extension of the fetlock	OMC (2d kinematics)	Gait quality sound horses	runway	[108]
Fetlock joint angle pattern	OMC (2d kinematics)	Descriptive Variability of fetlock joint	rubber runway	[98]

		angle patterns in sound horses		
Fetlock range of motion	OMC	Lameness (induced)	treadmill	[109]
Angle of fetlock at mid stance-negative angular velocity-positive angular velocity	OMC (2d kinematics)	Descriptive in galloping horses with different ages	overground	[110]
Maximum fetlock joint angle extension-occurrence time of max fetlock joint extension	OMC (2-d kinematics)	Evaluation of supporting boots on fetlock	treadmill	[111]
Fetlock joint angle at contact-fetlock joint angle a toe off-min and max joint excursion	OMC (2d kinematics)	Descriptive effects of fatigue on loading in Standardbreds	treadmill	[112]
Fetlock joint angle in time (entire stride)	OMC (2-d kinematics)	Descriptive Effects of raised heels on joint angles	treadmill	[113]
Flexion/extension-adduction/abduction-internal-external rotation	OMC (3d kinematics)	Descriptive (sound horses)	Rubberized runaway Bone fixed markers	[97]
Maximum fetlock extension angle	Biplanar video-radiography (3d kinematics)	Descriptive (limb support)	Flat track way	[96]

Maximal extension-% stride at maximal extension-maximal flexion-% stride at maximal flexion-ROM	OMC (2d Kinematics)	Descriptive during swimming (sound horses)	Straight Swimming pool	[114]

Table 4.

4.2 Specific Aims

To the authors' knowledge, there are no reported data investigating FJA and FJROM using IMUs in horses. As Limb movement and joint angle patterns are important indicator of both physiologic locomotor capacity [102] and disturbance due to lameness [76,76], detection of FJA and FJROM could furnish objective quantification of temporal gaits event (hoof on/off stride-swing-stance duration) and a preliminary step to the development of an on-board tool for the detection of degradation of horse locomotion trough left and right coefficient of asymmetry between FJA of the legs.

The advantages of quantify those parameters with IMU's system would be the portability that could enable the use at various gait, speed, conditions.

Objective quantification of fetlock of fetlock joint angle (FJA), fetlock joint ROM (FJROM) and stride associated temporal parameters (duration of stance and swing) could be applied for:

- asymmetry index for lameness detection

- gait quality and training judgments

-efficacy of rehabilitation modalities

-influence of support tools on fetlock angle

-assessment of range of motion for joint functional mobility and treatment progression

The first aim of this thesis was to prove the feasibility of IMU in detecting sagittal range of motion of the fetlock joint and validate the quantification in sound horses using a comparison with OMC and values present in the current literature. The hypotheses of this study are:

1. the placement of IMU sensors over the metacarpal/phalangeal joint would be feasible and well accepted by the horse
2. the Imu system under investigation could successfully record relative fetlock joint angle during walk and trot in sound horses. Amplitude and shape of the recorded curves would be comparable to curves already present in literature obtained with other systems in sound horses

3. There will be an agreement between curves obtained with IMU system under investigation and a 2-D optical motion capture system in horses sound and affected by natural occurring lameness
4. The shape and the amplitudes of curves detected with the IMU system will reflect variability related to lameness

4.3 Materials and Methods

4.3.1.Study design

In this prospective observational study, fourteen horses were subsequentially enrolled with a 1:1 ratio between groups (sound vs. lame horses). Enrollment started in January 2021 and ended in November 2021. The sound horses were recruited from a jumping training center affiliated with our institution. The lame horses were recruited among cases referred to the Equine Clinical Service at the Veterinary Teaching Hospital of University of Turin. A written informed consent was obtained by all owners of the horses. The ethical approval of the study protocol was obtained by local competent committee (protocol n. 2796/2020; approval date 15/12/2020).

Horses were assigned to the sound group after subjective assessment by two experienced clinicians (ACVSMR diplomates) and consensual agreement on the absence of lameness or any relevant gait alterations secondary to neurological or non-orthopedic disorders. To be included in the sound group, horses had to be in training and free of orthopedic disease for at least 2 years. We deliberately chose sound horses with similar physical conformation (withers heigh-weight) to reduce variability in FJA [98] . The sound horses were all Warmbloods (3 mares and 4 geldings), all used for show jumping, aged 10.8±3.5 years (mean± SD; range: 7-18 years). Their weight was 509±45 kg (range: 450–580 kg) and withers height 163±9 cm (range: 153–175 cm). All sound subjects were trained regularly at the time of the study and were shoed. Signalment details of the horses included in the sound group are resumed in table n 5.

Horse code	Age		weight		heigh
S01	7		450		1.53
S02	18		580		1.75
S03	11		527		1.65
S04	11		550		1.54
S05	11		484		1.67
S08	9		485		1.57
S09	9		489		1.71

Table 5.

As no other objective lameness detection system was used for comparison, lame horses were included in the study if they presented a moderate to severe single limb lameness ranging from grade 3 to 4 based on AAEP scale scoring system [115] due to an orthopedic disease. The diagnosis in each horse was confirmed based on a combination of a subjective examination of lameness, results of intra-articular or perineural nerve blocks, and diagnostic imaging. Lame horses were of different breeds. They were 4 mares and 3 geldings, 2 used for leisure activity, 2 for breeding purposes, and 3 for show jumping. Their mean age was 12.3±6.6 years (range: 4-23 years), weight 514±70.91 kg (range: 410-600 kg) and height at the withers 158±10 cm (range: 145-175 cm). All horses studied were shoed at the time of the test. Characteristics of the 7 lame horses are resumed in table 6.

Horse code	Age (y)	Breed	Sex	Lameness degree	Lame limb	Diagnosis
Z01	8	TB	M	4/5	RF	Fetlock joint OA
Z02	4	ST	M	4/5	LF	Scapulo-humeral OA
Z03	23	Criollo	G	3/5	RH	SDFT tendonitis
Z05	17	WB	M	3/5	RH	Proximal interphalangeal joint OA
Z06	7	WB	G	3/5	LH	Centrotarsal joint OA

Z07	15	Pony	G	3/5	RH	Medial femoro-tibial joint OA
Z08	12	IS	M	3/5	RF	DDFT tendonitis and NV

Table 6.

Each horse enrolled in the study underwent a standardized locomotion test during which FJAP were simultaneously evaluated in all 4 limbs with the two-system tested (IMU and OMC) at walk and trot as detailed below.

4.3.2 Positioning on the horse of IMU system and OMC technology

Relative orientation data from IMU yielded information on the dorsal fetlock joint angles by tracking movements of the pastern relative to the metacarpus or metatarsus. The elastic bands were fixed around each distal metacarpal/metatarsal bone and pastern, with the sensor positioned on the dorsal aspect of the limb (Fig.18). Conventionally, FJA were set at 0° during calibration. Thus, positive and negative sagittal FJA indicate flexion and extension of the joint, respectively, compared to the initial calibration point (Fig.19). Sampling rate was set to 200 Hz and internal memory storage.

Three flat circular retroreflective markers (40 mm diameter) per limb were glued on the lateral aspect of the center of rotation of each joint (Fig. 18), precisely:

-carpus/tarsus landmark: head of the IV° metatarsal/metacarpal bone

-fetlock landmark: distal condyle of metacarpus/metatarsus over lateral collateral ligament

-distal interphalangeal joint landmark: lateral collateral ligament of the distal interphalangeal joint at the level of the coronary band of the hoof.

As the movement of the proximal interphalangeal joint is very narrow, P1 and P2 were considered as a unique segment.

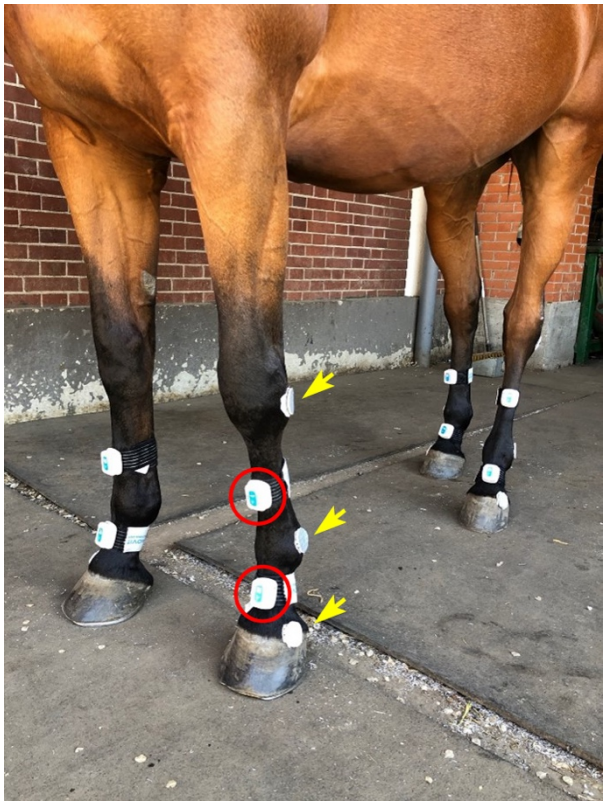

***Fig 18**. Placement of IMUs (red circle, identified only in one limb) and optical markers (yellow arrows, OMC technology) on equine distal limbs for data acquisition. The IMUs were fixed to the dorsal metacarpus/metatarsus and to the dorsal aspect of the pastern in the four limbs by means of plastic docking bases attached to elastic bands. Optical markers were glued to the skin on the lateral aspect of the joints studied.*

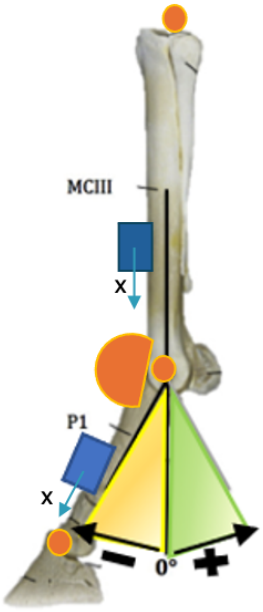

***Fig 19.** Schematic representation of the positioning and the fetlock angles measurments by the two systems. OMC-three markers (orange): Fetlock joint angles expressed as the dorsal angle of the pastern axis relative to the vertical (0°) angle of the metacarpus/metatarsus axis. IMU-two (blue): negative angle values express extension of the fetlock joint (yellow area); positive angle values express flexion of the joint (green area)*

Optical data were obtained in a standardized environment (testing area). A digital camera[d] (full HD-camera resolution 1920 width*1080 height) with a recording time resolution of 60 Hz was used, placed at a distance of approximately 8 m from the center of the testing area through its transverse axis. The position of the camera was chosen to include the whole testing area (10 m long) within a single field of view. This was based on what is currently considered the minimal data requirement for equine gait analysis, corresponding to three complete and consecutive strides [83]. More in detail, as the average speed of the horse during trot is 3 m/s and average stride length is 250 cm [116], we calculated the distance required for capturing a minimum of 3 strides at trot at constant speed and we choose 10 m as the optimal length of our testing area. The objective of the camera was positioned perpendicular to the long axis of the testing area.

4.3.3 Locomotion test

For the standardized locomotion test performed, horses were first walked and then trotted (if allowed by their pathological condition) forth and back led in hand, with the animal's handler at the opposite side of the camera (Fig.20). The standardized locomotion test was performed on a firm surface (concrete). The surface was the same for all the trials, defined testing area, consisting in a 10 x 2 m rectangle within a dedicated trotting-up area (Fig.20). Horses walked or trotted in line starting approximately 8 m before the testing area at both sides to obtain a constant speed and maintained throughout the test.

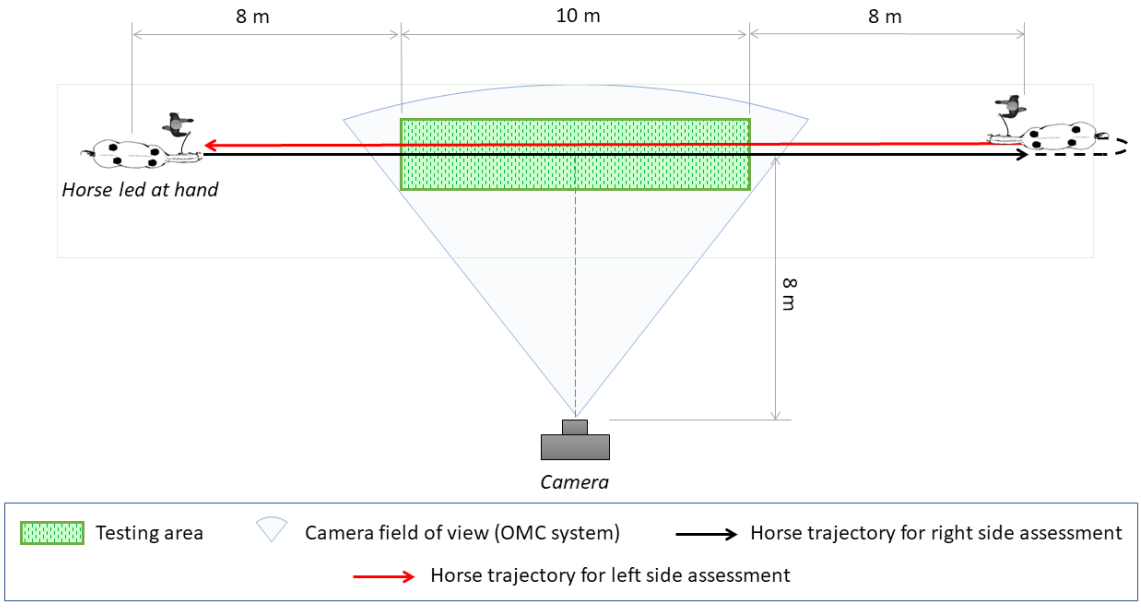

Fig 20. *Schematic representation of the set up used for the standardized locomotion test performed*

4.3.4 Data acquisition

Data acquisition with the IMUs was started manually before the horse entered into the testing area and was stopped manually when the horse exits the area.

Videorecording was focused on the pair of limbs on the side of the camera (right fore [RF] and right hind [RH] while walking and trotting forth, and left fore [LF] and left hind [LH] while walking and trotting back), and lasted as long as possible from the moment the horse entered in the field of view of the camera (testing area) to when it went out. A trial was rejected if the horse was judged by the observer as moving inconsistently or not freely within the testing area.

Video recordings were digitized with a dedicated software for gait analysis[e]. Testing area was calibrated in the 2 dimensions by using a reference stake. The fetlock joint angles of all limbs were computed at 60 Hz from reflective marker trajectories (Fig.21), by means of a dedicated software tool, and exported in an excel file. Fetlock joint angles were expressed as the dorsal angle of the pastern axis relative to the vertical (0°) angle of the metacarpus/metatarsus axis. In this way, fetlock extension produced a decrease in FJA while fetlock flexion produced an increase in FJA, and patterns were more easily comparable to those obtained with IMU system.

Both OMC and IMU systems generated Excel files (one per limb per test) with FJA measurements in time.

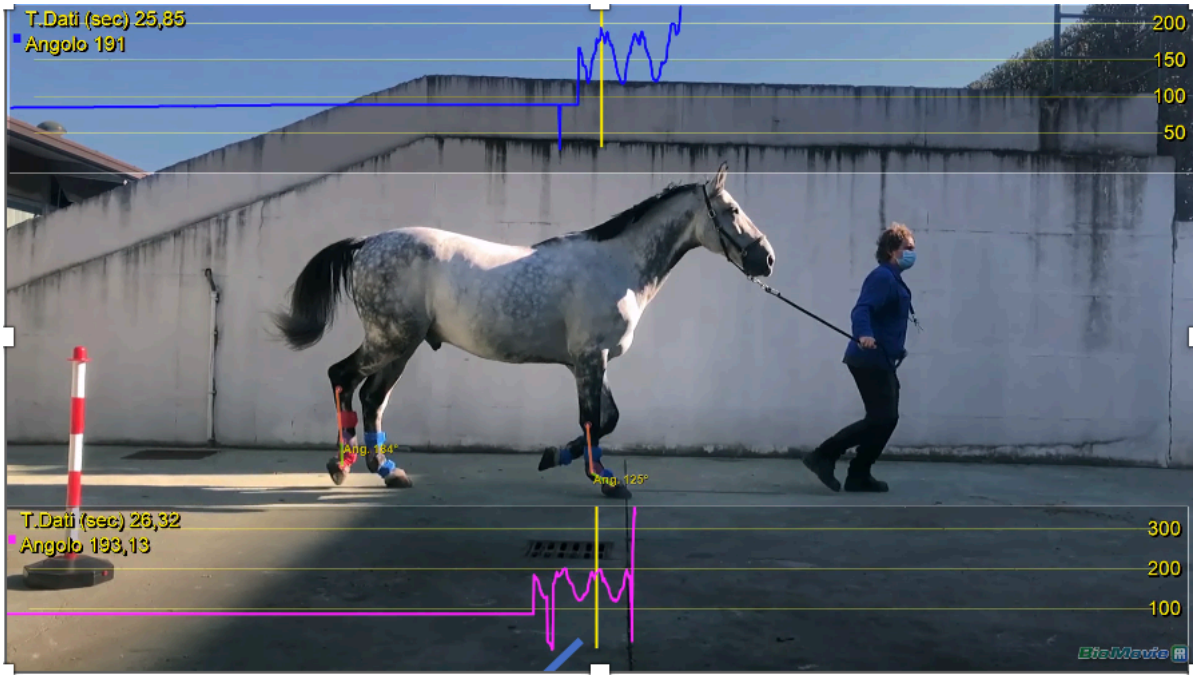

Fig 21. Reflective markers trajectories of the fetlock joint and angle values on RF and RH at trot of horse S01.

4.3.5 Data processing

Fetlock joint angles data derived from the two systems were imported in MATLAB[f]. A custom-written specific script was designed to compare FJAP (Suppl. Mat. 1). Briefly, resampling of the video signal (from 60 to 200 Hz) was performed using MATLAB's spline interpolation function in order to have both data at 200 Hz. Both signals were low-pass filtered with a 4-order Butterworth filter with a cutoff frequency of 10 Hz. The data obtained from the two systems were synchronized at the point of absolute minimum between the first two maxima of the two signals. Absolute FJAP obtained with the two systems were also aligned on the y axis (°) by subtracting the difference of the two patterns calculated at the synchronization point.

Stride segmentation and detection of toe-on and toe-off events was performed based on peak detection of the resultant angular velocity data recorded from the gyroscope in the IMU sensor mounted on the pastern on the light of the results of the work of Briggs and Mazzà [88] (Fig.22) .

After stride segmentation, the fetlock joint range of motion (FJROM) was computed from IMU system data as the difference between the maximal and minimal FJA recorded within the same stride (Fig 22). Mathematically, this was calculated as:

$$FJROM_{stride} = \text{absolute value } [\max(FJA_{stride}) - \min(FJA_{stride})]$$

FJROM was calculated as mean of ROM of three strides for every limb.

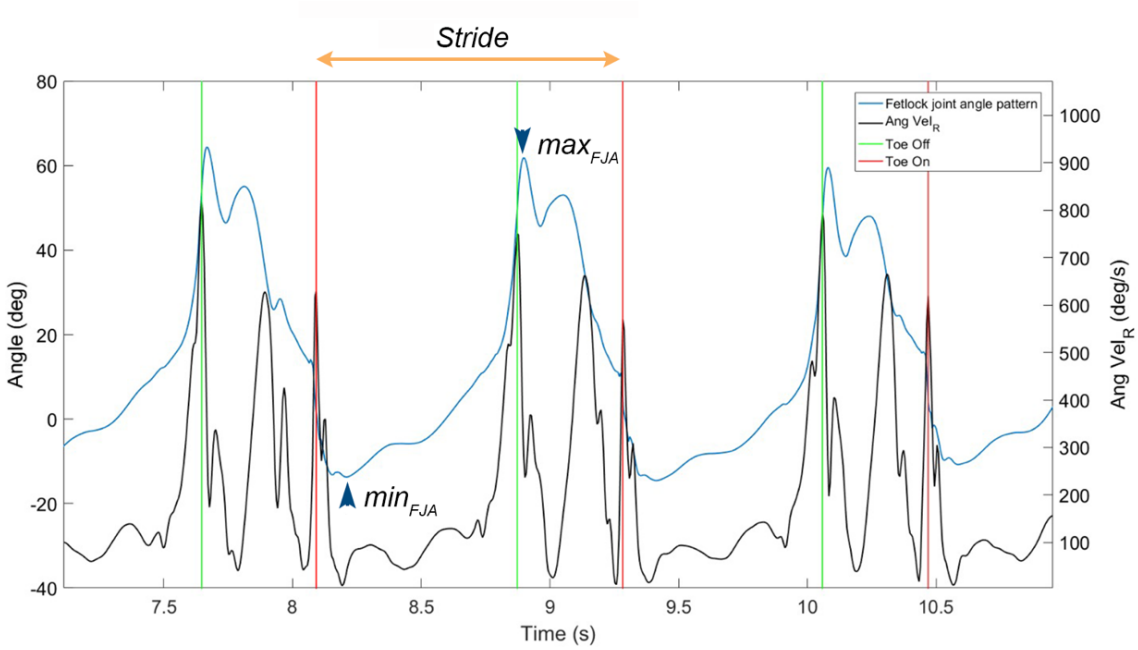

Fig 22. Results of stride segmentation by means of the gyroscope signal quantified at the pastern and identification of minimal and maximal FJA during the stride used for calculation of fetlock joint range of motion (FJROM). Data from a lame horse at walk on asphalt. Ang vel$_R$: resultant angular veolcty; min$_{FJA}$: minimal FJA within the stride; max$_{FJA}$: maximal FJA within the stride.

4.3.6 Statistical analysis

Pearson correlation coefficient (PCC) and root mean square error (RMSE) between the FJA detected with the two systems under investigation at each time point (200 Hz) were calculated using the MATLAB corrcoef function (PCC) and the following formula (RMSE) for each fetlock joint studied (RF-RH-LF-LH) and for each gait (walk-trot):

$$RMSE = \sqrt{\frac{\sum_{i=1}^{n}(x_i - y_i)^2}{n}}$$

PCC was used to measure the strength of the linear relationship between the two patterns and RMSE (°) to measure the difference between FJA values detected with IMUs and OMC for each joint at each gait. The mean values of PCC, RMSE, and their standard deviation were calculated at walk and trot in sound and lame horses using Microsoft Excel[9].

To calculate the agreement between the two systems, Bland-Altman analyses were run separately on data of single FJA values (200 FJA/second) and FJROM (mean of valued calculated from 3 strides) measured by the two systems, accounting for repeated measures [25]. Data obtained at walk and trot were analyzed separately. The Granger causality test (α = 0.01) was also computed to predict temporal agreement between IMUs patterns and 2-D OMC patterns in sound and lame horses.

The coefficient of variation, calculated as

(CV [%] =sd/mean* 100) of the FJROM

detected by IMU between right and left forelimbs and between right and left hindlimbs were calculated for all animals enrolled in the studied over 3 consecutive strides, for each considered gait (walk and trot). In lame horses, only the lame limb and its contralateral were studied to this aim.

The effect of gait (walk/trot), lameness (sound/lame), and pair of limbs (front-hind) on CVs was assessed by means of a three-way ANOVA (α = 0.05) after verifying normal distribution of the data with Shapiro-Wilk normality test. The model did not consider the horse as a clustering or independent variable.

4.4 RESULTS

The horses did not show any sign of stress or discomfort due to the presence of IMUs fixed to their distal limbs and were judged to move freely after a brief initial adaptation period. The average walking speed was 1.53±0.19 and 1.51±0.35 m/s in sound and lame horses, respectively. The average trotting speed was 3.56 ± 0.78 and 3.92 ± 0.85 m/s in sound and lame horses, respectively. Horse z1 was not tested at trot because too lame to trot at constant velocity. Detailed velocity for each horse at the two gaits is shown in table n 7.

sound	Walk (m/s)	Trot (m/s)
S01	1.79	4.21
S02	1.48	3.22
S03	1.32	2.93
S04	1.41	2.77
S05	1.76	4.37
S08	1.37	4.53
S09	1.55	2.89
lame	Walk (m/s)	Trot (m/s)
Z01	1.11	X
Z02	1.68	4.46
Z03	1.95	2.6
Z05	1.32	4.22
Z06	1.37	4.55
Z07	1.17	3.11
Z08	1.95	4.58

Table.7

4.4.1 FJA curves generated by MOVIT IMU system

Median values (tab. 8), shape and amplitude (fig.23) of sagittal FJA in the population of sound horses quantified by IMUs were comparable with previous studies on sagittal plane kinematics at walk and trot obtained with OMC.

range of motion ° flex/ext	stride		stance		swing	
	walk	trot	walk	trot	walk	trot
IMU Captiks	57.69	82.83	27.42	45.74	40.62	47.12
SD	4.50	6.64	2.58	3.30	3.66	2.67
Clayton et al. [97]	62	77	31	42	38	47
SD	7	5	3	10	7	5

Tab.8

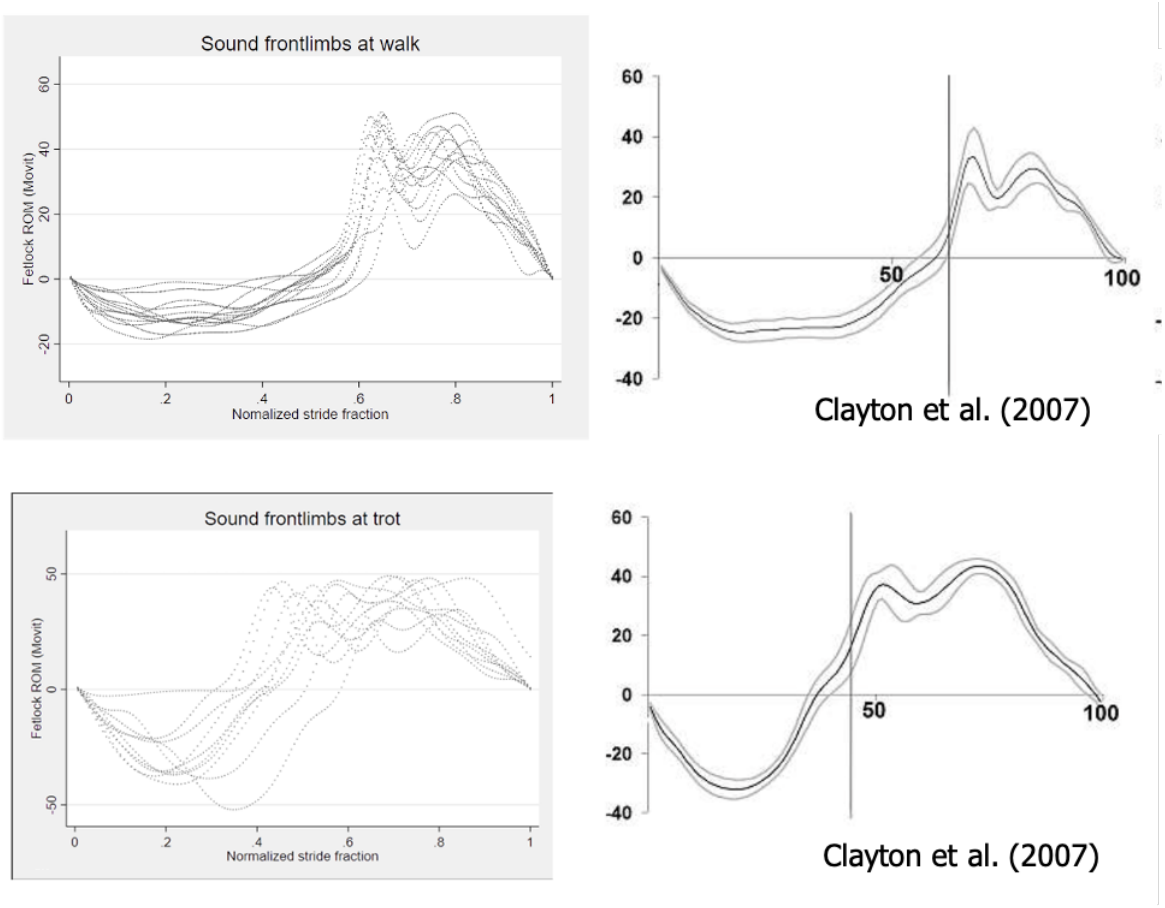

Fig 23. Comparison of shape and amplitude of fetlock joint angle curve detected with IMUs of sound horses in this study and fetlock joint angle curve detected with 3-D OMC on sound horses in the work of Clayton [97]

In sound horses, the pattern describing sagittal FJA at walk showed a symmetric double peak of flexion and two extension peaks (Fig. 24 panel a- b). At trot, the curve was characterized by a symmetric double peak of flexion and a single peak of extension for each stride (Fig. 24 panel c-d). The shape and the amplitude of FJA curves were similar between pairs of limbs (left vs right forelimbs and left vs right hindlimbs; fig.24).

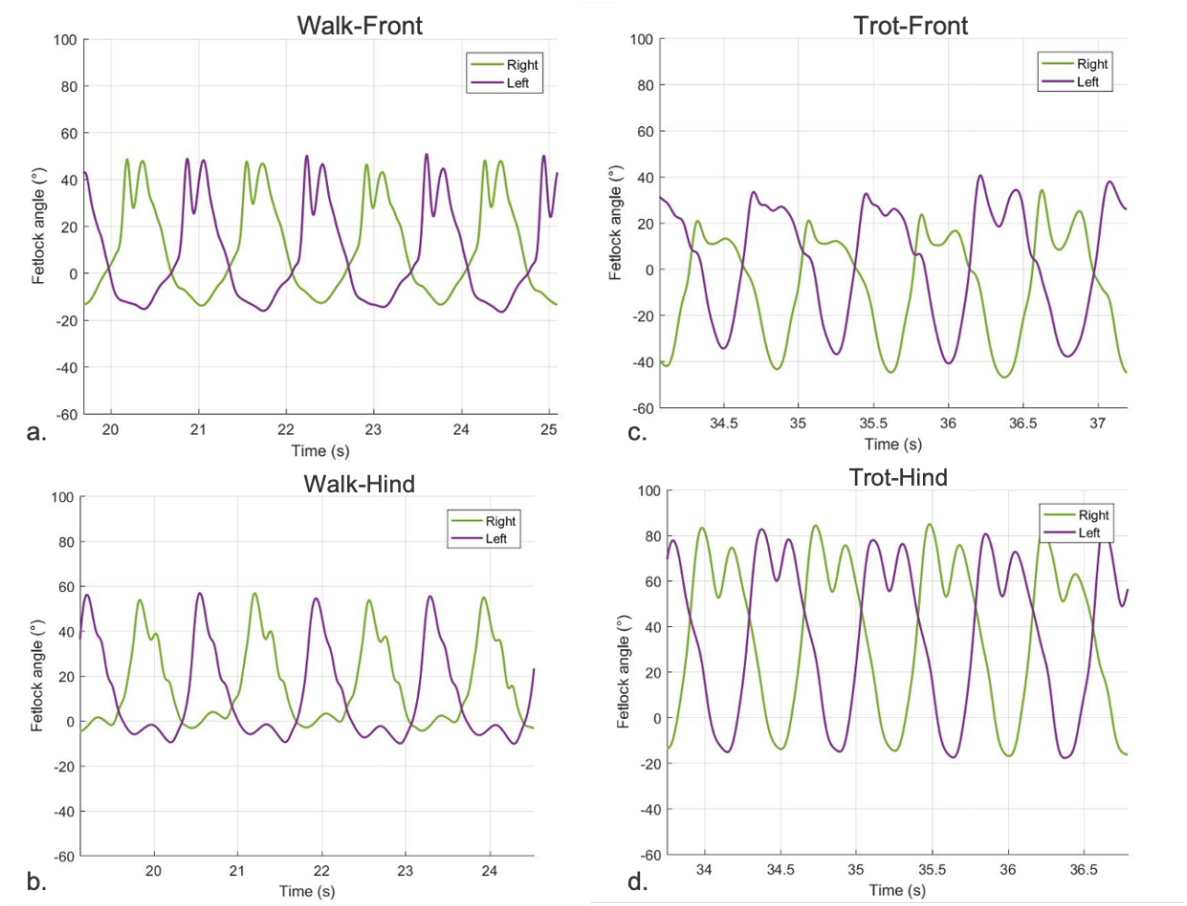

Fig 24. Fetlock joint angle pattern quantified by the MOVIT IMU system in a sound horse over time. Positive values of angles (°) represent flexion and negative values extension of the fetlock joint. a. left front (violet-mean 57.84°) and right front (green-mean 56.72°) at walk.; b. left hind (violet-mean 67.01°) and right hind (green-mean 63.55°) at walk; c. left front (violet-mean 78.92°) and right front (green-mean 78.05°) at trot d. left hind (violet-mean 94.14°) and right hind (green-mean 92.03°) at trot.

In lame horses, the curves describing FJA at walk and trot in the lame limb were characterized by an asymmetric pair-to-pair double peak of flexion for each stride and an asymmetric pair-to-pair single peak of extension at each stride at the trot. The shape and the amplitude of the patterns were different between the lame limb and its contra-lateral, with the lame limb showing a constant decrease in amplitude resulting in a smaller ROM compared to the contra-lateral. This pattern was similar either at walk (fig.25 panel a-b) or trot (fig. 25 panel c-d).

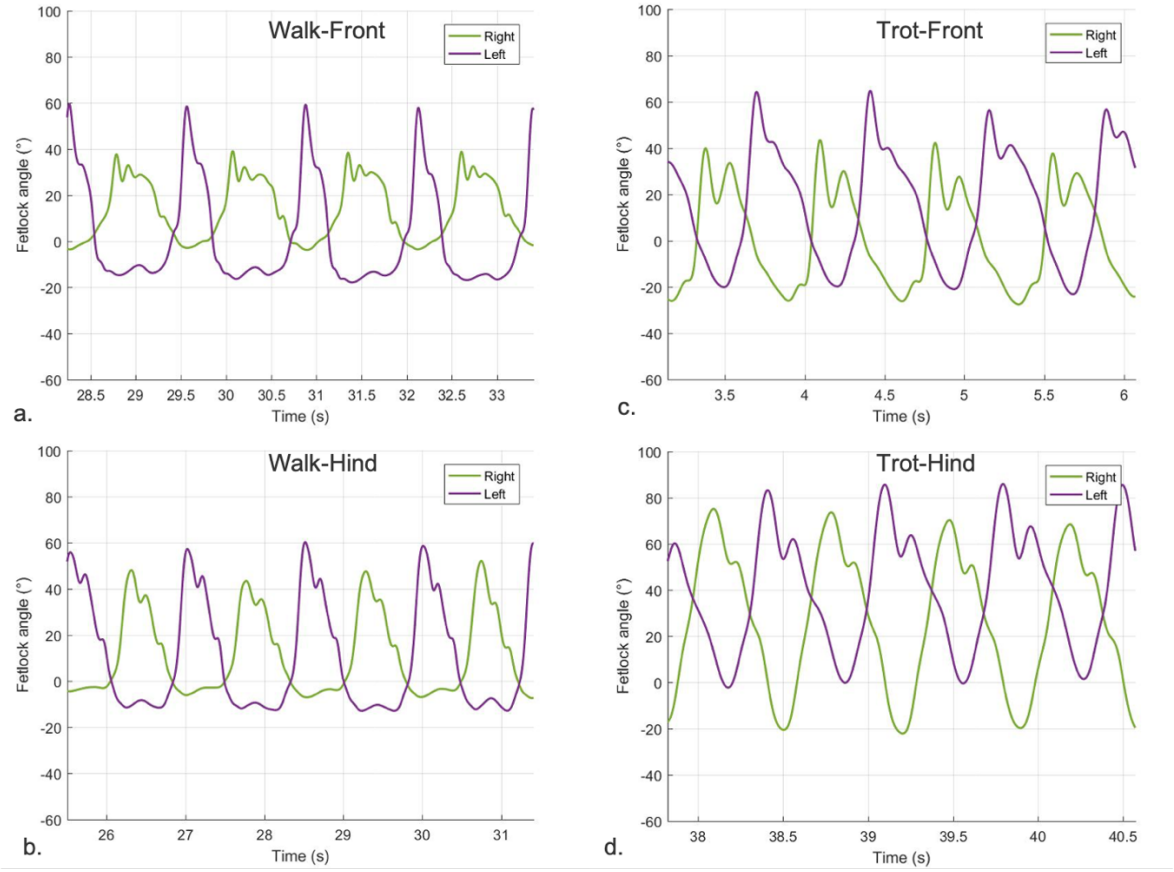

Fig 25. Panels show fetlock joint angle pattern quantified by the MOVIT IMU system in the lame limb and its contra-lateral over time in 4 different horses. Positive values of angles (°) represent flexion and negative values extension of the fetlock joint a. horse z01- right front lame (green-mean 44.22°) and left front contralateral (violet-mean 75.60°) at the walk; b. horse z05-right hind lame (green-mean 52.88°) and left hind contralateral (violet-mean 70.38°) at walk; c. horse z08-right front lame (green-mean 87.98°) and left front contralateral (violet-mean 98.69°) at trot d. horse z06-left hind lame (violet-mean 73.35°) and right hind contralateral (green-mean ROM 94.34°) at trot.

In sound horses, the mean FJROM value in front-limbs captured by the MOVIT IMU system was 57.79° ± 4.50° at walk and 82.83° ± 6.64° at trot. The mean FJROM in hind-limbs at walk was 60.48°± 6.10°, and 89.40°±4.89° at trot. The FJROM coefficient of variation (CV) between pairs of front limbs (left vs right) was 3% at the walk and 2.51% at the trot. The CV between paired hind limbs (left vs right) was 3.91% at the walk and 3.60% at the trot. The mean degree of difference in FJROM between paired front limbs was 1.76° at walk and 0.57° at trot, and between hind limbs was 0.86° at walk and 1.58° at trot.

In lame horses, the CV of FJROM between the lame limb and the contralateral was 15.47% at the walk and 7.06% at the trot. The mean degree of difference in the FJROM between the lame limb and contralateral was 19.84° in lame at the walk and 8.44° when considering all lame horses at two gaits.

4.4.2 Determinants of FJROM variability in IMU system-acquired data

The CVs of FJROM of consecutive strides (up to three) of the same limb were consistently <5%, irrespective of gait, front vs. hindlimbs, and the presence of lame-ness. The CV between right and left FJROM was significantly affected by lameness ($p<0.0001$), gait ($p=0.0029$), and front vs hindlimbs ($p=0.0233$). Left to right CV FJROM differences in lame and sound horses are shown in figure 26.

The presence of lameness per se, as most significant, accounted for 28.46% of total variation to explain the left to right FJROM difference. The gait accounted for 10.44%, whereas the presence of front vs hind limb lameness accounted for only 5.7% of the total variation.

Fig 26. Effect of lameness, gait, and front vs hindlimbs on CV between left and right limb of the horses in the study.

4.4.3 Agreement between IMU system and 2-D OMC technology

In sound horses, RMSE between the two methods was 7.77 °± 3.42° at walk and 8.06°± 2.99° at trot, while PCC was 0.96 ± 0.03 ($p<0.001$) at walk and 0.97 ± 0.02 ($p<0.001$) at trot.

WALK		TROT	
RMSE SOUND	PCC SOUND	RMSE SOUND	PCC SOUND
7.38	0.97	5.84	0.98
9.67	0.94	14.83	0.96
8.02	0.94	12.47	0.89
7.38	0.97	8.41	0.96
9.24	0.98	10.87	0.98
4.27	0.98	15.12	0.99
4.40	0.98	4.38	0.98
6.71	0.98	8.12	0.97
8.40	0.94	12.13	0.96
9.75	0.94	5.52	0.98
3.42	0.99	5.86	0.99
6.05	0.97	7.42	0.99
16.55	0.98	6.34	0.97
12.64	0.92	6.22	0.98
8.70	0.93	9.31	0.95
5.20	0.97	6.82	0.98
10.78	0.88	7.01	0.98
6.23	0.97	4.25	0.99
8.32	0.90	8.05	0.93
7.097	0.96	10.31	0.95
4.90	0.99	5.33	0.98
4.85	0.98	6.58	0.98
17.40	0.95	5.24	0.98
9.12	0.94	4.83	0.99
5.85	0.96	7.84	0.97
5.01	0.97	7.47	0.97
6.17	0.98	7.47	0.98
4.04	0.98	11.50	0.95

Table 9.

In lame horses, RMSE between the two systems was 8.68° ± 4.03 at walk and 10.06° ± 4.39 at trot, while PCC was 0.95 ± 0.04 ($p<0.001$) at walk and 0.96±0.03 ($p<0.001$) at trot.

WALK		TROT	
RMSE LAME	PCC LAME	RMSE LAME	PCC LAME
4.79	0.98	5.90	0.96
3.36	0.99	8.97	0.97
3.81	0.98	12.38	0.99
5.94	0.97	9.84	0.96
4.70	0.95	19.20	0.87
10.00	0.92	19.67	0.95
8.95	0.88	14.68	0.95
8.85	0.95	8.21	0.98
13.98	0.89	7.75	0.97
8.00	0.97	13.50	0.91
18.56	0.91	8.33	0.97
18.58	0.95	10.94	0.96
6.46	0.97	10.74	0.95
4.20	0.99	21.82	0.95
12.84	0.82	7.18	0.96
8.37	0.94	7.68	0.98
6.95	0.94	7.66	0.97
9.15	0.96	12.67	0.94
4.44	0.96	13.96	0.93
15.01	0.96	7.44	0.98
9.43	0.92	7.53	0.96
7.18	0.95	8.66	0.98
7.88	0.92	13.94	0.93
9.02	0.96	6.70	0.99
5.93	0.98		
7.08	0.99		
11.04	0.96		
8.66	0.96		

Tab.10

In sound horses, according to the Granger causality test, the pattern of the two systems studied was in temporal agreement in 54/56 cases at walk (94.7%) and in 55/56 cases at trot ($p<0.01$) (fig. 27 a, 27 c).

According to the Granger causality test, the pattern of the two systems studied was in temporal agreement in 55/56 cases at both walk and trot ($p<0.01$) in lame horses (fig. 27 b, 27 d).

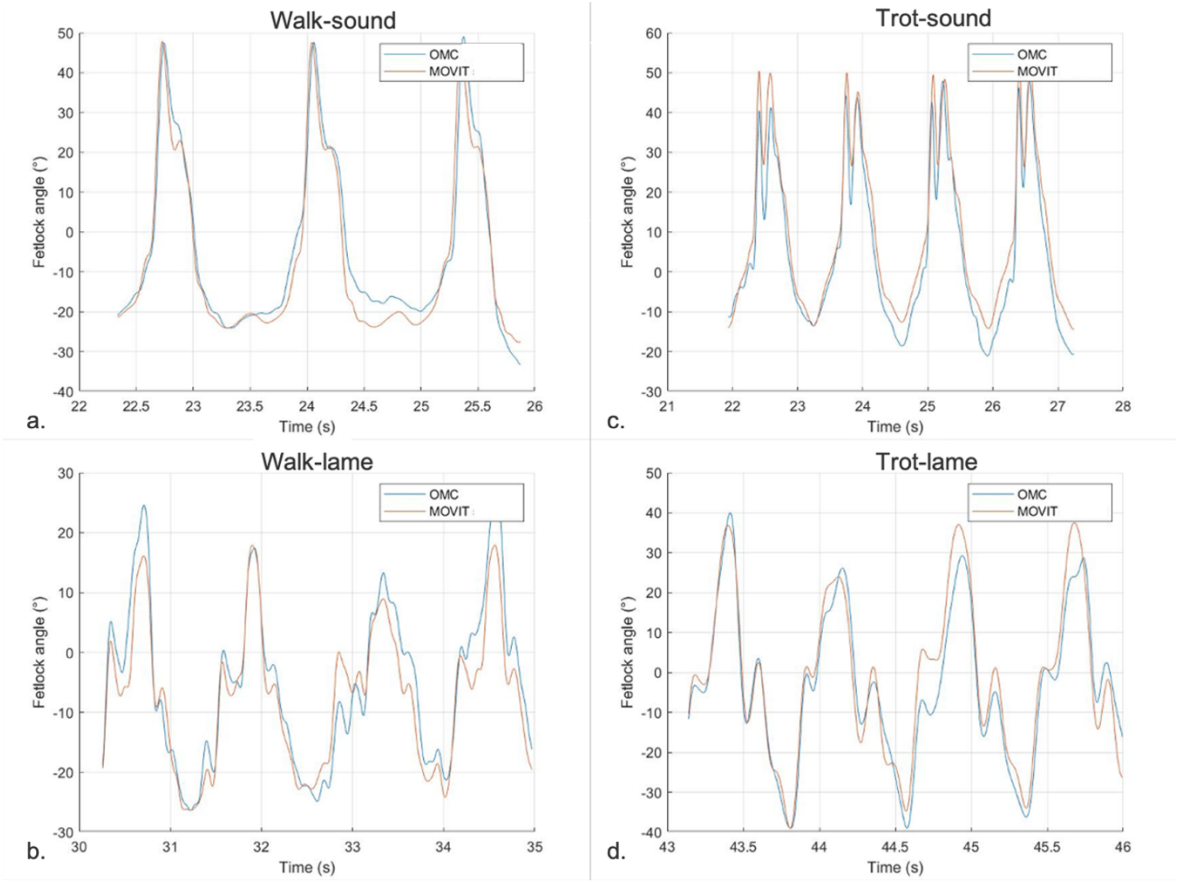

Fig 27. Pattern of FJA over time measured by the MOVIT IMU system (MOVIT-orange) and the 2-D OMC (OMC-blue) in four selected cases. a. Left hind at walk in a sound horse (RMSE=7.09°- PCC=0.96). b. Left front at walk in a lame horse (z2-RMSE=4.69°- PCC=0.95). c. Right front at trot in a sound horse (RMSE=7.47°- PCC=0.97). d. Left front at trot in a lame horse (z2-RMSE=5.91°- PCC=0.96).

According to Bland-Altman analyses, the MOVIT IMU system and the 2-D OMC measurements quantifying FJA in both lame and sound horses agreed at both walk (mean difference= -0.09; limits of agreement = -15.60,15.41) and trot (mean difference = 0.31; limits of agreement = -20.58,21.21). The agreement of FJROM assessed with Bland-Altman analysis revealed a reduction of mean bias between the two systems tested at both walk (mean difference= -1.96; limits of agreement= -14.26, 10.34) and trot (mean difference= -1.19; limits of agreement= -16.45, 14.08), as shown in figure 28.

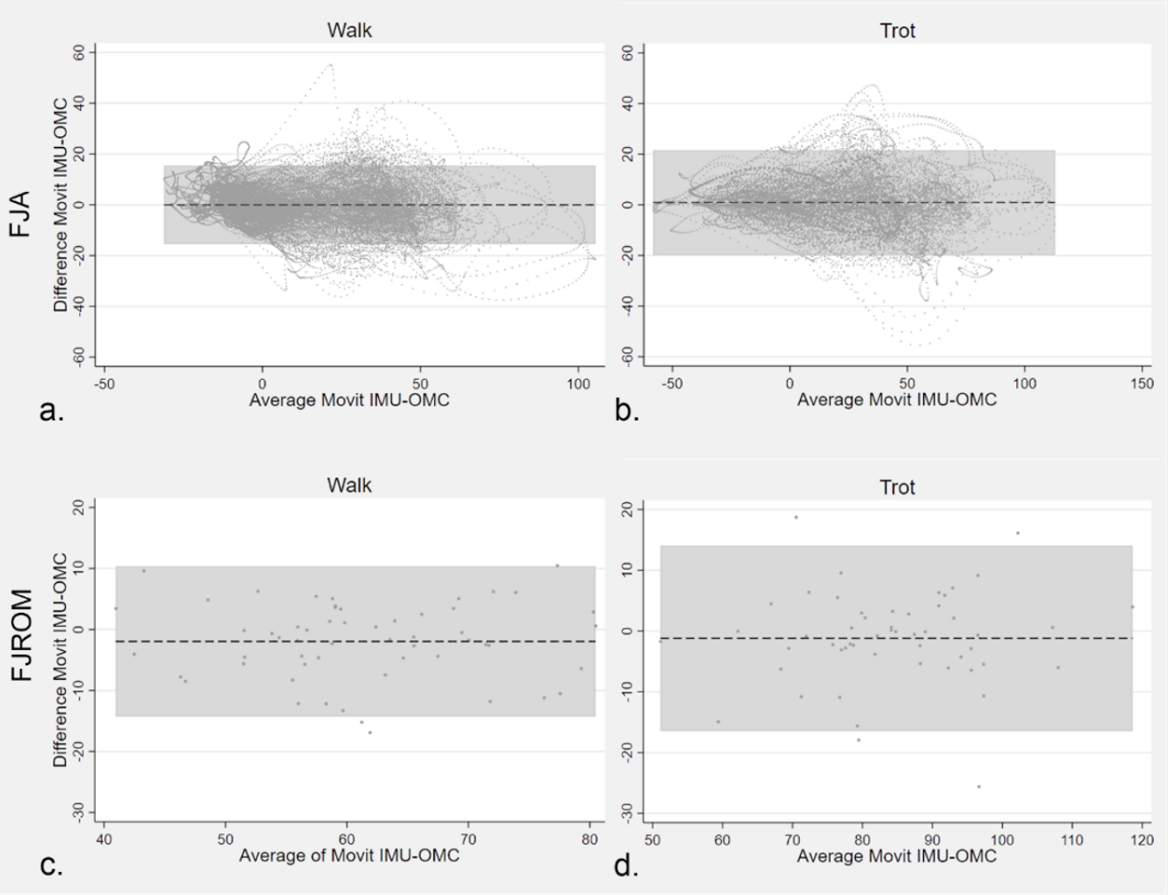

Fig 28. *Bland-Altman plots indicating agreement between MOVIT IMU system and 2-D OMC concerning FJA (panels a and b) sampled at 200 HZ and derived FJROM (panels c and d). Data were obtained at walk (panels a and c, respectively with n=389377 and n=14) and at trot (panels b and d, respectively with n=16333 and n=13). Dashed horizontal lines show the mean differences between measures taken with the IMU and OMC technology. The grey areas indicate a 95% CI of the differences*

4.5 Discussion

The aim of this research was to describe, for the first time, equine FJA curves quantified by the MOVIT IMUs system in field conditions at the walk and trot. Curves were obtained from sound horses and from horses with naturally occurring lameness localized to a single limb. The curves obtained with the MOVIT IMU system were also compared with those obtained with a 2-D OMC technology. Shape and amplitude of the curves obtained with the two systems agreed and were comparable.

Afterward, the study demonstrated that the variability of fetlock joint range of motion registered with IMUs in lame horses moving in a straight line was mainly related to the presence of lameness.

4.5.1 Equine FJA curves in sound and lame horses

Horses with induced forelimb lameness showed altered fetlock joint extension patterns compared to sound horses, detectable at walk and trot [31,103,107]. Sound horses show a similar degree of fetlock extension in lateral pairs of limbs (right and left forelimbs or hindlimbs). In lame horses, fetlock extension is reduced in the lame limb while increased in the contralateral limb [103]. Of note, all available work concerning the effect of lameness on fetlock extension and, more broadly, on FJA, employed experimentally induced forelimb lameness models, in the absence of validation in spontaneously occurring lameness. Our data confirm that the shape and amplitude of FJA patterns differ in sound and natural occurring lame horses, irrespectively of the anatomical localization of the lameness.

In sound horses, FJROM variability calculated over 3 strides of the same limb was approximatively 3% at both walk and trot for both front and hindlimbs, in line with the work of Degueurce [98]. Considering that absolute gait symmetry is unnatural and that some horses are characterized by natural gait laterality [117], we considered 3% as very low. Although maximal joint extension and flexion were repeatable between strides of the same animal for the same limb, the observed FJA pattern in the lame limb was asymmetric compared to the contralateral sound limb in our study. The variability of FJORM was higher in lame (11%) compared to sound horses (3%), and at walk (15%) compared to trot (7%). The almost halved variability at trot in the group of lame horses could be a spurious result but was considered mainly linked to the fact that the FJROM is grater at trot compared to

walk and symmetry and regularity increase with velocity [118]. FJROM variability at trot was higher in the lame group compared to the sound (7%- 3%) but, although not standardized in our study, average velocity at trot was similar in both groups. So, as velocity could have accounted for the same variability between the groups, the difference in FJROM variability between lame and contra-lateral limb could be considered relevant.
In our study, the inclusion criteria were only based on the severity of lameness, so animals of different breeds were inserted in the lame group. This could have played a consistent role in the variability of kinematic parameters due to different motion patterns in the fetlock joints in terms of animation of the movement and elasticity between animals. However, it has been demonstrated that the effect of height at the withers is minimal when considering angular parameters and does not affect temporal parameters of the stride [119]. In the work of Ishihara et al. [28], a larger coefficient of variation for kinematics variables and larger variation from the optimal motion pattern have been present in horses showing more severe lameness, reflecting the findings of our study where horses with severe lameness were included.

4.5.2 Agreement between the systems studied

The precision of the MOVIT IMU system in detecting FJA in sound and lame horses was considered good, as according to Cuesta et al. [120], RMSE between the two methods ranged between 5° to 10° at both walk and trot in lame and sound horses (mean RMSE =8.83°). According to Poitras et al.[121], the values of PCC showed an excellent correlation between the IMU system and 2-D OMC as it was ranging over 0.9 at two gaits and in the two groups (mean PCC=0.95).
Based on the Bland-Altman analysis, the mean bias between the two systems under study was negligible, when both FJA and FJROM were used as input data. Limits of agreement were narrower for FJROM compared to FJA data. For FJA, the 95% CIs indicated that bias could range from 20° to -20° which prompted further data inspection and analysis. The following observations were made, which could explain our result: 1. patterns were not perfectly aligned, which produced the largest differences when the slope of the curve was proximal to the vertical; 2. larger differences were observed for higher positives averages corresponding to the swing phase of the stride during fetlock joint flexion. A limited marked movement could certainly happen during fast oscillating events and marker displacement is a possible source of error for cranio-caudal estimates[122]. In addition, acquiring videos at 60 Hz makes the comparison with a 200 Hz system less reliable. For FJROM, the bias between the systems was ranging between 10° to 16° degrees which was considered

acceptable in relation to the large variation in angle degree values and the nature of the experimental settings. Farber et al.[123] found a 10%-15% error in flexion extension assessment of dorsal spinous processes due to skin displacement of reflective markers. That said, the agreement was judged satisfying and the reported bias error was overestimated. Although the MOVIT IMU system could retrieve angles in all three dimensions, only data concerning the sagittal dimension have been taken into consideration for the purpose of this study as the comparison has been done with the 2-D OMC technology. However, movement in the sagittal plane is the predominant type of motion of the fetlock joint [14] and the variability between sound horses in fetlock joint movement in the sagittal plane has been reported to be low [98].

The previous study on fetlock joint kinematics in the horse has been reported using 2-D OMC technology and 3-D OMC on hard surfaces at walk [124,125] and trot [97] with horses exercising on the treadmill [126]. Values of FJROM measured with the MOVIT IMU system in our study are in line with previous results of sagittal plane kinematics for a walk [127] and trot [17,97,128] in sound horses. More precisely, the mean FJROM of forelimbs at walk quantified by MOVIT IMU system was 58.56°± 4.41°, in comparison to 62° ±1.4° in the work of Back et al. [128] with 2-D OMC and 62° ±7° in the work by Clayton et al. [97] by 3-D OMC. At the trot, the mean FJROM of forelimbs measured by the MOVIT IMU system was 80.66°±5.86°, in comparison to 80.6°±7.1° and 77°±5° in the previously cited works, respectively.

4.5.3 Pros of IMU system recording FJA

The portability of the MOVIT IMU system (due to its internal memory storage) could enable the possibility of its use to study limb kinematics in-vivo during different types of clinical conditions and gait velocity encountered in practice as demonstrated by the findings of this article. One of the main limitations of OMC technology is, in fact, the limited camera field of view. Tridimensional OMC requires a high number of cameras and supporting infrastructure, so has mostly been limited to a fixed laboratory environment.

To the best author's knowledge, two commercial systems rely on extremity-mounted IMUs that detect angular parameters in the sagittal plane (EquiMoves-Pegasus). The EquiMoves system relies on a single sensor positioned on a bone segment (metacarpal/metatarsal bone) and it could only measure the orientation of the cannon bone as a rigid element (absolute angle). In our study, the position of two IMUs over the fetlock joint has allowed the quantification of the relative angular pattern of the anatomical joint. This advantage permits, in addition to a complete and realistic spatial study of the kinematics of this joint, a

detailed quantification of temporal variables (stride, stance, and swing duration). The IMU system under investigation could register and quantify the ROM for all individual limbs enabling a complete comprehension of limb motion that could be useful to objectively assess performance, symmetry of movement, clinical improvement, and efficacy of rehabilitation protocols.

4.5.4 Limitations

This study has some limitations, first of all, the use of 2-D instead of 3-D OMC for validation purpose. The studies on the validation of the EquiMoves and Pegasus systems were realized on a treadmill[12,89]] and reported an overall accuracy between the systems higher than ours. To compare the IMU system under investigation, we used a 2-D OMC technology with a lower sampling rate (60Hz) than those reported in the previously mentioned study, so this method is suboptimal for considering it as a gold standard. Since this IMU system is designed for everyday use by practitioners working-up clinical cases, we decided to perform an experiment that best matched this condition, precluding any laboratory setting. The accuracy of the IMU system has not been assessed on different surfaces.
The inclusion of horses with natural occurring limb lameness with different sources of lameness related pain could have led to a greater inhomogeneity in the shape of fetlock joint angle curves in this group.

4.5.5 Conclusions

The IMU technology can be used to assess FJA, approving its use in gait and performance analysis. The system presented in this study provides real-time wireless FJA patterns detection, with the potential for real-time biofeedback to the user. Although the proposed IMU system registers FJROM for all individual limbs simultaneously and could enable to comprehend more extensively affected limb related patterns during lameness, the wide limits of agreement found in this experiment suggest that use of IMUs on fetlock joint as sole quantification method could not be precise in detection of more subtle lameness.
To the authors' best knowledge, this is the first study in which IMUs are applied over fetlock joints to record relative angle pattern overground. Its use in the field of objective lameness evaluation is under investigation and further studies aimed at quantify biological significant differences in FJROM, FJA patterns and limb phasing related to lameness are still needed.

5.EXPERIMENTAL PART- CARPUS

5.1 Introduction

The equine carpus is a high-motion joint composed of 2 rows of carpal bones positioned between the distal radius and the proximal metacarpal bones, creating 3 joint spaces:
-the antebrachiocarpal joint;
- the middle carpal joint
- the carpometacarpal joint.
The antebrachiocarpal and the middle carpal joints are hinge-type joints, while the low-motion carpometacarpal joint is arthrodial in function [129]. The antebrachiocarpal joint ROM is the most extensive of the 3 joints with up to 100° of flexion; the middle carpal joint ROM approaches 45°, and the carpometacarpal joint allows no flexion but undergoes shear stress [129].
The bones comprising the carpus are the distal radius;
the proximal row of carpal bones:
-radial carpal bone (CR)
-intermediate carpal bone (CI)
-ulnar carpal bone (CU)
- accessory carpal bone (CA)
The distal row of carpal bone
-2nd carpal bone, (C2)
-3rdcarpal bone (C3)
-4th carpal bone (C4)
and
the metacarpal bones (2nd 3rd and 4th metacarpal bones)

There are intercarpal ligaments passing between each of the carpal bones holding them in place. Medial and lateral collateral ligaments support the whole carpus. The lateral collateral ligament originates from the lateral styloid process of the radius and has a variety of insertions on the ulnar and 4th carpal bones, and the 3rd and 4th metacarpal bones. The medial collateral ligament originates from the medial styloid process of the radius and has a variety of insertions on the radial and 2nd carpal bones and 2nd and 3rd metacarpal bones. The palmar carpal ligament is an important thick broad fibrous layer of the joint capsule that spans the palmar aspect of the carpus and serves as the dorsal surface of the carpal canal. Deep to the palmar carpal ligament is a

group of smaller supportive palmar ligaments (radiocarpal ligament, palmar middle carpal ligament, and palmar carpometacarpal ligament). Together these ligaments act to prevent joint hyperextension.

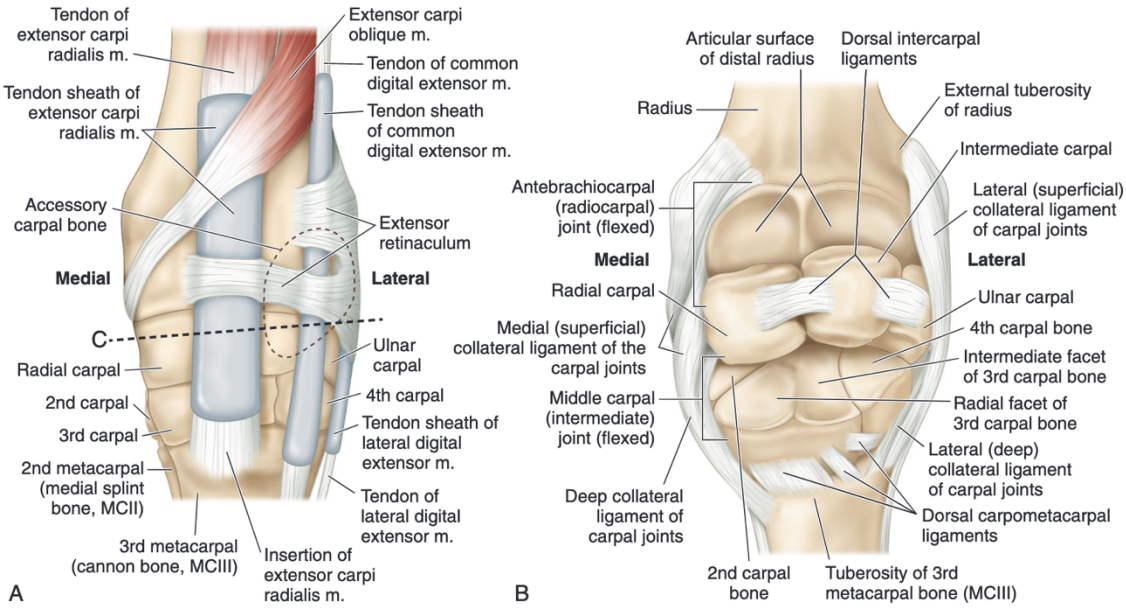

***Fig 29**. The equine carpal bones, ligaments, sheaths and retinaculum. From [129]*

The carpus is a common location of fracture in racehorses [130]. Bone fractures in racehorses are the most commonly occurring problem in the racing industry worldwide [131,132].

Fractures of the carpal bones during training or racing may account for 1–8% of all injuries in some populations and C3 represent the more commonly injured carpal bones [130]. Most of the carpal articulations allow an interlocking wedge arrangement to be formed when are load axially during maximal exercise [130]. Some of the load is transferred to the intercarpal ligaments [133]. Through this mechanism, when supra-physiologic loads are applied, the energy could be absorbed as the carpus has limited elastic ability to over-extend because of the palmar soft tissues [134]. This dispersal of energy may not occur on the medial aspect of the intercarpal joint, as loads from the radius may pass to the CR and directly on to the radial facet of C3 without being dissipated to the intercarpal ligaments [130]. This predisposes the 3 major weight bearing bones to injury (radius CR and C3), in particular the radial facet of C3 [133] .

Pathologic evidence indicates that most fractures in racehorses represent the end of repetitive overuse injuries (stress related bone injury) [135].

Evidence of stress remodeling was observed in association with fracture interfaces of equine long (eg., third metacarpal bone, humerus, scapula, or tibia), cuboidal (e.g., carpal), and irregular (egg, pelvis or vertebrae) bone [135]. During exercise the subchondral bone deforms when placed under a mechanical load. Repetitive loading stimulates the osteoblasts lining the spongiosa to upregulate leading to thickening of the trabeculae. As subchondral bone density increases the shock-absorptive capacity decreases.

The severity of these injuries varies greatly although they can be broadly divided into those that are classified as ‘catastrophic’ which necessitate euthanasia of the horse on humane grounds and the rest that do not.

Usually Carpal injuries are common non-catastrophic injuries [135].

5.2 Aims

The study aimed at developing a computer model of the equine forelimb of a horse sustained a catastrophic carpal fracture during a Palio competition. Although an elevate incidence of musculoskeletal catastrophic injuries during Palios is only anecdotally reported, there is a perception between veterinarians involved in those competitions that catastrophic fractures of the carpus are overrepresented in comparison to flat racing [136]

Italian Palios

Italian Palios are traditional races held in many medieval cities once a year. Jockeys ride bareback at high speeds on a dirt track. The track is obtained in the main square of the city center and racing surface is composed by a mixture of tuff clay and sand. Racehorses run clockwise on triangular or quadrangular track with a perimeter raging from 300 to 450 mt circuits. Due to the racetrack design and geometry, turns in traditional races are characterized by an extremely narrow curve radius (between 14 and 30 m in the Palio of Asti and two bends with an angle of 95° and 92°, in the Palio of Siena).

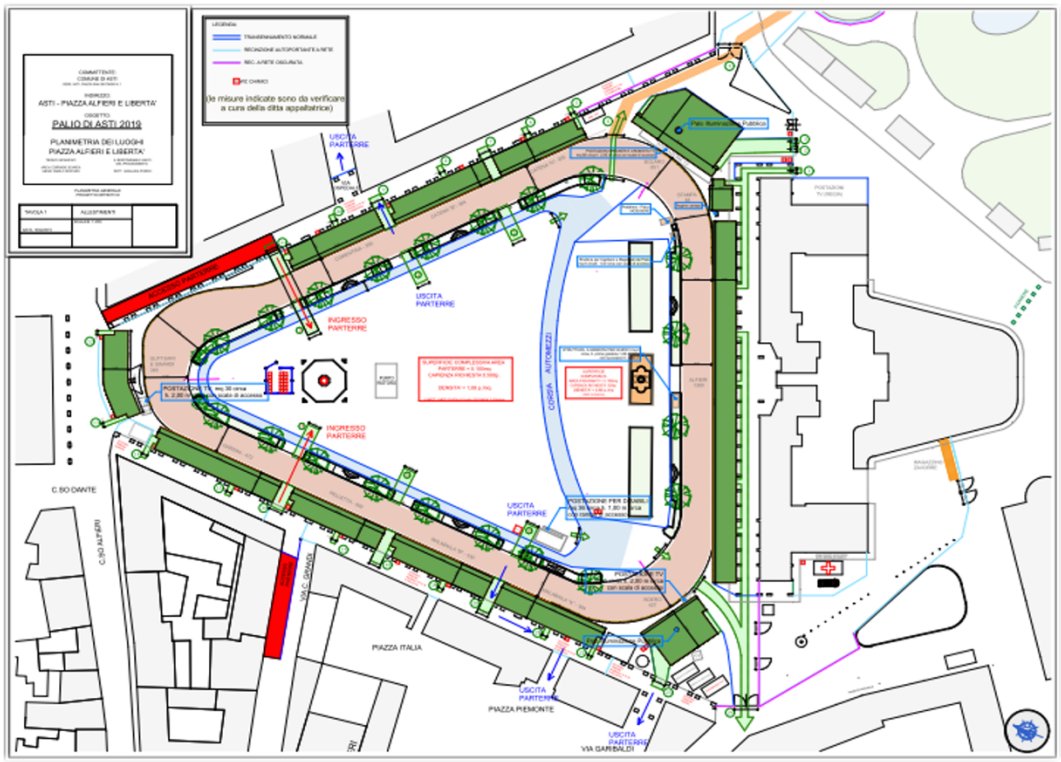

***Fig 30**. Map of racetrack of Palio Asti obtained in the main square of the city. Courtesy of municipality of Asti*

Proper designed flat racing racecourses show constant radius of the curves, with gradual transition in the radius of the turns, with measure between 85 and 200 m, and optimal banking superelevation to reduce centripetal force on the horses' body negotiating curves.

Despite organizational efforts to reduce potential causes of accidents, the characteristic of Palios racetrack raises many issues about the safety of horse involved in these competitions and significant concerns in the public opinion exist.

Horses that race during Palios are likely to be exposed to biomechanical forces that are different from those measured during conventional races. Due to the unfeasibility to experimentally reproduce the features of the Palios track conditions, a direct biomechanical analysis of racehorses during competitions is not feasible.

Computational modelling represents a viable alternative to experimentation in the field of biomechanics. Especially, numerical multibody models have proven to be a valuable tool for addressing open issues related to the musculoskeletal system as well as improving the understanding of complex anatomical structures, like those constituting diarthrodial joints. By exploiting these models, kinematics and dynamics quantities that are difficult, or even impossible to be directly measured experimentally (e.g., intra-articular contact forces), can be estimated to enable the identification of detrimental biomechanical conditions, and allowing the prediction of injuries [69,70].

The aim of this study is to evaluate, using computer modelling, the magnitude and the location of contact forces generated at the level of the carpus in the specific context of a turn in the Palio race. Our hypothesis is that an accordance exists between the internal forces generated in the radio-carpal joint based on the prevision of the model and the in vivo damage observed in the carpus of the injured racehorse.

5.3 Material and methods

5.3.1 Input data

Our model was based on Computer Tomographic data[h] of an adult Thoroughbred (TB) racehorse (7 years old; weighting 480 kg), which was euthanized as consequence of a catastrophic fracture sustained during a traditional race (Palio of Asti; edition 2015). The horse sustained an injury in a 28 meters radius curve (Square Vittorio Alfieri), where it collapsed suddenly on the left forelimb (LF).

After the accident the horse was not weight-bearing, and the distal limb was barely unstable. First aid was immediately provided by immobilization of the limb in a well-padded splint and afterward the animal was transported to the closest equine hospital. At the admission, radiographic examination was performed and an instable fracture of the carpus due to a complete CR failure was diagnosed. The owner denied any treatment and the horse was humanely euthanatized. After obtaining the consent of the owner, the anatomical specimens were collected for further study.

5.3.2 Ct scan

The limb of the horse was amputated at the level of the proximal aspect of the radius and immediately frozen. The specimen was placed with the carpus in full extension on the CT table into a leg-supporting pad with the long axis of the limb parallel to the CT gantry. Contiguous 2.0 mm transverse slices were acquired of the region of interest (ROI), from the diaphysis of the radius to the distal phalanx. Specimen was examined in a proximal to distal direction along the transverse, sagittal and coronal cutting plans, and the generated images were viewed using a bone window. Elaboration in 2D and volume rendering of the bony structures was performed using a DICOM software[i] and evaluated by an experience radiologist.

5.3.3 In-vivo kinematic measurements

A 470 kg mass TB horse ridden by a jokey of 60 Kg mass was equipped with gait analysis system[b] consisting of 4 IMU (triaxial accelerometer and triaxial gyroscope) over both carpi in a surrogate track for the Palio racing circuit under study. After the calibration, each IMU was allocated in its docking base and placed around the distal end of the radius and the proximal metacarpus by a Velcro strap (Fig. 31). in order to secure the equipment, an adhesive band was used to wrap the sensors around the leg (Fig.31) Acquisitions were performed in a curve

with the same curve radius where the accident occurred (Fig.32). IMU sensors were set to a sampling rate of 200 Hz and the recordings were saved on internal memory. In order to measure instant velocity of the horse galloping on the curve, a drone was positioned at a height of 20 mt (Fig.33). A bright colored passive marker was positioned on the jockeys' hat and custom-made markers (circles of 50 cm of diameter) were positioned on the ground at 5 mt intervals along the outside of the curve. Two more cameras were positioned to make video footages of the horse from the side and from rear. All the videos were synchronized with IMU recordings. The horse reached maximum speed gallop over the 370 mt diameter track in a clockwise direction. The recording session was kept as short as possible to ensure genuine IMU high speed data without risk of miscalibration. Videos were digitized and analyzed with a gait analysis software[e]. Distance (m), instant velocity (m/sec), average velocity (m/sec) and acceleration (m/s2) far 50 mt of the curve at each lap on the video from above were calculated. The inclination (angle-degree) of metacarpus to the ground was calculated on the video from rear using the same gait analysis software (Fig.34).

***Fig 31**. Positioning of the IMUs over the carpal joint*

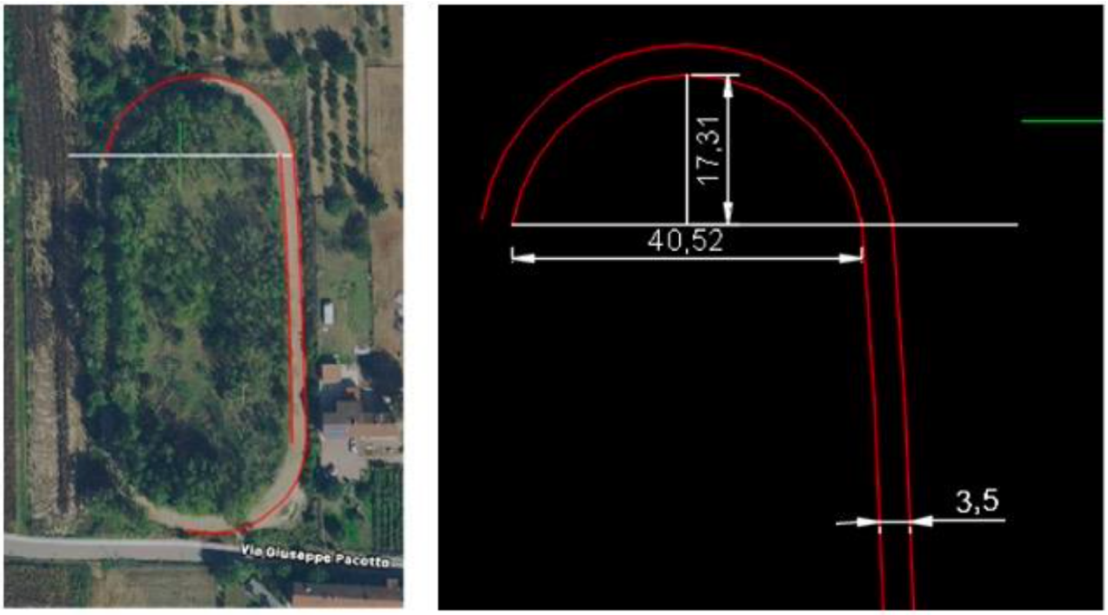

Fig 32. View from above and planimetry of the surrogate track used to simulate in vivo kinematic measurement during turn

***Fig 33**. Calculation of instant velocity and acceleration from the drone on curve*

***Fig 34**. Calculation of inclination of the body and the matacarpus to the ground on curve*

5.3.4 Computation modelling

The CT scans images were segmented, and the respective 3D solid geometries of the entire forelimb were created using commercial software for 3D image processing. Specifically, since the Cr was fractured into two main pieces, it was virtually reconstructed by aligning the bone fragments and applying a wrapping function to reproduce the non-fractured bone structure. Both the segmentation and reconstruction processes were supported by a veterinary surgeon. Therefore, the obtained 3D geometries were imported into a multibody software where a dynamic model was implemented. The model included the following bones obtained from the CT scans: the radius, the Cr, the intermediate carpal bone (Ci), the ulnar carpal bones (Cu), the second (C2), third (C3) and fourth (C4) carpal bones, and the proximal metacarpal bone. In addition to the mentioned bones, the humerus, the ulna, the distal metacarpal bone, and the phalanges were included by adapting standardized geometries to the specific horse sizes. A value of density equal to 1590 kg/m^3 was assigned to the bones based on published data [137]. Thus, the inertial characteristics and center of mass were computed for each body segment. Moreover, the body of the horse was simplified by using a cylindrical geometry having a mass equal to the body weight, that is around 500 kg.

As regarding the joints, the elbow, carpus, fetlock, and distal interphalangeal joint were modelled as hinges, thus, each of them allows for only a rotation movement (i.e., 1 degree of freedom) on the sagittal anatomical plane, whereas the articulations between proximal and middle phalanges were considered fixed. Since this study was focused on the investigation of the forces generated inside the carpal joint, contacts between the articulating surfaces of the carpal bones and the retaining actions of the articular ligaments were implemented. The complexity of the joint, due to the numerosity of its anatomical structures required the introduction of some modelling simplifications. First, the relative motion among the C2, C3 and C4 bones was neglected by fixing them together. Second, only the collateral ligaments, the dorsal retinaculum and the palmar carpal ligament were modelled whereas the constraining effect of the intercarpal ligaments and soft tissues that surround the joint was represented by means of bushing elements. Specifically, each collateral ligament was represented by means of two branches, i.e., the long and short medial collateral ligament (l-MCL and s-MCL), and the long and short lateral collateral ligament (l-LCL and s-LCL). The dorsal retinaculum was represented by two branches per joint side, i.e., the long and short medial retinaculum (l-MR and s-MR), the long and short lateral retinaculum (l-LR and s-LR). Each branch was modelled as a non-linear only-tension spring [138] having the characteristic stiffness parameters adapted from the literature [137] and the slack lengths of the ligaments tuned, by means of preliminary simulations, starting from the modelled ligament lengths

measured with the joint at its resting position. Origin and insertion points of the branches were deduced on the base of anatomical references. Each bushing element was implemented to generate a six-components force (i.e., 3 translational forces and 3 torques) acting between two bones proportionally to their relative linear and angular displacements and velocities. The palmar carpal ligament was modelled with a vinculum at the maximal extension of the carpal joint, at -6° as defined by previous work [139], to counterbalance the stabilization effect offered by the digital flexor tendons. Visual details of the model are reported in figure 35 (panels a-b-c-d) and the corresponding mathematical functions are reported in the supplemental material (Suppl. mat. 2a-2b-2c).

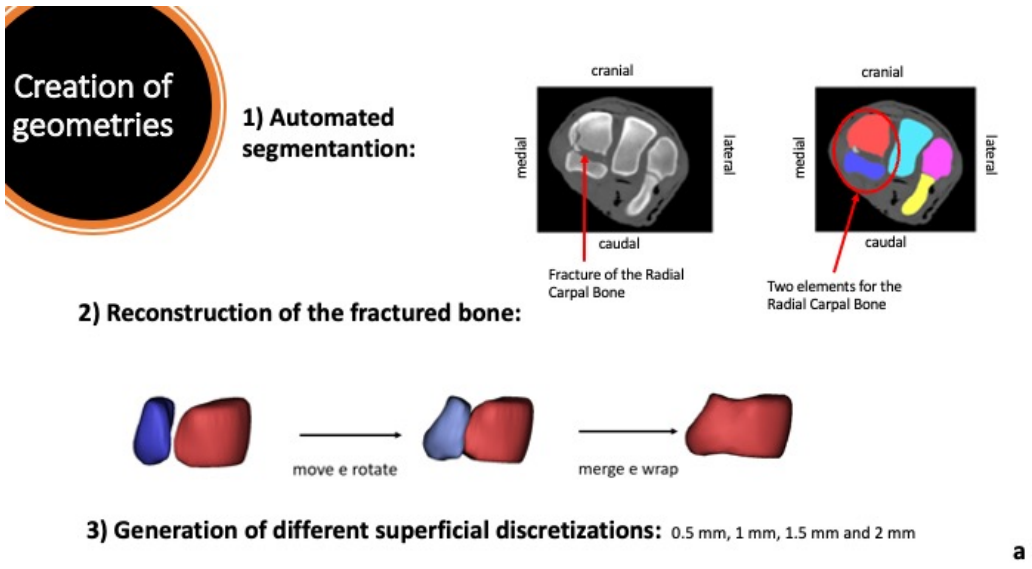

Fig 35.a *The radial carpal bone (Cr) was fractured into two main pieces, it was virtually reconstructed by aligning the bone fragments and applying a wrapping function to reproduce the non-fractured bone surface*

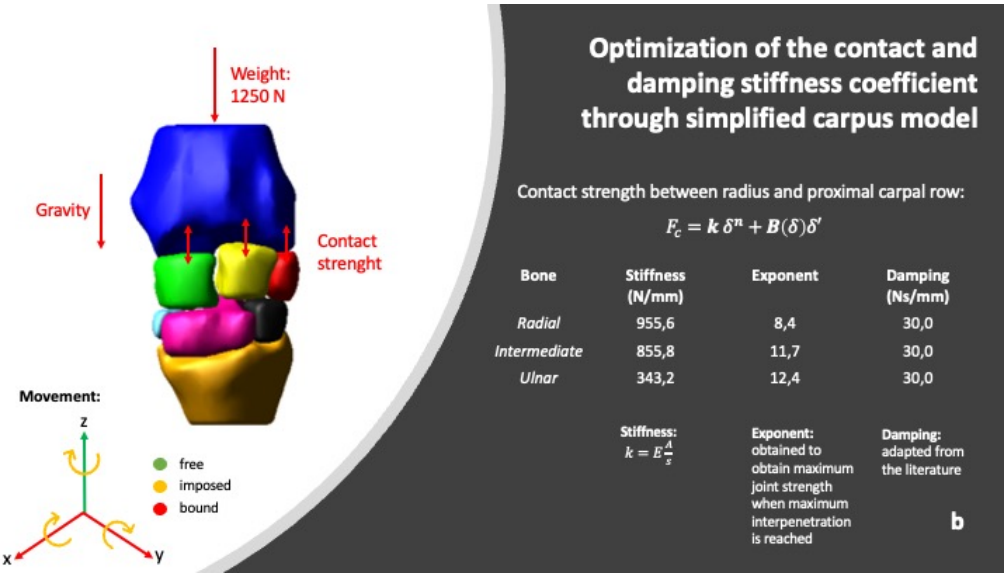

Fig 35.b *Articulating bones of the carpal joint were segmented and the respective three-dimensional (3D) solid geometries were created using software for 3D image processing. The 3D model was imported in a multibody software*

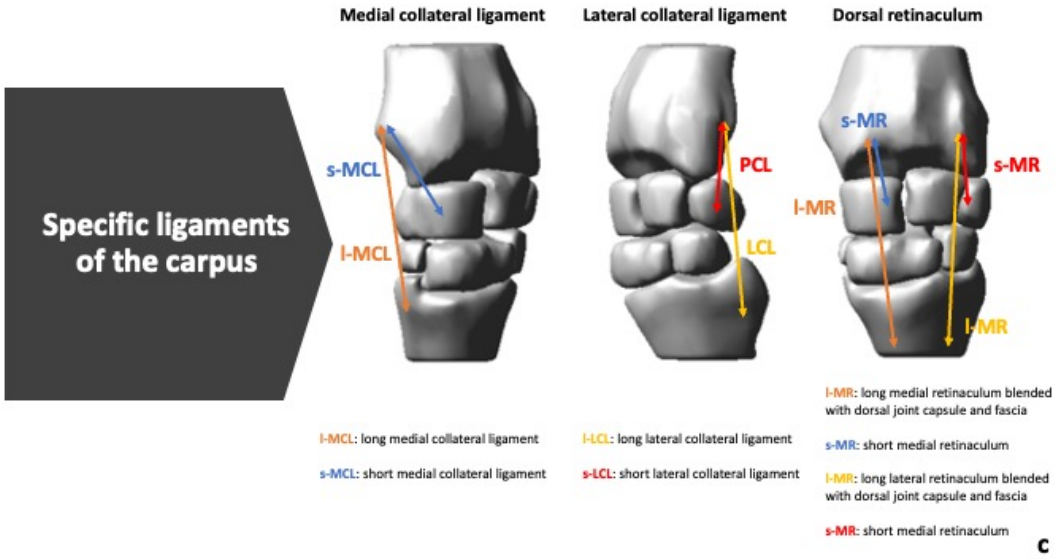

Fig 35.c *The collateral ligaments and the dorsal retinaculum were modelled*

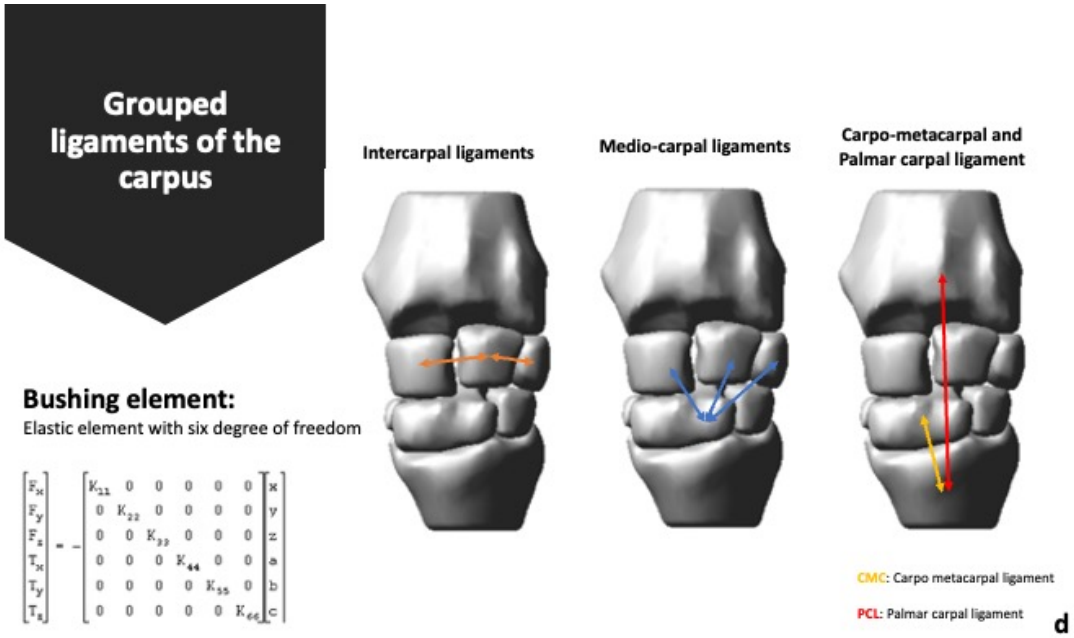

Fig 35.d *The intercarpal ligaments were modelled as bushing elements, acting between two bones proportionally to their relative linear and angular displacements and velocities.*

The intra-articular contact forces were calculated by means of an interpenetration function taking into account the total cartilage thickness (C.Th) between the contacting bones. The physiological value of the C.Th of the carpal bones and radius considered in the study has been previously reported in literature [140]. Three different contact pairs were defined between the distal radius and the Cr, between the distal radius and the Ci, and between the distal radius and the Cu bones, respectively. Articular contacts were assumed frictionless. In addition, a further contact was defined between the limb and the ground. Also, the gravity force was considered for the simulation. Lead and trail limb stride duration (s), stance duration (s), swing duration (s), carpus angle at impact (deg), angle of max extension (deg), angle of maximal flexion (deg), and range of motion (deg) were imported in the model in conjunction with gyroscope and accelerometer raw data captured by IMU sensors.

Furthermore, video footages of the race, acquired from different points of view, were analyzed to extract useful information to replicate the dynamic conditions of the accident, such the horse speed, which was calculated at 14 m/s. The front limb inclination of the external limb with respect to the ground was imported from the kinematic evaluation and calculated in relation to the speed of the horse and the radius of the curve at 56°. The whole simulated stride corresponds to 0.102 msec. Kinematic data introduced in the model are shown in figure 36.

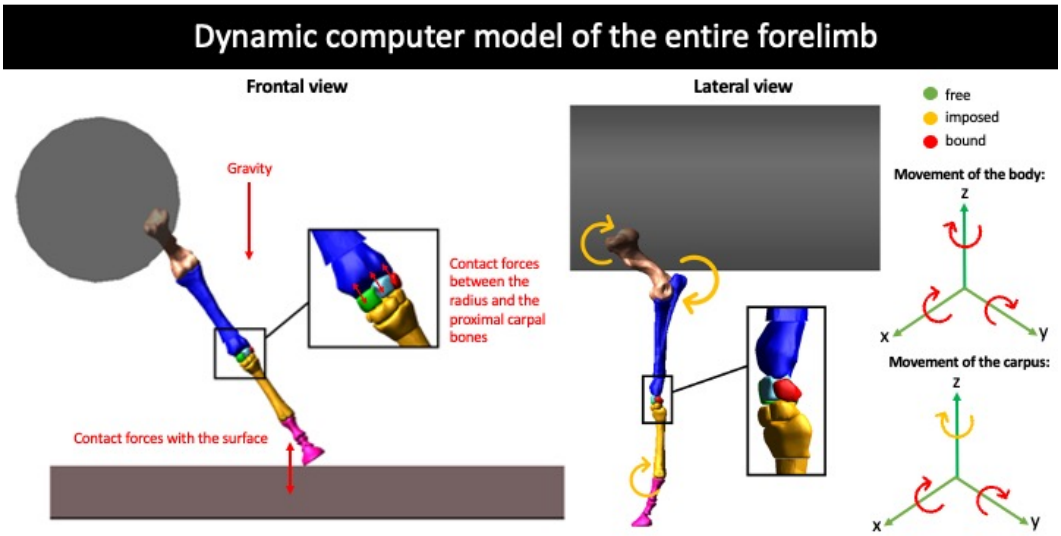

***Fig 36**. Simulation of the carpal joint movement during the stance phase of the stride under study. Input from inertial measurement units, horse speed and front limb inclination with respect to the ground are introduced in the simulation. The body of the horse was simplified by using a cylindrical geometry having a mass equal to the body weight*

As maximum speed reached by the horse along the curve during the experiment was 14 m/sec, kinematics measurements were properly scaled in time and prescribed to the joint. Locations and magnitudes of the center of contact (CoC) forces at the level of the radio-carpal joint were obtained as output from the computational simulation and compared with the location of the cartilage damage and the site of bone failure observed post-mortem.

5.3.5 Macroscopic evaluation of pathology

Macroscopic evaluation of the carpal joints of the euthanatized horses was performed after careful dissection and disarticulation of the joints compartments and scored accordingly [141]. Indian ink solution diluted with phosphate-buffered saline (1:5) was used to stain the superficial hyaline cartilage as described [142] and the stained specimens were photographed using a high-resolution digital camera (Fig.37). Findings were evaluated according to the classification reported in the table 11.

Macroscopic Score	
Grade 1	Surface was normal and smooth in appearance and did not retain Indian ink
Grade 2	Minimal fibrillation, surface retained Indian ink as elongated specks or light-grey patches
Grade 3	Overt fibrillation when areas were velvety in appearance and retained Indian ink as intense black patches
Grade 4	Erosion, when area of cartilage exposing the underlying subchondral bone was evident.

Tab.11

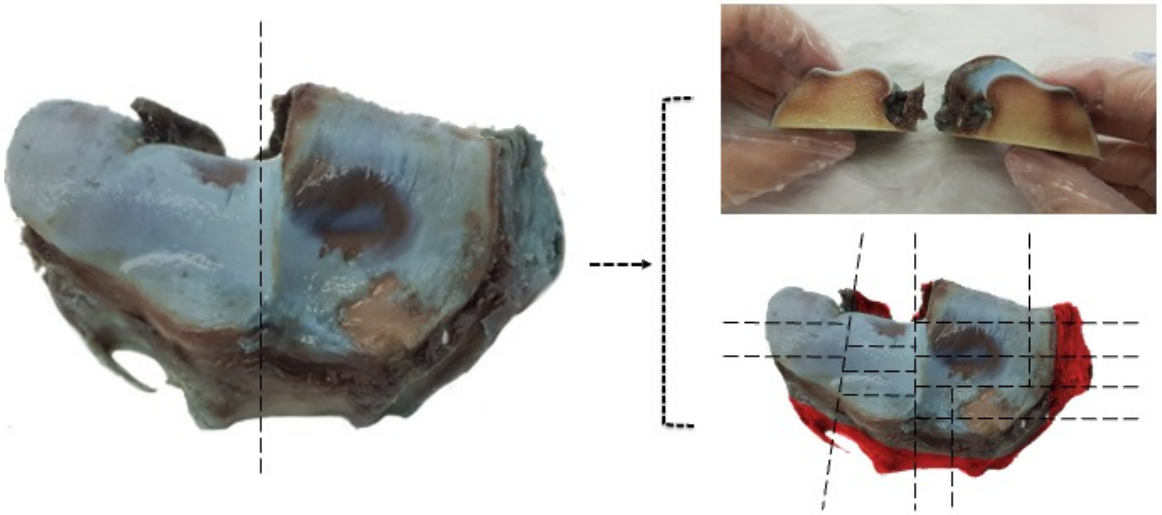

***Fig 37**. Articular surface is visualized after dissection of the antebrachio-carpal joint, and Indian ink deposition (left). Hyaline articular cartilage is severely damaged, as shown. Multiple cut-lines are planned in the articular surface of the radio-carpal joint to capture lesions in the entire hyaline articular cartilage at histopathology (right).*

5.3.6 Micro-computed tomographic examination

The radius and the cuboid carpal bones with the corresponding articular surfaces were carefully dissected and stored at -20°C. All specimens were identified with an ID number. Specimens were submitted to µCT scan at the Istituto Ortopedico Rizzoli (IOR, Bologna, Italy). During µCT acquisition a 65-kV voltage and a current of 385 µA were applied to the source, inter-posing a 1 mm thick aluminum filter. Specimens were rotated 180° following a 0.4° rotation steps. The scan images obtained (1336x3936 pixels) have a nominal resolution (pixel size) of 17.5 µm; and were then reconstructed with the NRecon program[m] to obtain 5911 micro-tomographic sections (each 3936x3936 pixels, keeping the relative pixel size). As correction factors for the reconstructions, in addition to the specific alignment relative to each single scan, beam hardening correction, smoothing and ring artefacts reduction were used. Specimens were examined along the transverse, sagittal, and coronal cutting plans. Further elaborations in 2D and volume rendering were performed. False colors were attributed to tissues in relation to their structural density using yellow ochre for the bone and light blue for the cartilage. The 2D sections were examined to identify a pattern of bone degenerative changes using a structural score [143]. Discrete volumes of interest (VOI) in the radial epiphysis and in the corresponding cuboid carpal bones were identified for quantitative analyses. Parameters measured included bone volume fraction (BV/TV), trabecular thickness (Tb.Th), trabecular separation (Tb.Sp) and number (Tb.N), trabecular pattern factor (Tb.Pf), structure model index (SMI), degree of anisotropy (Da) and C.Th. Bone mineral density was not considered for the analysis because the potential bias related to the freezing processing of the specimen.

5.3.7 Histopathology

After µCT assessment, specimens were stored again in PBS at +4°C. Specimens were processed for histological analysis. Multiple cut lines were planned in the articular surface of the distal radius to map the entire articular cartilage of this specimen in relation of the severity of the macroscopic lesions (Figure sopra). Cuboid carpal bone had not been processed for histopathology. Fourteen osteochondral pieces were obtained. Cuts for histological examination were preferentially performed in the regions where macroscopic cartilage lesions were observed. After fixation in 10% formalin for 24h and rinsing in water, specimens were decalcified with a 5% formic acid solution and 4% hydrochloric acid in 1 L distilled water, respecting the proportion for the desired volume and remained in a descaling solution for one month, where the hardness of the bone component was systematically checked. After

descaling, samples were rinsed in water and then dehydrated in an increasing series of ethyl alcohol (70%, 95% and 100%), passed in xylol and included in paraffin blocks. For each osteochondral piece, two sections of 5 µm thickness were cut along the transverse plane of the carpus to observe both the hyaline cartilage and the corresponding subchondral bone (SBC). Sections were stained with hematoxylin and eosin (H&E) and with safranin O fast green (SOFG). The stained sections were then acquired at 100x for further analysis through a digital scanner[n] and assessed by one author using the OARSI osteoarthritis cartilage histopathology assessment system [141,142] for grading the articular cartilage damage. A site-by-site comparison was performed between the histopathology evaluation of the hyaline cartilage and the corresponding µCT sections at the level of the SCB.

Grade 0	Intact cartilage surface and intact cartilage morphology
Grade 1	Surface fibrillation
Grade 2	Surface discontinuity
Grade 3	Wear lines in the cartilage
Grade 4	Cartilage erosion
Grade 5	Cartilage denudation

Tab. 12

5.4 Results

5.4.1 Radiology and CT scan

Radiographic examination of the carpus identified a biarticular and moderately displaced fracture of the radial carpal bone. The CT scan identified a complete fracture along the coronal plane of the Cr, propagating from the radio-carpal to the inter-carpal joints, with comminution of the palmaro-proximal aspect of the Ci. The main fracture line divided the Cr in 2 main pieces, with the dorsal portion approximately 2/3 and the palmar approximately 1/3 of the whole bone. The complete transverse CT scan from the mid portion of the radius to the proximal third metacarpal bone could be visualized as supplemental material (Suppl. Mat. 3.a QR code 1)

5.4.2 Computation modelling

In the computational model the radio-carpal joint of the left forelimb was analyzed in a simulated stride at the middle of the curve of the racetrack where the horse had the accident. The kinematic input in the model derived from the experimental acquisitions in the surrogate racetrack. All the proximal articular surfaces of the Cr, Ci, and Cu resulted in a contact with the articular surface of the radius after 0.18 msec from the beginning of the simulated stride (Fig. 38). Contact forces present a peak soon after the limb hit the ground, and maximal values differ among the three cuboid bones. The peak force between the radius and Cr had the higher value at around 7000 N, and the peak force between the radius and Cu had the lowest value. When the limb started the swing phase, contact forces decreases, to increase again during full flexion of radio-carpal joint, but without reaching similar values of those obtained during the contact with the ground. CoCs are localized on the convexity of the radial trochlea at the beginning of the simulation, when the carpus was in complete extension and then move, at approximately 0.40 msec from the start of the simulation, on the palmar aspect of the articular surface of the radius, during the flexion of the joint and then returning on dorsal aspect of the articular surface of the radius, during carpal extension. Video of the simulated stride and the migration of contact forces along the radius within the simulated stride are present as supplementary material (3b-QR code 2 and 3c-QR code 3)

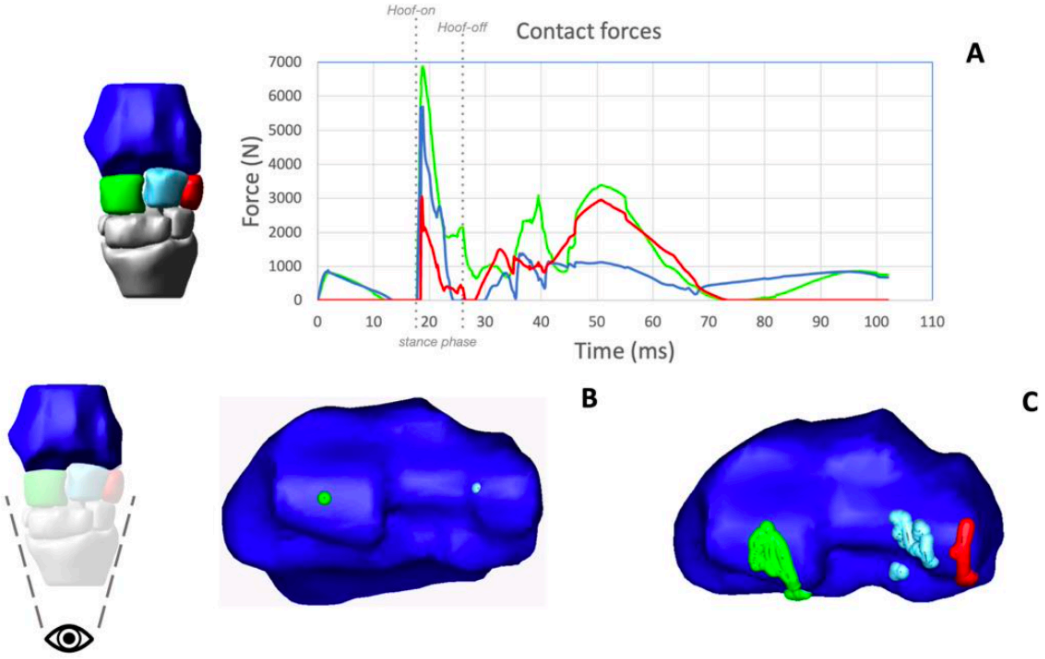

Fig. 38 *The plot shows the magnitude of the forces of contact between the radius (Ra) and the radial carpal bone (green), the intermediate carpal bone (light blue) and the ulnar carpal bone (red). The magnitude of the forces is reported in Newtons as a function of the time of the simulated stride. The hoof-on/hoof- off points and the duration of the stance phase are included in the graph (A). The articular surface of the 3D model of the distal Ra is shown in B. The green dots define the CoC between the Ra and radial carpal bone, the light blue dots define the CoC between the Ra and intermediate carpal bone and the red dots define the CoC between Ra and ulnar carpal bone. Tracking position of contact forces are shown in C. The dynamic simulation of the migration of the CoC can be visualized in Suppl. Mat. 3c-QR Code 3.*

5.4.3 Qualitative and quantitative µCT analysis

The articular surfaces of the radial and intermediate facets of the radius, medially and laterally to the medial parasagittal groove (MPG), and the ulnar facet of the radius exhibited diffuse wear lines, and two large patchy areas with an articular cartilage erosion (Fig. 37). The Cu presented multiple wear lines on the articular surface, whereas the articular surfaces of the Cr and Ci exhibited irregular and full thickness cartilage erosions. Articular surface of the radio-carpal joint was classified as having severe cartilage damage, due to the extensive retention of Indian Ink at the level of the hyaline cartilage. The direction of the wear lines was coincident with the physiologic rotation axis of the joint.

The µCT dataset allows to observe different anatomical planes and to analyze the trabecular pattern of the SCB of the distal radius and cuboid carpal bones. We used both Data viewer[l] and Image J[o] software loading the entire datasets as virtual stacks. Observing the articular surface of the radius using the false color light blue attributed to the hyaline cartilage, two regions with a focal cartilage damage were detected at the level of the radial facet of the radius (Suppl. Mat 3.d QR code 4), accordingly with macroscopic observation (Fig. 37). Lesions were localized medially to the MPG, on the dorso-medial border of the bone and in the palmar aspect of the radial trochlea. Further cartilage lesions were observed in the intermediate facet of the radius laterally to the MPG.

In the SBC, neither focal porosities nor surface irregularities were detected. Sections along the sagittal plans revealed only moderate bone densification in a limited area over the SCB regions at the level of the dorsal aspect of the radial facet of the radius, and at the dorsal aspect of the Cr and Ci (Fig.39).

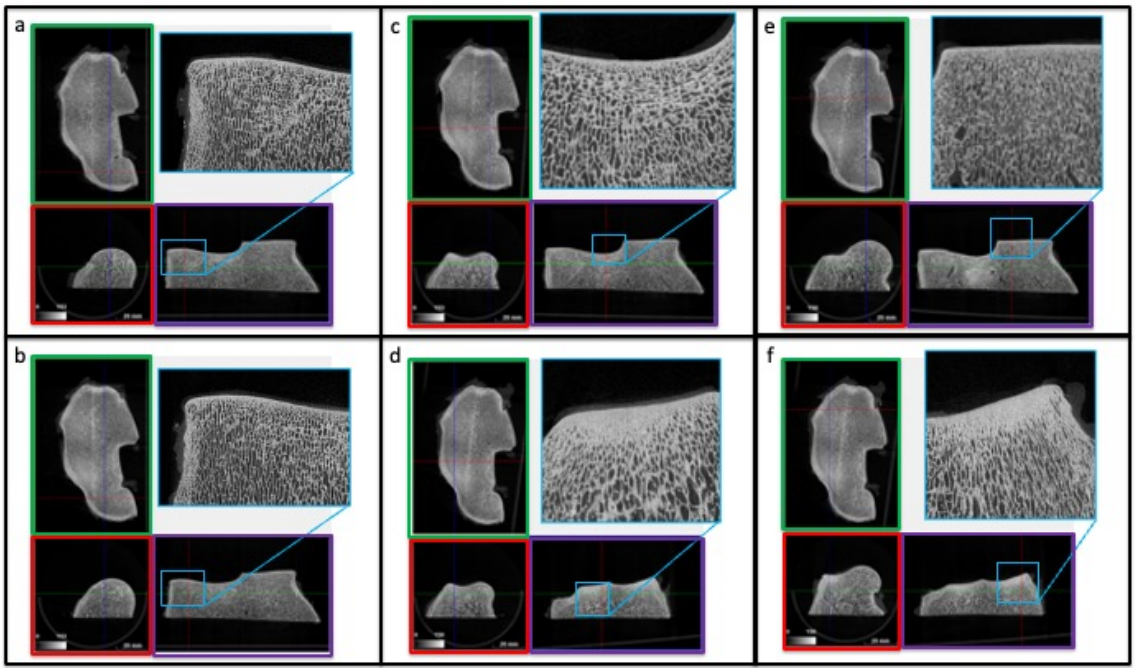

***Fig 39**. A moderate bone densification is limited over the SCB regions, at the level of the dorsal aspect of the radial facet of the radius (d and f). The sagittal, coronal, and transverse plans of the distal radial epiphysis are shown. Plane of cuts are indicated with the corresponding color borders.*

Those areas of bone sclerosis were considered in the physiologic range for a 7-years-old TB racehorse with an history of racing career. The fracture line along the Cr does not travel a region with bone sclerosis.

Three VOI of 15 mm in size were selected on the articular surface of radio-carpal joint, based on the severity of macroscopic aspect of the articular cartilage. The VOI 1 and 2 were localized medially to the MPR: the VOI 1 was opposite to the fracture line on the Cr. The VOI 3 is a negative control and is located abaxially to the MPR, at the level of the intermediate facet of the radius. The VOIs sampled in the distal articular surface of the radius showed marked differences in cartilage thickness (C.Th): in the area identified with 1, it was detected the minimum value of C.Th (76.78 µm). All structural µCT parameters were reported in detail in the corresponding table (Tab.13).

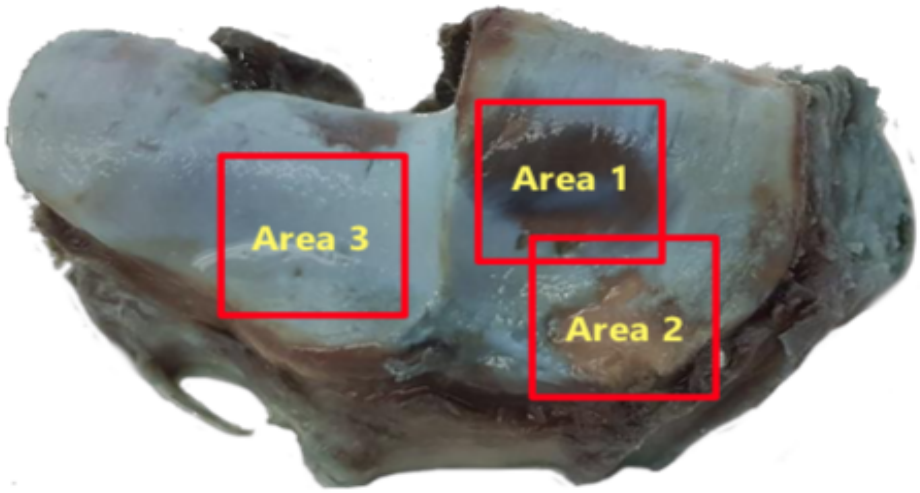

	Trabecular bone							Cartilage
VOI	**BV/TV**	**Tb.Th**	**Tb.SP**	**Tb.N**	**Tb.Pf**	**SMI**	**Da**	**C.th**
	%	µm	µm					µm (min-max)
Total	40.76	309.44	507.32	1.32	-0.19	-0.09	0.54	
Area 1	35.40	199.89	514.88	1.77	-0.44	0.15	0.32	224.59 (76.78-579.90)
Area 2	51.52	334.81	423.31	1.54	-2.44	-1.37	0.40	312.29 (99.61-567.29)
Area 3	41.21	273.97	515.78	1.50	-0.73	-0.35	0.56	629.83 (319.86-825.79)

Tab.13

5.4.3 Histopathology

Sections stained with safranin-O fast green (SOFG) were assessed using a validated grading system. The sections stained with hematoxylin and eosin (H&E) was assessed for

comparison. Hyaline cartilage at the level of the radial facet of the radius appeared extensively damaged (Fig.40).

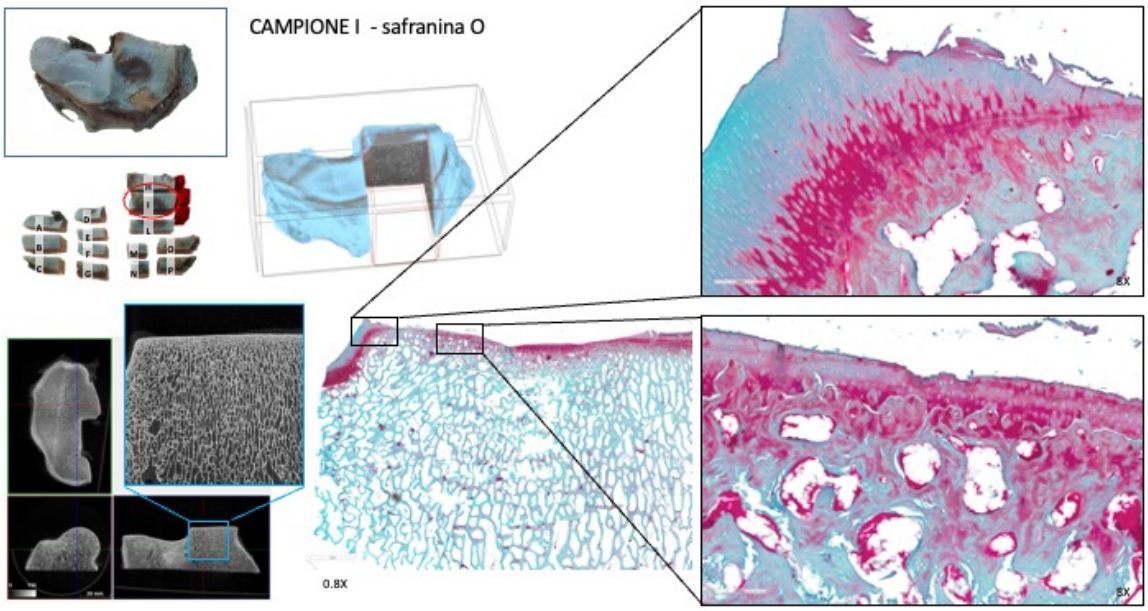

Fig 40. *The radial facets of the articular surface of the distal radius are shown. Particulars of the radial facet. The image captured the radial facet changes, with extensive loss of the hyaline cartilage*

5.5 Discussion

In this study a multibody computer model of the entire equine forelimb has been generated to derive the magnitude and the localization of the contact forces at the level of the radio-carpal joint in a horse experiencing a catastrophic carpal fracture during a traditional race. This point of failure computer model was informed with data that we obtained from the literature and from kinematic data taken from a live test that reproduced, as closely as possible, the condition under which the injury occurred.

Recently, a musculoskeletal model of the Thoroughbred forelimb was developed to test strain profiles of the tendons and ligaments at trot and canter and the same model was used to study the response related to changing ground surface [144]. Differently to that model, where bones were simulated by rigid elements, we developed a model of the carpal joint where biomechanical properties of tissues (cartilage, trabecular bone, ligaments) at the level of the carpus and their deformation were considered. The proposed approach is useful to study interaction between articular surfaces during motion and describe forces at the instant preceding failure, introducing specific conditions of speed and inclination in respect to ground.

The introduction of live kinematic data captured in simulated condition adds value to the output of the model in relation to the specific injury under study. Further validation of the model itself would be recommended before to use this model to describe different condition. The peak of contact forces in our simulation was identified at the level of the cartilage surface of the radial facet of the distal radius, axially to the medial parasagittal ridge, and occurred 18 m/s from the beginning of the stance phase of the stride in the simulated period. We assumed that these findings were explained by the consistent inclination of the leading forelimb and the consequent displacement of the center of mass of the horse' body negotiating the curve at elevated speed. The peak of the forces, based on the reconstruction of the entire horse' stride in this specific race circuit, is localized in correspondence to the articular surface where the fracture line would probably start. It is important to note that the amount of contact forces values predicted by our model do not provide a direct explanation of the fracture per se. We estimated a contact peak force close to 7000 N in a single point between the radial facet of the radius and the Cr. This value is only indicative, because the absence of the forces attributed the flexor and extensor tendons in our model underestimates the force acting on the campus in this horse. However, values obtained in the model are in line with those reported in the equine carpal joints in previous studies [61,145].

There are limited data on the fatigue properties of carpal bone due to the technical difficulties encountered in vivo to measure such loads without altering the physiological loading conditions [146]. Currently, there are any precise references on the amount of force that a carpal bone can withstand before failure. The study of Tidswell [147] shows that an increase in bone mineral density is a common finding in equine cuboidal bones leading to a greater stiffness in racehorses under training. However, no study can precisely define the cuboidal bones breaking point.

In literature it is reported that the curve in a circuit is a significative factor in the pathogenesis of racehorses' injuries [148–150]. Kinematics of movement on curved track has been recently investigated in horses at trot [151] and at gallop [152] in racetracks where the radius of the curve ranged from 85 to 200 m. In horses galloping on a curve at around 14 m/s, the entire limb and the third metacarpal bone inclination increase, to counter-balance the elevated centripetal acceleration acting perpendicular to the direction of motion [148,152]. At the extremal point of a curve a horse generally experiences forces that are smaller than what would be predicted by mathematical models [153]. It has been suggested that increased force associate with the galloping on a curve may be associated with in-creased injury risk [125,150]. Commonly horses at gallop enter curves with the leading limb on the inside of the curve, however the horse in the current study had the leading limb, which is the one that sustained the fracture, on the outside of the curve. It is possible that this choice could be the result of the horse's preference [154] or it could be led by the lack of specific training to race on such a small track.

The simulation of the migration of the forces during an entire stride in our model represents a useful indication of the potential detrimental effect of the force concentration on the proximal aspect of the cuboid bones of the carpus when the horse is leaning on a curve. The pattern of migration of the center of contacts of the forces in that joint matches with the observed pattern of hyaline cartilage injuries observed in the horse under study. The maximum load experienced by the radial carpal bone peaked when the carpal joint was in closed position, at the beginning of the stance phase, and the load reached a point where bone failure could have been possible. Furthermore, as the response of the trabecular bone to repetitive loading is anisotropic, the resistance of the bone is higher when the cyclic loading is applied in the direction of the physiological loading angle and lower at other loading angles [155]. In case of extreme leaning, like in the condition under study, the specific load was applied in a non-axial direction so the resistance of the bone could be further decreased.

Complete fractures of the radial carpal bone are uncommon in racehorses in flat racing [156]. It seems logical to correlate the unusual design of the circuit in the traditional race, mainly the small radius of the curves (28.4 m) of the track travelled at such high speed, with the observed injury. Load on the equine limb is proportional to speed [157]: as galloping speed increases a lower number of stride cycles are required to induce an injury [158]. In the specific context of Palio, horse is not regularly trained in the condition as the circuit is built once a year, so we have concerns about the ability to develop bone adaptation necessary to this specific race. However, there is substantial inter-horse variation in fatigue accumulation based on individual horses' stride characteristics [159].

At the entry of the curve considered in our modelling, the carpal joint of the forelimb negotiating the curve outwardly is overwhelmed by the elevated centripetal acceleration [152] due to the displacement of the center of mass of the animal, with a tremendous increase of the contact forces in the medial aspect of the radio-carpal joint.

The identification of a severe cartilage breakdown on the radial facets of the distal radius requires some specific considerations concerning data introduced in the model. We must consider that catastrophic fractures in horse could be the consequence of pre-existing osteoarthritis of the carpus, as a risk factor for the fracture. However, histopathology and microstructural analysis on the specimen under study did not support pre-existing lesions in this horse. The lesions observed in the hyaline cartilage appear acute rather than related to chronic injury. The cartilage damages were not uniformly distributed, and interestingly, they were localized with good approximation to the points where the model predicted the higher contact in the joint. We observed no histological evidence of chronicity of the lesions, such as chondrocytes cluster or a reduction of chondrocytes density.

Micro-CT revealed increased bone density only in very small areas of the joint, such the dorsal aspect of the intermediate carpal bone and on the radial facet of the distal radius, as we expected in a racehorse and reflecting bone physiological adaptation to training [147,160]. Based on current knowledge, the fracture of the radial carpal bone in this horse was generated under compression, due to the high loading rate [161–163]. Bone geometry, material properties, load direction and the speed of application of the force are the main factors involved in this failure [164]. Furthermore, the cuboid bones in the lateral aspect of the carpus allow greater dissipation of the axial loading thanks to the arrangement of the fourth carpal bone between the ulnar and the intermediate carpal bone due to the horizontal translation of

the bones and their recoil, and the strong intercarpal ligaments [133,134]. This type of mechanism is not possible on the medial aspect of the joint.

The proposed model highlighted some critical elements that could lead to acute bone failure during traditional race. This is only a pilot study, and more work is required to validate this model. The future goal will be to examine more cases of catastrophic fractures to identify specific forces generated in this type of circuits and compare data derived from the simulation to yield point of equine carpal bones. These types of models, like the one used in this study, which integrated in vivo kinematics within silico modelling could be useful for designing racetracks in order to simulate the potential risks for horse competing on these courses. In term of prevention of this type of injury, this study supports the consideration that city tracks should be redesigned to increase the safety of turns and to accommodate horses running at high-speed.

Our model presents some limitations: first of all, not all the sites where macroscopic lesions were observed were completely predicted by the model. This could be probably due to the necessary simplifications introduced in the model. The palmar contention performed by the flexor tendons were not fully considered in the model. The model was retrospectively created and refers to a single horse. Therefore, the findings reported by this study cannot be translated to the whole population of racehorses competing in traditional races. Also, it is no possible to experimentally simulate the track conditions where the accident occurred for obvious ethical reasons.

5.5.1 Conclusions

Computer simulation at the point of failure can define with precision internal forces exceeding yield point of the bone and cartilage and causing catastrophic fracture of the carpus in a horse galloping during a traditional competition. This study describes a new approach to investigate fractures in racehorses, requiring further validation studies. The model is simpler than finite element simulation and could be applied to specific fractures introducing proper input. This approach has the potential to be applied to other fractures than the one studied and offers the opportunity to simulate new racetrack design to improve racehorses' welfare and hopefully reducing catastrophic accidents.

Manufacturer's addresses

a. Qualisys AB. Kvarnbergsgatan 2, 41105 Gothenburg, Sweden [76]
b. MOVIT G1 Captiks SRL Rome
c. MPU9250 by InvenSense, San Jose, US
d. Exilim EX-FH20, Casio, Europe
e. Bio movie, Infolab media, Aosta, Italy
f. Mathlab version 2020R, The MathWorks Inc., Natick, Massachusetts, USA
g. Microsoft Excel Version 16.58, 2013
h. General Electric Hi-Speed Fx; detector rows of 2.0 mm each; collimation, 120 kVp; tube charge, 130 mAs; and pitch, 1.0
i. OsiriX Lite; Pixmeo SARL, Bernex, Switzerland
j. Mimics, Materialize, USA
k. MD Adams, MSC Software Corporation, USA
l. high-resolution µCT Skyscan 1176 Bruker, Belgium
m. NRecon program version 1.6.10.4, Bruker
n. Leica Biosystems
o. U. S. National Institutes of Health, Bethesda, Maryland, USA

REFERENCES

1. van Weeren, P.R.; Gómez Álvarez, C.B. Equine Gait Analysis: The Slow Start, the Recent Breakthroughs and the Sky as the Limit? *Equine Vet J* **2019**, *51*, 809–810, doi:10.1111/evj.13161.
2. Aristotle De Incessu Animalium. In *Parts of animals; movements of animals; progression of animals.*; A.L. Peck and E.S. Forster: Heinemann, London, 1961.
3. Xenophon Uber Die Reitkunst. In *Xenophon. Reitkunst*; Widdra, Schriften und Quellen der Alten Welt: Berlin, 1965.
4. Muybridge,E. *Animals in Motion*; L.S. Brown, 1899;
5. Marey, E-J *La Machine Animale. Locomotion Terrestre et Aérienne*; G.Baillie.; Paris, 1873;
6. Fredricson, I.; Drevemo, S. A New Method of Investigating Equine Locomotion. *Equine Vet J* **1971**, *3*, 137–140, doi:10.1111/j.2042-3306.1971.tb04456.x.
7. Egan, S.; Brama, P.; McGrath, D. Research Trends in Equine Movement Analysis, Future Opportunities and Potential Barriers in the Digital Age: A Scoping Review from 1978 to 2018. *Equine Veterinary Journal* **2019**, *51*, 813–824, doi:10.1111/evj.13076.
8. Clayton, H.M.; Hobbs, S.-J. The Role of Biomechanical Analysis of Horse and Rider in Equitation Science. *Applied Animal Behaviour Science* **2017**, *190*, 123–132, doi:10.1016/j.applanim.2017.02.011.
9. Keegan, K.G. Evidence-Based Lameness Detection and Quantification. *Vet Clin North Am Equine Pract* **2007**, *23*, 403–423, doi:10.1016/j.cveq.2007.04.008.
10. Barrey, E.; Hermelin, M.; Vaudelin, J.L.; Poirel, D.; Valette, J.P. Utilisation of an Accelerometric Device in Equine Gait Analysis. *Equine Veterinary Journal* **1994**, *26*, 7–12, doi:10.1111/j.2042-3306.1994.tb04864.x.
11. Keegan, K.G.; Kramer, J.; Yonezawa, Y.; Maki, H.; Pai, P.F.; Dent, E.V.; Kellerman, T.E.; Wilson, D.A.; Reed, S.K. Assessment of Repeatability of a Wireless, Inertial Sensor–Based Lameness Evaluation System for Horses. *American Journal of Veterinary Research* **2011**, *72*, 1156–1163, doi:10.2460/ajvr.72.9.1156.
12. Bosch, S.; Serra Bragança, F.; Marin-Perianu, M.; Marin-Perianu, R.; Van der Zwaag, B.J.; Voskamp, J.; Back, W.; Van Weeren, R.; Havinga, P. EquiMoves: A Wireless Networked Inertial Measurement System for Objective Examination of Horse Gait. *Sensors* **2018**, *18*, 850, doi:10.3390/s18030850.
13. Ross, M.W. Chapter 7 - Movement. In *Diagnosis and Management of Lameness in the Horse (Second Edition)*; Ross, M.W., Dyson, S.J., Eds.; W.B. Saunders: Saint Louis, 2011; pp. 64–80 ISBN 978-1-4160-6069-7.
14. Back, W.; Clayton, H.M. *Equine Locomotion*; 2nd ed.; 2012; ISBN 978-0-7020-2950-9.
15. Barrey, E. Methods, Applications and Limitations of Gait Analysis in Horses. *The Veterinary Journal* **1999**, *157*, 7–22, doi:10.1053/tvjl.1998.0297.
16. Maria The 4 Basic Horse Gaits Explained [Diagrams & Animations]. *Horses and Us* 2020.
17. Back, W.; Schamhardt, H.C.; Savelberg, H.H.; van den Bogert, A.J.; Bruin, G.; Hartman, W.; Barneveld, A. How the Horse Moves: 1. Significance of Graphical Representations of Equine Forelimb Kinematics. *Equine Vet J* **1995**, *27*, 31–38, doi:10.1111/j.2042-3306.1995.tb03029.x.
18. Thomason, J.J.; Peterson, M.L. Biomechanical and Mechanical Investigations of the Hoof-Track Interface in Racing Horses. *Vet Clin North Am Equine Pract* **2008**, *24*, 53–77, doi:10.1016/j.cveq.2007.11.007.
19. Hobbs, S.; Northrop, A.; Mahaffey, C.; Martin, J.; Clayton, H.; Murray, R.; Roepstorff, L.; Peterson, M. *Equine Surfaces White Paper*; 2014;

20. Rubin, C.T.; Lanyon, L.E. Limb Mechanics as A Function of Speed and Gait: A Study of Functional Strains in the Radius and Tibia of Horse and Dog. *Journal of Experimental Biology* **1982**, *101*, 187–211, doi:10.1242/jeb.101.1.187.
21. Clayton, H.M.; Hodson, E.; Lanovaz, J.L. The Forelimb in Walking Horses: 2. Net Joint Moments and Joint Powers. *Equine Vet J* **2000**, *32*, 295–300, doi:10.2746/042516400777032174.
22. Clayton, H.M. Locomotion. In *Equine Sports Medicine*; Lea & Febiger: Philadelphia; pp. 149–187.
23. Serra Bragança, F.M.; Rhodin, M.; van Weeren, P.R. On the Brink of Daily Clinical Application of Objective Gait Analysis: What Evidence Do We Have so Far from Studies Using an Induced Lameness Model? *Vet J* **2018**, *234*, 11–23, doi:10.1016/j.tvjl.2018.01.006.
24. Carr, B.J.; Resident, A.; Dycus, D.L. CANINE GAIT ANALYSIS. 7.
25. Merkens, H. w.; Schamhardt, H. c. Distribution of Ground Reaction Forces of the Concurrently Loaded Limbs of the Dutch Warmblood Horse at the Normal Walk. *Equine Veterinary Journal* **1988**, *20*, 209–213, doi:10.1111/j.2042-3306.1988.tb01501.x.
26. Bragança, F.M.S.; Hernlund, E.; Thomsen, M.H.; Waldern, N.M.; Rhodin, M.; Byström, A.; Weeren, P.R. van; Weishaupt, M.A. Adaptation Strategies of Horses with Induced Forelimb Lameness Walking on a Treadmill. *Equine Veterinary Journal* **2021**, *53*, 600–611, doi:https://doi.org/10.1111/evj.13344.
27. Weishaupt, M.A.; Wiestner, T.; Hogg, H.P.; Jordan, P.; Auer, J.A. Compensatory Load Redistribution of Horses with Induced Weightbearing Hindlimb Lameness Trotting on a Treadmill. *Equine Vet J* **2004**, *36*, 727–733, doi:10.2746/0425164044848244.
28. Ishihara, A.; Bertone, A.L.; Rajala-Schultz, P.J. Association between Subjective Lameness Grade and Kinetic Gait Parameters in Horses with Experimentally Induced Forelimb Lameness. *American Journal of Veterinary Research* **2005**, *66*, 1805–1815, doi:10.2460/ajvr.2005.66.1805.
29. E.a, M.; H.j, S. *Redistribution of Ground Reaction Forces in Experimentally Induced Equine Carpal Lameness.*; 1987;
30. Keg, P.R.; Barneveld, A.; Schamhardt, H.C.; van den Belt, A.J. Clinical and Force Plate Evaluation of the Effect of a High Plantar Nerve Block in Lameness Caused by Induced Mid-Metatarsal Tendinitis. *Vet Q* **1994**, *16 Suppl 2*, S70-75.
31. Clayton, H.M.; Schamhardt, H.C.; Willemen, M.A.; Lanovaz, J.L.; Colborne, G.R. Kinematics and Ground Reaction Forces in Horses with Superficial Digital Flexor Tendinitis. *Am J Vet Res* **2000**, *61*, 191–196, doi:10.2460/ajvr.2000.61.191.
32. Williams, G.E.; Silverman, B.W.; Wilson, A.M.; Goodship, A.E. Disease-Specific Changes in Equine Ground Reaction Force Data Documented by Use of Principal Component Analysis. *Am J Vet Res* **1999**, *60*, 549–555.
33. Weishaupt, M.A.; Hogg, H.P.; Wiestner, T.; Denoth, J.; Stüssi, E.; Auer, J.A. Instrumented Treadmill for Measuring Vertical Ground Reaction Forces in Horses. *Am J Vet Res* **2002**, *63*, 520–527, doi:10.2460/ajvr.2002.63.520.
34. Weishaupt, M.A.; Wiestner, T.; Hogg, H.P.; Jordan, P.; Auer, J.A. Compensatory Load Redistribution of Horses with Induced Weight-Bearing Forelimb Lameness Trotting on a Treadmill. *Vet J* **2006**, *171*, 135–146, doi:10.1016/j.tvjl.2004.09.004.
35. Weishaupt, M.A. Adaptation Strategies of Horses with Lameness. *Vet Clin North Am Equine Pract* **2008**, *24*, 79–100, doi:10.1016/j.cveq.2007.11.010.
36. Müller-Quirin, J.; Dittmann, M.T.; Roepstorff, C.; Arpagaus, S.; Latif, S.N.; Weishaupt, M.A. Riding Soundness-Comparison of Subjective With Objective Lameness Assessments of Owner-Sound Horses at Trot on a Treadmill. *J Equine Vet Sci* **2020**, *95*, 103314, doi:10.1016/j.jevs.2020.103314.
37. Ratzlaff, M.H.; Wilson, P.D.; Hyde, M.L.; Balch, O.K.; Grant, B.D. Relationship between Locomotor Forces, Hoof Position and Joint Motion during the Support Phase of the Stride of Galloping Horses. *Acta Anat (Basel)* **1993**, *146*, 200–204, doi:10.1159/000147447.

38. Roepstorff, L.; Drevemo, S. Concept of a Force-Measuring Horseshoe. *Acta Anat (Basel)* **1993**, *146*, 114–119, doi:10.1159/000147431.
39. Hjertén, G.; Drevemo, S. Semi-Quantitative Analysis of Hoof-Strike in the Horse. *J Biomech* **1994**, *27*, 997–1004, doi:10.1016/0021-9290(94)90216-x.
40. Kai, M.; Aoki, O.; Hiraga, A.; Oki, H.; Tokuriki, M. Use of an Instrument Sandwiched between the Hoof and Shoe to Measure Vertical Ground Reaction Forces and Three-Dimensional Acceleration at the Walk, Trot, and Canter in Horses. *Am J Vet Res* **2000**, *61*, 979–985, doi:10.2460/ajvr.2000.61.979.
41. Roland, E.S.; Hull, M.L.; Stover, S.M. Design and Demonstration of a Dynamometric Horseshoe for Measuring Ground Reaction Loads of Horses during Racing Conditions. *J Biomech* **2005**, *38*, 2102–2112, doi:10.1016/j.jbiomech.2004.08.024.
42. Chateau, H.; Robin, D.; Simonelli, T.; Pacquet, L.; Pourcelot, P.; Falala, S.; Denoix, J.-M.; Crevier-Denoix, N. Design and Validation of a Dynamometric Horseshoe for the Measurement of Three-Dimensional Ground Reaction Force on a Moving Horse. *J Biomech* **2009**, *42*, 336–340, doi:10.1016/j.jbiomech.2008.11.017.
43. Munoz-Nates, F.; Chateau, H.; Van Hamme, A.; Camus, M.; Pauchard, M.; Ravary-Plumioen, B.; Denoix, J.-M.; Pourcelot, P.; Crevier-Denoix, N. Accelerometric and Dynamometric Measurements of the Impact Shock of the Equine Forelimb and Hindlimb at High Speed Trot on Six Different Tracks - Preliminary Study in One Horse. *Comput Methods Biomech Biomed Engin* **2015**, *18 Suppl 1*, 2012–2013, doi:10.1080/10255842.2015.1069601.
44. THOMASON, J.J.; BIEWENER, A.A.; BERTRAM, J.E. Surface Strain on the Equine Hoof Wall In Vivo: Implications for the Material Design and Functional Morphology of the Wall. *Journal of Experimental Biology* **1992**, *166*, 145–168, doi:10.1242/jeb.166.1.145.
45. Thomason, J.J.; Bignell, W.W.; Sears°, W. Components of Variation of Surface Hoof Strain with Time. *Equine Veterinary Journal* **2001**, *33*, 63–66, doi:10.1111/j.2042-3306.2001.tb05361.x.
46. Thomason, J.J.; Bignell, W.W.; Batiste, D.; Sears, W. Effects of Hoof Shape, Body Mass and Velocity on Surface Strain in the Wall of the Unshod Forehoof of Standardbreds Trotting on a Treadmill. *Equine and Comparative Exercise Physiology* **2004**, *1*, 87–97, doi:10.1079/ECEP20034.
47. Thomason, J.J.; McClinchey, H.L.; Jofriet, J.C. Analysis of Strain and Stress in the Equine Hoof Capsule Using Finite Element Methods: Comparison with Principal Strains Recorded in Vivo. *Equine Vet J* **2002**, *34*, 719–725, doi:10.2746/042516402776250388.
48. Clayton, H.M.; Schamhardt H.C. Measurement Techniques for Gait Analysis. In *Equine Locomotion*; Saunders Ltd: Philadelphia, 2013.
49. Van Weeren, P.R.; Van Den Bogert, A.J.; Barneveld, A. Quantification of Skin Displacement near the Carpal, Tarsal and Fetlock Joints of the Walking Horse. *Equine Veterinary Journal* **1988**, *20*, 203–208, doi:10.1111/j.2042-3306.1988.tb01500.x.
50. Van Weeren, P.R.; Van Den Bogert, A.J.; Barneveld, A. Quantification of Skin Displacement in the Proximal Parts of the Limbs of the Walking Horse. *Equine Veterinary Journal* **1990**, *22*, 110–118, doi:10.1111/j.2042-3306.1990.tb04746.x.
51. Bogert, A.J. van den; Weeren, P.R. van; Schamhardt, H.C. Correction for Skin Displacement Errors in Movement Analysis of the Horse. *Journal of Biomechanics* **1990**, *23*, 97–101, doi:10.1016/0021-9290(90)90374-C.
52. Kastner, J.; Knezevic, P.F.; Girtler, D.; Toeltsch, M. Die 3-Dimensionale Bewegungsanalyse Als Klinische Methode Zur Objektivierung von Lahmheiten Beim Pferd. **1990**, *35*, 171–172, doi:10.1515/bmte.1990.35.s2.171.
53. Pfau, T.; Witte, T.H.; Wilson, A.M. A Method for Deriving Displacement Data during Cyclical Movement Using an Inertial Sensor. *Journal of Experimental Biology* **2005**, *208*, 2503–2514, doi:10.1242/jeb.01658.
54. Elftman, H. Forces and Energy Changes in the Leg during Walking. *American Journal*

of Physiology-Legacy Content **1939**, *125*, 339–356, doi:10.1152/ajplegacy.1939.125.2.339.
55. Clayton, H.M.; Hodson, E.; Lanovaz, J.L.; Colborne, G.R. The Hindlimb in Walking Horses: 2. Net Joint Moments and Joint Powers. *Equine Vet J* **2001**, *33*, 44–48, doi:10.2746/042516401776767359.
56. Clayton, H.M.; Lanovaz, J.L.; Schamhardt, H.C.; Willemen, M.A.; Colborne, G.R. Net Joint Moments and Powers in the Equine Forelimb during the Stance Phase of the Trot. *Equine Vet J* **1998**, *30*, 384–389, doi:10.1111/j.2042-3306.1998.tb04505.x.
57. Lanovaz, J.L.; Clayton, H.M.; Colborne, G.R.; Schamhardt, H.C. Forelimb Kinematics and Net Joint Moments during the Swing Phase of the Trot. *Equine Vet J Suppl* **1999**, 235–239, doi:10.1111/j.2042-3306.1999.tb05225.x.
58. Dutto, D.J.; Hoyt, D.F.; Clayton, H.M.; Cogger, E.A.; Wickler, S.J. Moments and Power Generated by the Horse (Equus Caballus) Hind Limb during Jumping. *J Exp Biol* **2004**, *207*, 667–674, doi:10.1242/jeb.00808.
59. Khumsap, S.; Lanovaz, J.L.; Rosenstein, D.S.; Byron, C.; Clayton, H.M. Effect of Induced Unilateral Synovitis of Distal Intertarsal and Tarsometatarsal Joints on Sagittal Plane Kinematics and Kinetics of Trotting Horses. *Am J Vet Res* **2003**, *64*, 1491–1495, doi:10.2460/ajvr.2003.64.1491.
60. Putame, G.; Aldieri, A.; Audenino, A.; Terzini, M. Chapter 4 - Orthopedic Biomechanics: Multibody Analysis. In *Human Orthopaedic Biomechanics*; Innocenti, B., Galbusera, F., Eds.; Academic Press, 2022; pp. 39–69 ISBN 978-0-12-824481-4.
61. Harrison, S.M.; Whitton, R.C.; Kawcak, C.E.; Stover, S.M.; Pandy, M.G. Relationship between Muscle Forces, Joint Loading and Utilization of Elastic Strain Energy in Equine Locomotion. *J Exp Biol* **2010**, *213*, 3998–4009, doi:10.1242/jeb.044545.
62. Malekipour, F.; Whitton, R.C.; Lee, P.V.-S. Distribution of Mechanical Strain in Equine Distal Metacarpal Subchondral Bone: A MicroCT-Based Finite Element Model. *Medicine in Novel Technology and Devices* **2020**, *6*, 100036, doi:10.1016/j.medntd.2020.100036.
63. Merritt, J.S.; Pandy, M.G.; Brown, N.A.T.; Burvill, C.R.; Kawcak, C.E.; McIlwraith, C.W.; Davies, H.M.S. Mechanical Loading of the Distal End of the Third Metacarpal Bone in Horses during Walking and Trotting. *Am J Vet Res* **2010**, *71*, 508–514, doi:10.2460/ajvr.71.5.508.
64. Bogert, A.J.V. den; Schamhardt, H.C. Multi-Body Modelling and Simulation of Animal Locomotion. *CTO* **1993**, *146*, 95–102, doi:10.1159/000147428.
65. Schiehlen, W. Multibody System Dynamics: Roots and Perspectives. *Multibody System Dynamics* **1997**, *1*, 149–188, doi:10.1023/A:1009745432698.
66. van den Bogert, A.J.; Schamhardt, H.C.; Crowe, A. Simulation of Quadrupedal Locomotion Using a Rigid Body Model. *Journal of Biomechanics* **1989**, *22*, 33–41, doi:10.1016/0021-9290(89)90182-6.
67. Zarucco, L.; Swanstrom, M.D.; Driessen, B.; Hawkins, D.; Hubbard, M.; Steffey, E.P.; Stover, S.M. An in Vivo Equine Forelimb Model for Short-Term Recording of Peak Isometric Force in the Superficial and Deep Digital Flexor Muscles. *Veterinary Surgery* **2003**, *32*, 439–450, doi:10.1053/jvet.2003.50058.
68. Lawson, S.E.M.; Chateau, H.; Pourcelot, P.; Denoix, J.-M.; Crevier-Denoix, N. Sensitivity of an Equine Distal Limb Model to Perturbations in Tendon Paths, Origins and Insertions. *Journal of Biomechanics* **2007**, *40*, 2510–2516, doi:10.1016/j.jbiomech.2006.11.010.
69. Putame, G.; Terzini, M.; Bignardi, C.; Beale, B.; Hulse, D.; Zanetti, E.; Audenino, A. Surgical Treatments for Canine Anterior Cruciate Ligament Rupture: Assessing Functional Recovery Through Multibody Comparative Analysis. *Front. Bioeng. Biotechnol.* **2019**, *7*, doi:10.3389/fbioe.2019.00180.
70. Terzini, M.; Zanetti, E.M.; Audenino, A.L.; Putame, G.; Gastaldi, L.; Pastorelli, S.; Panero, E.; Sard, A.; Bignardi, C. Multibody Modelling of Ligamentous and Bony Stabilizers in the Human Elbow. *Muscles Ligaments Tendons J* **2018**, *7*, 493–502,

doi:10.11138/mltj/2017.7.4.493.
71. Nielsen, T.D.; Dean, R.S.; Robinson, N.J.; Massey, A.; Brennan, M.L. Survey of the UK Veterinary Profession: Common Species and Conditions Nominated by Veterinarians in Practice. *Vet Rec* **2014**, *174*, 324, doi:10.1136/vr.101745.
72. Buchner, H.H.; Savelberg, H.H.; Schamhardt, H.C.; Barneveld, A. Head and Trunk Movement Adaptations in Horses with Experimentally Induced Fore- or Hindlimb Lameness. *Equine Vet J* **1996**, *28*, 71–76, doi:10.1111/j.2042-3306.1996.tb01592.x.
73. Rhodin, M.; Roepstorff, L.; French, A.; Keegan, K.G.; Pfau, T.; Egenvall, A. Head and Pelvic Movement Asymmetry during Lungeing in Horses with Symmetrical Movement on the Straight. *Equine Vet J* **2016**, *48*, 315–320, doi:10.1111/evj.12446.
74. Audigié, F.; Pourcelot, P.; Degueurce, C.; Geiger, D.; Denoix, J.M. Fourier Analysis of Trunk Displacements: A Method to Identify the Lame Limb in Trotting Horses. *Journal of Biomechanics* **2002**, *35*, 1173–1182, doi:10.1016/S0021-9290(02)00089-1.
75. Buchnefp, H.H.F.; Savelberg, H.H.C.M.; Schamhardt, H.C.; Barneveld, A. Temporal Stride Patterns in Horses with Experimentally Induced Fore- or Hindlimb Lameness. *Equine Veterinary Journal* **1995**, *27*, 161–165, doi:10.1111/j.2042-3306.1995.tb04911.x.
76. Keegan, K.G.; Wilson, D.J.; Wilson, D.A.; Frankeny, R.L.; Loch, W.E.; Smith, B. Effects of Anesthesia of the Palmar Digital Nerves on Kinematic Gait Analysis in Horses with and without Navicular Disease. *Am J Vet Res* **1997**, *58*, 218–223.
77. Dyson, S.; Mb, V. Equine Lameness: Clinical Judgment Meets Advanced Diagnostic Imaging. 31.
78. Sapone, M.; Martin, P.; Ben Mansour, K.; Chateau, H.; Marin, F. The Protraction and Retraction Angles of Horse Limbs: An Estimation during Trotting Using Inertial Sensors. *Sensors* **2021**, *21*, 3792, doi:10.3390/s21113792.
79. Dyson, S. Recognition of Lameness: Man versus Machine. *The Veterinary Journal* **2014**, *201*, 245–248, doi:10.1016/j.tvjl.2014.05.018.
80. Parkes, R.S.V.; Weller, R.; Groth, A.M.; May, S.; Pfau, T. Evidence of the Development of 'Domain-Restricted' Expertise in the Recognition of Asymmetric Motion Characteristics of Hindlimb Lameness in the Horse. *Equine Veterinary Journal* **2009**, *41*, 112–117, doi:10.2746/042516408X343000.
81. Keegan, K.G.; Wilson, D.A.; Wilson, D.J.; Smith, B.; Gaughan, E.M.; Pleasant, R.S.; Lillich, J.D.; Kramer, J.; Howard, R.D.; Bacon-Miller, C.; et al. Evaluation of Mild Lameness in Horses Trotting on a Treadmill by Clinicians and Interns or Residents and Correlation of Their Assessments with Kinematic Gait Analysis. *Am J Vet Res* **1998**, *59*, 1370–1377.
82. Keegan, K.G.; Dent, E.V.; Wilson, D.A.; Janicek, J.; Kramer, J.; Lacarrubba, A.; Walsh, D.M.; Cassells, M.W.; Esther, T.M.; Schiltz, P.; et al. Repeatability of Subjective Evaluation of Lameness in Horses. *Equine Vet J* **2010**, *42*, 92–97, doi:10.2746/042516409X479568.
83. Drevemo, S.; Dalin, G.; Fredricson, I.; Hjertén, G. Equine Locomotion; 1. The Analysis of Linear and Temporal Stride Characteristics of Trotting Standardbreds. *Equine Vet J* **1980**, *12*, 60–65, doi:10.1111/j.2042-3306.1980.tb02310.x.
84. Olsen, E.; Andersen, P.H.; Pfau, T. Accuracy and Precision of Equine Gait Event Detection during Walking with Limb and Trunk Mounted Inertial Sensors. *Sensors (Basel)* **2012**, *12*, 8145–8156, doi:10.3390/s120608145.
85. Bragança, F.M.; Bosch, S.; Voskamp, J.P.; Marin-Perianu, M.; Van der Zwaag, B.J.; Vernooij, J.C.M.; van Weeren, P.R.; Back, W. Validation of Distal Limb Mounted Inertial Measurement Unit Sensors for Stride Detection in Warmblood Horses at Walk and Trot. *Equine Vet J* **2017**, *49*, 545–551, doi:10.1111/evj.12651.
86. Sapone, M.; Martin, P.; Ben Mansour, K.; Château, H.; Marin, F. Comparison of Trotting Stance Detection Methods from an Inertial Measurement Unit Mounted on the Horse's Limb. *Sensors (Basel)* **2020**, *20*, 2983, doi:10.3390/s20102983.
87. Hatrisse, C.; Macaire, C.; Sapone, M.; Hebert, C.; Hanne-Poujade, S.; De Azevedo,

E.; Marin, F.; Martin, P.; Chateau, H. Stance Phase Detection by Inertial Measurement Unit Placed on the Metacarpus of Horses Trotting on Hard and Soft Straight Lines and Circles. *Sensors* **2022**, *22*, 703, doi:10.3390/s22030703.
88. Briggs, E.V.; Mazzà, C. Automatic Methods of Hoof-on and -off Detection in Horses Using Wearable Inertial Sensors during Walk and Trot on Asphalt, Sand and Grass. *PLOS ONE* **2021**, *16*, e0254813, doi:10.1371/journal.pone.0254813.
89. Roepstorff, L.; Wiestner, T.; Weishaupt, M.A.; Egenvall, E. Comparison of Microgyro-Based Measurements of Equine Metatarsal/Metacarpal Bone to a High Speed Video Locomotion Analysis System during Treadmill Locomotion. *Vet J* **2013**, *198 Suppl 1*, e157-160, doi:10.1016/j.tvjl.2013.09.052.
90. Darbandi, H.; Serra Bragança, F.; van der Zwaag, B.J.; Voskamp, J.; Gmel, A.I.; Haraldsdóttir, E.H.; Havinga, P. Using Different Combinations of Body-Mounted IMU Sensors to Estimate Speed of Horses-A Machine Learning Approach. *Sensors (Basel)* **2021**, *21*, 798, doi:10.3390/s21030798.
91. Cruz, A.M.; Maninchedda, U.E.; Burger, D.; Wanda, S.; Vidondo, B. Repeatability of Gait Pattern Variables Measured by Use of Extremity-Mounted Inertial Measurement Units in Nonlame Horses during Trotting. *Am J Vet Res* **2017**, *78*, 1011–1018, doi:10.2460/ajvr.78.9.1011.
92. Anderson, K.; Morrice-West, A.V.; Walmsley, E.A.; Fisher, A.D.; Whitton, R.C.; Hitchens, P.L. Validation of Inertial Measurement Units to Detect and Predict Horse Behaviour Whilst Stabled. *Equine Veterinary Journal n/a*, doi:10.1111/evj.13909.
93. Saggio, G.; Tombolini, F.; Ruggiero, A. Technology-Based Complex Motor Tasks Assessment: A 6-DOF Inertial-Based System Versus a Gold-Standard Optoelectronic-Based One. *IEEE Sensors Journal* **2021**, *21*, 1616–1624, doi:10.1109/JSEN.2020.3016642.
94. Teufl, W.; Miezal, M.; Taetz, B.; Fröhlich, M.; Bleser, G. Validity, Test-Retest Reliability and Long-Term Stability of Magnetometer Free Inertial Sensor Based 3D Joint Kinematics. *Sensors (Basel)* **2018**, *18*, 1980, doi:10.3390/s18071980.
95. Santschi, E.M. Articular Fetlock Injuries in Exercising Horses. *Vet Clin North Am Equine Pract* **2008**, *24*, 117–132, doi:10.1016/j.cveq.2007.11.011.
96. Childs, B.A.; Pugliese, B.R.; Carballo, C.T.; Miranda, D.L.; Brainerd, E.L.; Kirker-Head, C.A. Three-Dimensional Kinematics of the Equine Metacarpophalangeal Joint Using x-Ray Reconstruction of Moving Morphology - a Pilot Study. *Vet Comp Orthop Traumatol* **2017**, *30*, 248–255, doi:10.3415/VCOT-16-06-0095.
97. Clayton, H.M.; Sha, D.; Stick, J.; Elvin, N. 3D Kinematics of the Equine Metacarpophalangeal Joint at Walk and Trot. *Vet Comp Orthop Traumatol* **2007**, *20*, 86–91, doi:10.1160/vcot-07-01-0011.
98. Degueurce, C.; Pourcelot, P.; Audigié, F.; Denoix, J.M.; Geiger, D. Variability of the Limb Joint Patterns of Sound Horses at Trot. *Equine Vet J Suppl* **1997**, 89–92, doi:10.1111/j.2042-3306.1997.tb05062.x.
99. Wilson, A.M.; McGuigan, M.P.; Su, A.; van Den Bogert, A.J. Horses Damp the Spring in Their Step. *Nature* **2001**, *414*, 895–899, doi:10.1038/414895a.
100. Riemersma, D.J.; Schamhardt, H.C.; Hartman, W.; Lammertink, J.L. Kinetics and Kinematics of the Equine Hind Limb: In Vivo Tendon Loads and Force Plate Measurements in Ponies. *Am J Vet Res* **1988**, *49*, 1344–1352.
101. McGuigan, M.P.; Wilson, A.M. The Effect of Gait and Digital Flexor Muscle Activation on Limb Compliance in the Forelimb of the Horse Equus Caballus. *Journal of Experimental Biology* **2003**, *206*, 1325–1336, doi:10.1242/jeb.00254.
102. Back, W.; Barneveld, A.; Bruin, G.; Schamhardt, H.C.; Hartman, W. Kinematic Detection of Superior Gait Quality in Young Trotting Warmbloods. *Veterinary Quarterly* **1994**, *16*, 91–96, doi:10.1080/01652176.1994.9694510.
103. Buchner, H.H.; Savelberg, H.H.; Schamhardt, H.C.; Barneveld, A. Limb Movement Adaptations in Horses with Experimentally Induced Fore- or Hindlimb Lameness. *Equine Vet*

J **1996**, *28*, 63–70, doi:10.1111/j.2042-3306.1996.tb01591.x.
104. Back, W; Calyton, H.M. Gait Adaptation in Lameness. In *Equine locomotion*; Elsevier Health Sciences, 2012.
105. Back, W.; Clayton, H.M. Gait Adaptation in Lameness. In *Equine Locomotion*; Saunders Ltd, 2013.
106. Back, W.; Schamhardt, H.C.; Savelberg, H.H.C.M.; Van Den Bogert, A.J.; Bruin, G.; Hartman, W.; Barneveld, A. How the Horse Moves: 2. Significance of Graphical Representations of Equine Hind Limb Kinematics. *Equine Veterinary Journal* **1995**, *27*, 39–45, doi:10.1111/j.2042-3306.1995.tb03030.x.
107. Keegan, K.G.; Wilson, D.A.; Smith, B.K.; Wilson, D.J. Changes in Kinematic Variables Observed during Pressure-Induced Forelimb Lameness in Adult Horses Trotting on a Treadmill. *American Journal of Veterinary Research* **2000**, *61*, 612–619, doi:10.2460/ajvr.2000.61.612.
108. Holmström, M.; Fredricson, I.; Drevemo, S. Biokinematic Differences between Riding Horses Judged as Good and Poor at the Trot. *Equine Veterinary Journal* **1994**, *26*, 51–56, doi:10.1111/j.2042-3306.1994.tb04874.x.
109. Peloso, J.G.; Stick, J.A.; Soutas-Little, R.W.; Caron, J.C.; DeCamp, C.E.; Leach, D.H. Computer-Assisted Three-Dimensional Gait Analysis of Amphotericin-Induced Carpal Lameness in Horses. *Am J Vet Res* **1993**, *54*, 1535–1543.
110. Butcher, M.T.; Ashley-Ross, M.A. Fetlock Joint Kinematics Differ with Age in Thoroughbred Racehorses. *Journal of Biomechanics* **2002**, *35*, 563–571, doi:10.1016/S0021-9290(01)00223-8.
111. Kicker, C.J.; Peham, C.; Girtler, D.; Licka, T. Influence of Support Boots on Fetlock Joint Angle of the Forelimb of the Horse at Walk and Trot. *Equine Vet J* **2004**, *36*, 769–771, doi:10.2746/0425164044848208.
112. Johnston, C.; Gottlieb-Vedi, M.; Drevemo, S.; Roepstorff, L. The Kinematics of Loading and Fatigue in the Standardbred Trotter. *Equine Vet J Suppl* **1999**, 249–253, doi:10.1111/j.2042-3306.1999.tb05228.x.
113. Peham, C.; Girtler, D.; Kicker, C.; Licka, T. Raising Heels of Hind Hooves Changes the Equine Coffin, Fetlock and Hock Joint Angle: A Kinematic Evaluation on the Treadmill at Walk and Trot. *Equine Vet J Suppl* **2006**, 427–430, doi:10.1111/j.2042-3306.2006.tb05581.x.
114. Santosuosso, E.; Leguillette, R.; Vinardell, T.; Filho, S.; Massie, S.; McCrae, P.; Johnson, S.; Rolian, C.; David, F. Kinematic Analysis During Straight Line Free Swimming in Horses: Part 1 - Forelimbs. *Front Vet Sci* **2021**, *8*, 752375, doi:10.3389/fvets.2021.752375.
115. AAEP Horse Show Committee Guide to Veterinary Services for Horse Shows. 1999.
116. Clayton, H.M. Comparison of the Stride Kinematics of the Collected, Working, Medium and Extended Trot in Horses. *Equine Vet J* **1994**, *26*, 230–234, doi:10.1111/j.2042-3306.1994.tb04375.x.
117. Lynch, J.A.; Clayton, H.M.; Mullineaux, D.R. The Reliability of Force Platform Data from Trotting Horses. *Equine and Comparative Exercise Physiology* **2005**, *2*, 129–132, doi:10.1079/ECP200555.
118. Lewczuk, D.; Maśko, M. Symmetry and Regularity of Recreation Horse during Treadmill Training. *Livestock Science* **2021**, *254*, 104773, doi:10.1016/j.livsci.2021.104773.
119. Galisteo, A.M.; Cano, M.R.; Morales, J.L.; Vivo, J.; Miró, F. The Influence of Speed and Height at the Withers on the Kinematics of Sound Horses at the Hand-Led Trot. *Vet Res Commun* **1998**, *22*, 415–424, doi:10.1023/A:1006105614177.
120. Cuesta-Vargas, A.I.; Galán-Mercant, A.; Williams, J.M. The Use of Inertial Sensors System for Human Motion Analysis. *Phys Ther Rev* **2010**, *15*, 462–473, doi:10.1179/1743288X11Y.0000000006.
121. Poitras, I.; Dupuis, F.; Bielmann, M.; Campeau-Lecours, A.; Mercier, C.; Bouyer, L.J.; Roy, J.-S. Validity and Reliability of Wearable Sensors for Joint Angle Estimation: A

Systematic Review. *Sensors (Basel)* **2019**, *19*, E1555, doi:10.3390/s19071555.
122. Olsen, E.; Pfau, T.; Ritz, C. Functional Limits of Agreement Applied as a Novel Method Comparison Tool for Accuracy and Precision of Inertial Measurement Unit Derived Displacement of the Distal Limb in Horses. *Journal of Biomechanics* **2013**, *46*, 2320–2325, doi:10.1016/j.jbiomech.2013.06.004.
123. Farber, M.; Schamhardt, H.; van Weeren, R.; Barneveld, A. Methodology and Validity of Assessing Kinematics of the Thoracolumbar Vertebral Column in Horses on the Basis of Skin-Fixated Markers. *Am J Vet Res* **2001**, *62*, 301–306, doi:10.2460/ajvr.2001.62.301.
124. Chateau, H.; Degueurce, C.; Denoix, J.-M. Evaluation of Three-Dimensional Kinematics of the Distal Portion of the Forelimb in Horses Walking in a Straight Line. *Am J Vet Res* **2004**, *65*, 447–455, doi:10.2460/ajvr.2004.65.447.
125. Hobbs, S.J.; Richards, J.; Matuszewski, B.; Brigden, C. Development and Evaluation of a Noninvasive Marker Cluster Technique to Assess Three-Dimensional Kinematics of the Distal Portion of the Forelimb in Horses. *Am J Vet Res* **2006**, *67*, 1511–1518, doi:10.2460/ajvr.67.9.1511.
126. Chateau, H.; Degueurce, C.; Denoix, J.M. Three-Dimensional Kinematics of the Distal Forelimb in Horses Trotting on a Treadmill and Effects of Elevation of Heel and Toe. *Equine Vet J* **2006**, *38*, 164–169, doi:10.2746/042516406776563260.
127. Hodson, E.; Clayton, H.M.; Lanovaz, J.L. The Forelimb in Walking Horses: 1. Kinematics and Ground Reaction Forces. *Equine Vet J* **2000**, *32*, 287–294, doi:10.2746/042516400777032237.
128. Back, W.; Schamhardt, H.C.; Barneveld, A. Are Kinematics of the Walk Related to the Locomotion of a Warmblood Horse at the Trot? *Vet Q* **1996**, *18 Suppl 2*, S79-84.
129. Getman, L. Case 14.4 - Radial Fracture. In *Comparative Veterinary Anatomy*; Orsini, J.A., Grenager, N.S., de Lahunta, A., Eds.; Academic Press, 2022; pp. 891–897 ISBN 978-0-323-91015-6.
130. Secombe, C.J.; Firth, E.C.; Perkins, N.R.; Anderson, B.H. Pathophysiology and Diagnosis of Third Carpal Bone Disease in Horses: A Review. *N Z Vet J* **2002**, *50*, 2–8, doi:10.1080/00480169.2002.36241.
131. Jeffcott, L.B.; Rossdale, P.D.; Freestone, J.; Frank, C.J.; Towers-Clark, P.F. An Assessment of Wastage in Thoroughbred Racing from Conception to 4 Years of Age. *Equine Vet J* **1982**, *14*, 185–198, doi:10.1111/j.2042-3306.1982.tb02389.x.
132. Robinson, R.A.; Kobluk, C.; Clanton, C.; Martin, F.; Gordon, B.; Ames, T.; Trent, M.; Ruth, G. Epidemiological Studies of Musculoskeletal Racing and Training Injuries in Thoroughbred Horses, Minnesota, U.S.A. *Acta Vet Scand Suppl* **1988**, *84*, 340–343.
133. Bramlage, L.R.; Schneider, R.K.; Gabel, A.A. A Clinical Perspective on Lameness Originating in the Carpus. *Equine Veterinary Journal* **1988**, *20*, 12–18, doi:https://doi.org/10.1111/j.2042-3306.1988.tb04642.x.
134. Deane, N.J.; Davies, A.S. The Function of the Equine Carpal Joint: A Review. *New Zealand Veterinary Journal* **1995**, *43*, 45–47, doi:10.1080/00480169.1995.35845.
135. Stover, S.M. The Epidemiology of Thoroughbred Racehorse Injuries. *Clinical Techniques in Equine Practice* **2003**, *2*, 312–322, doi:10.1053/j.ctep.2004.04.003.
136. Parkin, T.D.H.; French, N.P.; Riggs, C.M.; Morgan, K.L.; Clegg, P.D.; Proudman, C.J.; Singer, E.R.; Webbon, P.M. Risk of Fatal Distal Limb Fractures among Thoroughbreds Involved in the Five Tpes of Racing in the United Kingdom. *Veterinary Record* **2004**, *154*, 493–497, doi:https://doi.org/10.1136/vr.154.16.493.
137. Swanstrom, M.D.; Zarucco, L.; Hubbard, M.; Stover, S.M.; Hawkins, D.A. Musculoskeletal Modeling and Dynamic Simulation of the Thoroughbred Equine Forelimb During Stance Phase of the Gallop. *Journal of Biomechanical Engineering* **2004**, *127*, 318–328, doi:10.1115/1.1865196.
138. Blankevoort, L.; Kuiper, J.H.; Huiskes, R.; Grootenboer, H.J. Articular Contact in a Three-Dimensional Model of the Knee. *Journal of Biomechanics* **1991**, *24*, 1019–1031,

doi:10.1016/0021-9290(91)90019-J.
139. Back, W.; Schamhardt, H.C.; Barneveld, A. Kinematic Comparison of the Leading and Trailing Fore- and Hindlimbs at the Canter. *Equine Veterinary Journal* **1997**, *29*, 80–83, doi:https://doi.org/10.1111/j.2042-3306.1997.tb05060.x.
140. Lee, H.; Kirkland, W.G.; Whitmore, R.N.; Theis, K.M.; Young, H.E.; Richardson, A.J.; Jackson, R.L.; Hanson, R.R. Comparison of Equine Articular Cartilage Thickness in Various Joints. *Connective Tissue Research* **2014**, *55*, 339–347, doi:10.3109/03008207.2014.949698.
141. McIlwraith, C.W.; Frisbie, D.D.; Kawcak, C.E.; Fuller, C.J.; Hurtig, M.; Cruz, A. The OARSI Histopathology Initiative – Recommendations for Histological Assessments of Osteoarthritis in the Horse. *Osteoarthritis and Cartilage* **2010**, *18*, S93–S105, doi:10.1016/j.joca.2010.05.031.
142. Schmitz, N.; Laverty, S.; Kraus, V.B.; Aigner, T. Basic Methods in Histopathology of Joint Tissues. *Osteoarthritis and Cartilage* **2010**, *18*, S113–S116, doi:10.1016/j.joca.2010.05.026.
143. Lacourt, M.; Gao, C.; Li, A.; Girard, C.; Beauchamp, G.; Henderson, J.E.; Laverty, S. Relationship between Cartilage and Subchondral Bone Lesions in Repetitive Impact Trauma-Induced Equine Osteoarthritis. *Osteoarthritis and Cartilage* **2012**, *20*, 572–583, doi:10.1016/j.joca.2012.02.004.
144. Bardin, A.L.; Tang, L.; Panizzi, L.; Rogers, C.W.; Colborne, G.R. Development of An Anybody Musculoskeletal Model of The Thoroughbred Forelimb. *Journal of Equine Veterinary Science* **2021**, *103*, 103666, doi:10.1016/j.jevs.2021.103666.
145. Palmer, J.L.; Bertone, A.L.; Litsky, A.S. Contact Area and Pressure Distribution Changes of the Equine Third Carpal Bone during Loading. *Equine Veterinary Journal* **1994**, *26*, 197–202, doi:https://doi.org/10.1111/j.2042-3306.1994.tb04369.x.
146. Martig, S.; Chen, W.; Lee, P.V.S.; Whitton, R.C. Bone Fatigue and Its Implications for Injuries in Racehorses: Bone Fatigue in Racehorses. *Equine Vet J* **2014**, *46*, 408–415, doi:10.1111/evj.12241.
147. Tidswell, H.K.; Innes, J.F.; Avery, N.C.; Clegg, P.D.; Barr, A.R.S.; Vaughan-Thomas, A.; Wakley, G.; Tarlton, J.F. High-Intensity Exercise Induces Structural, Compositional and Metabolic Changes in Cuboidal Bones — Findings from an Equine Athlete Model. *Bone* **2008**, *43*, 724–733, doi:10.1016/j.bone.2008.06.003.
148. Peterson, M.; Sanderson, W.; Kussainov, N.; Hobbs, S.J.; Miles, P.; Scollay, M.C.; Clayton, H.M. Effects of Racing Surface and Turn Radius on Fatal Limb Fractures in Thoroughbred Racehorses. *Sustainability* **2021**, *13*, 539, doi:10.3390/su13020539.
149. Parkin, T.D.H.; Clegg, P.D.; French, N.P.; Proudman, C.J.; Riggs, C.M.; Singer, E.R.; Webbon, P.M.; Morgan, K.L. Catastrophic Fracture of the Lateral Condyle of the Third Metacarpus/Metatarsus in UK Racehorses – Fracture Descriptions and Pre-Existing Pathology. *The Veterinary Journal* **2006**, *171*, 157–165, doi:10.1016/j.tvjl.2004.10.009.
150. Ueda, Y.; Yoshida, K.; Oikawa, M. Analyses of Race Accident Conditions through Use of Patrol Video. *Journal of Equine Veterinary Science* **1993**, *13*, 707–710, doi:10.1016/S0737-0806(06)81572-8.
151. Kallerud, A.S.; Hernlund, E.; Byström, A.; Persson-Sjodin, E.; Rhodin, M.; Hendrickson, E.H.S.; Fjordbakk, C.T. Non-Banked Curved Tracks Influence Movement Symmetry in Two-Year-Old Standardbred Trotters. *Equine Vet J* **2020**, doi:10.1111/evj.13409.
152. Parkes, R.S.V.; Pfau, T.; Weller, R.; Witte, T.H. The Effect of Curve Running on Distal Limb Kinematics in the Thoroughbred Racehorse. *PLOS ONE* **2020**, *15*, e0244105, doi:10.1371/journal.pone.0244105.
153. Brocklehurst, C.; Weller, R.; Pfau, T. Effect of Turn Direction on Body Lean Angle in the Horse in Trot and Canter. *Vet J* **2014**, *199*, 258–262, doi:10.1016/j.tvjl.2013.11.009.
154. Williams, D.E.; Norris, B.J. Laterality in Stride Pattern Preferences in Racehorses.

Animal Behaviour **2007**, *74*, 941–950, doi:10.1016/j.anbehav.2007.01.014.
155. Dendorfer, S.; Maier, H.J.; Taylor, D.; Hammer, J. Anisotropy of the Fatigue Behaviour of Cancellous Bone. *Journal of Biomechanics* **2008**, *41*, 636–641, doi:10.1016/j.jbiomech.2007.09.037.
156. Pd, R.; R, H.; Nj, D.; K, O. Epidemiological Study of Wastage among Racehorses 1982 and 1983. *Vet Rec* **1985**, *116*, 66–69, doi:10.1136/vr.116.3.66.
157. Witte, T.H.; Hirst, C.V.; Wilson, A.M. Effect of Speed on Stride Parameters in Racehorses at Gallop in Field Conditions. *Journal of Experimental Biology* **2006**, *209*, 4389–4397, doi:10.1242/jeb.02518.
158. Martig, S.; Lee, P.V.S.; Anderson, G.A.; Whitton, R.C. Compressive Fatigue Life of Subchondral Bone of the Metacarpal Condyle in Thoroughbred Racehorses. *Bone* **2013**, *57*, 392–398, doi:10.1016/j.bone.2013.09.006.
159. Morrice-West, A.V.; Hitchens, P.L.; Walmsley, E.A.; Tasker, K.; Lim, S.L.; Smith, A.D.; Whitton, R.C. Relationship between Thoroughbred Workloads in Racing and the Fatigue Life of Equine Subchondral Bone. *Sci Rep* **2022**, *12*, 11528, doi:10.1038/s41598-022-14274-y.
160. Martig, S.; Hitchens, P.L.; Lee, P.V.S.; Whitton, R.C. The Relationship between Microstructure, Stiffness and Compressive Fatigue Life of Equine Subchondral Bone. *Journal of the Mechanical Behavior of Biomedical Materials* **2020**, *101*, 103439, doi:10.1016/j.jmbbm.2019.103439.
161. Radin, E.L.; Parker, H.G.; Pugh, J.W.; Steinberg, R.S.; Paul, I.L.; Rose, R.M. Response of Joints to Impact Loading — III: Relationship between Trabecular Microfractures and Cartilage Degeneration. *Journal of Biomechanics* **1973**, *6*, 51–57, doi:10.1016/0021-9290(73)90037-7.
162. Lynch, M.E.; Main, R.P.; Xu, Q.; Schmicker, T.L.; Schaffler, M.B.; Wright, T.M.; van der Meulen, M.C.H. Tibial Compression Is Anabolic in the Adult Mouse Skeleton despite Reduced Responsiveness with Aging. *Bone* **2011**, *49*, 439–446, doi:10.1016/j.bone.2011.05.017.
163. Browner, B.D. *Skeletal Trauma: Basic Science, Management, and Reconstruction*; Elsevier Health Sciences, 2009; ISBN 978-1-4160-2220-6.
164. DeGoede, K.M.; Ashton-Miller, J.A.; Schultz, A.B. Fall-Related Upper Body Injuries in the Older Adult: A Review of the Biomechanical Issues. *Journal of Biomechanics* **2003**, *36*, 1043–1053, doi:10.1016/S0021-9290(03)00034-4.

SUPPLEMENTAL MATERIAL

1.

```
clc
clear all
close all

%% General defines

fs_Movit= 200;  %% Sampling freq IMU
fs_OMC = 60;  %% Sampling freq OMC
ft_angle_peaks = 3; % cutoff frequency for minimum selection
ft_angle = 10;  % cutoff frequency for data smoothing

order = 4; % butterworth filter order

%% IMPORT FILE

% IMPORT IMU FILE

[Movit] = import_anatomical_angle_cavalli();

% IMPORT OCM FILE

[OMC] = import_OMC_angle();


%% RESAMPLE
% Resampling of the OMC data from 60 Hz to 200 Hz

Fsa = fs_OMC;
Fsd = fs_Movit;  % Desired Sampling Frequency

OMC_TIME = OMC.TIME(1,1):1/Fsd:OMC.TIME(end,1);
OMC_Angle_resampled = spline(OMC.TIME, OMC.ANGLE(:,1), OMC_TIME);

%% LOW PASS FILTER (10 HZ)

[B_low,A_low]=butter(order,ft_angle/(fs_Movit/2),'low');
OMC_filt = filtfilt(B_low,A_low,OMC_Angle_resampled);
MOVIT_filt = filtfilt(B_low,A_low,MOVIT.ANGLE);

%% LOW PASS FILTER (3 HZ)
% signal used to find the first two maximum value among which to search the
% absolute minimum point (point used to sync IMU and OMC data in time and to remove
% the offset between the OMC and IMU data)
```

```
[B_low_angle, A_low_angle] = butter(order, ft_angle_peaks/(fs_Movit/2),'low');
OMC_Angle_filt_3 = filtfilt(B_low_angle,A_low_angle,OMC_filt);
MOVIT_Angle_filt_3 = filtfilt(B_low_angle,A_low_angle,MOVIT_filt);

%% SESSION CUT

% from the data, the user select the start and the end of the
% valid session, removing tha recording parts to not consider into analysis

figure()
plot(OMC_TIME, OMC_Angle_resampled)
hold on
plot(MOVIT.TIME, MOVIT.ANGLE)
A = ginput(2)
legend('OMC', 'MOVIT')

Start_Point = A(1);
Stop_Point = A(2);

Movit_start_interval = find(MOVIT.TIME>= Start_Point, 1);
Omc_start_interval = find(OMC_TIME>= Start_Point, 1);

Movit_stop_interval = find(MOVIT.TIME>= Stop_Point, 1);
Omc_stop_interval = find(OMC_TIME>= Stop_Point, 1);

% cut 10 hz signal

MOVIT_Angle_selection = MOVIT_filt(Movit_start_interval: Movit_stop_interval);
MOVIT_Time_selection = MOVIT.TIME(Movit_start_interval: Movit_stop_interval);

OMC_Angle_selection = OMC_filt(Omc_start_interval: Omc_stop_interval);
OMC_Time_selection = OMC_TIME(Omc_start_interval: Omc_stop_interval);

% cut 3 hz signal
OMC_Angle_filt_3_selection = OMC_Angle_filt_3(Omc_start_interval: Omc_stop_interval);
MOVIT_Angle_filt_3_selection = MOVIT_Angle_filt_3(Movit_start_interval:
Movit_stop_interval);

%% In the 3 hz filtered signal, find the first two maximum value

[ OMC_first_max, OMC_second_max ] = findFirstAndSecondMax( OMC_Time_selection,
OMC_Angle_filt_3_selection );
[ MOVIT_first_max, MOVIT_second_max ] = findFirstAndSecondMax(
MOVIT_Time_selection, MOVIT_Angle_filt_3_selection );
```

```
%% knowing the first two maximum value in time, find the absolute minimum value
between the two maximum in the 10 hz filtered data
[ OMC_t_min, OMC_value_min ] = findAbsoluteMinPoint( OMC_first_max,
OMC_second_max, OMC_Angle_selection, OMC_Time_selection);
[ MOVIT_t_min, MOVIT_value_min ] = findAbsoluteMinPoint( MOVIT_first_max,
MOVIT_second_max, MOVIT_Angle_selection, MOVIT_Time_selection);

% delta time and delta value between the minimum of the OMC signal and the
% minimum of the IMU signal

DELTA_TIME = OMC_t_min - MOVIT_t_min ;
DELTA_VALUE = OMC_value_min - MOVIT_value_min;

% remove time and value offset in the OMC signal
OMC_Time_selection_delta = OMC_Time_selection - DELTA_TIME;
OMC_Angle_selection_delta = OMC_Angle_selection - DELTA_VALUE;

%% After the temporal alignment, cut the signal and resample the OMC signal in order to
have the same number of samples to perform RMSE and Pearson coefficient calculation

TIME_START = max(OMC_Time_selection_delta(1) , MOVIT_Time_selection(1));
TIME_STOP = min(OMC_Time_selection_delta(end) , MOVIT_Time_selection(end));

Movit_time_start_sample = find(MOVIT_Time_selection>= TIME_START, 1);
Movit_time_stop_sample = find(MOVIT_Time_selection>= TIME_STOP, 1);

t_resample = MOVIT_Time_selection(Movit_time_start_sample:Movit_time_stop_sample);
OMC_signal = spline(OMC_Time_selection_delta, OMC_Angle_selection_delta, t_resample);
MOVIT_signal =
MOVIT_Angle_selection(Movit_time_start_sample:Movit_time_stop_sample);

%% CALCOLO PEARSON E RMSE

for i = 1:length(t_resample)
      error(i) = OMC_signal(i) - MOVIT_signal(i);
end
RMSE = sqrt(mean(error.^2))

Corr = corrcoef([OMC_signal, MOVIT_signal]);
Pearson = Corr(1,2
```

3.

a. Spring element implementation

The force-strain relationship of each spring element is described by the following nonlinear piecewise function:

$$f = \begin{cases} -k(\varepsilon - \varepsilon_L), & \varepsilon > 2\varepsilon_L \\ -0.25\, k \dfrac{\varepsilon^2}{\varepsilon_L}, & 0 \le \varepsilon \le 2\varepsilon_L \\ 0, & \varepsilon < 0 \end{cases}$$

where ε is the ligament strain, ε_L is a reference value of strain assumed to be 0.03 and k is the stiffness parameter, expressed as force per unit strain, of each different spring element. The spring strain ε is defined as:

$$\varepsilon = \frac{(l - l_0)}{l_0}$$

where l is the actual element length and l_0 is the no load length (i.e., slack length). Moreover, to avoid high frequency vibrations during simulations, a parallel damper with a damping coefficient of 0.5 Ns/mm was added to each spring element.

Characteristic parameters of the spring elements.

Element	k (N)	l_o (mm)
l-MCL	48000	102.0
l-LCL	48000	105.9
l-MR	10000	106.9
l-LR	10000	107.2
s-MCL	24000	51.4
s-LCL	24000	50.0
s-MR	1000	53.0
s-LR	1000	42.4

b. Bushing element implementation

The force-displacement relationship of each bushing element is described as following:

$$\begin{bmatrix} F_x \\ F_y \\ F_z \\ T_x \\ T_y \\ T_z \end{bmatrix} = \begin{bmatrix} K_{11} & 0 & 0 & 0 & 0 & 0 \\ & K_{22} & 0 & 0 & 0 & 0 \\ & & K_{33} & 0 & 0 & 0 \\ & & & K_{44} & 0 & 0 \\ & sym & & & K_{55} & 0 \\ & & & & & K_{66} \end{bmatrix} \cdot \begin{bmatrix} x \\ y \\ z \\ \alpha \\ \beta \\ \gamma \end{bmatrix} + \begin{bmatrix} C_{11} & 0 & 0 & 0 & 0 & 0 \\ & C_{22} & 0 & 0 & 0 & 0 \\ & & C_{33} & 0 & 0 & 0 \\ & & & C_{44} & 0 & 0 \\ & sym & & & C_{55} & 0 \\ & & & & & C_{66} \end{bmatrix} \cdot \begin{bmatrix} Vx \\ Vy \\ Vz \\ W\alpha \\ W\beta \\ W\gamma \end{bmatrix}$$

where: *F* and *T* are the translational and torsional force components, respectively; *x, y,* and *z* are the relative translational displacements between connected bodies; *α, β* and *γ* are the relative rotational displacements between connected bodies; K_{11}, K_{22}, and K_{33} are the translational stiffness coefficients; K_{44}, K_{55}, and K_{66} are the rotational stiffness coefficients; *Vx, Vy,* and *Vz* are the relative translational velocities between connected bodies; *Wα, Wβ* and *Wγ* the relative rotational velocities between connected bodies; C_{11}, C_{22}, and C_{33} are the translational damping coefficients; C_{44}, C_{55}, and C_{66} are the rotational damping coefficients.

Characteristic parameters of the defined bushing elements

Connected bodies	**K_{11} (N/mm)**	**K_{22} (N/mm)**	**K_{33} (N/mm)**	**K_{44} (N/°)**	**K_{55} (N/°)**	**K_{66} (N/°)**	**C_{11} (Ns/mm)**	**C_{22} (Ns/mm)**	**C_{33} (Ns/mm)**	**C_{44} (Ns/°)**	**C_{55} (Ns/°)**	**C_{66} (Ns/°)**
Metacarpus – Radius #1 *	1	1	1	10	10	10	0	0	0	0	0	0
Metacarpus – Radius #2 *	0	0	0	5	5	5	0	0	0	0	0	0
Metacarpus – Radius #3 *	0	0	0	50	50	50	0	0	0	0	0	0
C3 – Cu	3000	1000	3000	15	15	15	3000	3000	500	15	15	15
C3 – Ci	500	500	500	4	4	4	3000	3000	500	15	15	15
C3 – Cr	1000	1000	500	5	5	5	3000	3000	500	15	15	15
C3 – Metacarpus	1500	1500	1500	15	15	15	3000	3000	3000	15	15	15
Ci – Cu	0	0	0	0	0	0	0	0	2000	0	0	0
Ci – Cr	0	0	0	0	0	0	0	0	2000	1	1	1

* Three alternative bushing elements were used for the Metacarpus – Radius coupling. Such bushings were activated sequentially during the simulation. In detail, the bushing #1 was activated for the 0 – 26 ms time interval, the #2 for the 26 – 46 ms time interval, and the #3 for the 46 – 102 ms time interval.

c. Contact implementation

Contact forces F_c were calculated by using the following interpenetration formulation:

$$F_c = K_c\delta^e + C_c(\delta, \delta_{max}, C_{max})\dot{\delta}$$

where K_c is the contact stiffness constant, δ is the interpenetration depth between contacting rigid bodies, e is a nonlinear power exponent, $\dot{\delta}$ is the penetration velocity and C_c is a damping function defined as:

$$C_c(\delta) = \begin{cases} 0, & \delta \leq 0 \\ C_{max}\left(\frac{\delta}{\delta_{max}-\delta}\right)^2\left(3-\frac{2\delta}{\delta_{max}-\delta}\right), & 0 < \delta \leq \delta_{max} \\ C_{max}, & \delta \geq \delta_{max} \end{cases}$$

where δ_{max} is the maximum interpenetration depth, defined equal to 0.1 mm, at which the damping function reaches its maximum value C_{max} of 30 Ns/mm, which was adapted from data reported for the human knee.
Specifically, the parameter K_c was computed by combining the following formulas:

$$E = \frac{H(1+\nu)(1-2\nu)}{1-\nu}$$
$$K_c = E\frac{A}{s}$$

where E is the Young's modulus, H is the aggregate modulus, ν is the Poisson's ratio and s is the thickness relative to the cartilage layers of the contacting bones. Moreover, the contacting area A between bones was initially estimated from the CT scans.
The nonlinear power exponent was iteratively refined so that a maximum reported contact force equal to 15000 N can be reached for the maximum considered interpenetration depth, that is the total cartilage thickness.
Based on the same formulation, a further contact was defined between the ground and the front limb. In this case, friction was considered by using a Coulomb's model. Due to the lack of data in literature, generic contact parameters were iteratively adapted to the case study.

Parameters involved in the articular contact

Contact pair	Aggregate modulus H (MPa)	Young's modulus E (MPa)	Poisson's ratio ν	Area A (mm^2)	Cartilage thickness s (mm)	Max damping C_{max} (Ns/mm)	Max penetration δ_{max} (mm)	Power exponent e	Stiffness K_c (N/mm)
Radius – Cr	1.58	1.38	0.22	958.7	2.23	30	0.1	8.4	955.6
Radius – Ci	1.42	1.29	0.19	845.9	2.16	30	0.1	11.65	855.8
Radius - Cu	1.62	1.34	0.26	347.8	2.20	30	0.1	12.35	343.2

Parameters involved in the ground-limb contact.

Contact pair	Max damping C_{max} (Ns/mm)	Max penetration δ_{max} (mm)	Power exponent e	Static friction coefficient	Dynamic friction coefficient	Stiffness K_c (N/mm)
Limb - Ground	150	20	2.2	0.58	0.46	20000

3. QR CODES- VIDEO

a. QR CODE 1

b. QR CODE 2

c. QR CODE 3

a. QR CODE 4

RESEARCH PRODUCTS

Articles related to the PhD project

1.Pagliara, E., Marenchino, M., Antenucci, L., Costantini, M., Zoppi, G., Giacobini, M. D. L., ... & Bertuglia, A. (2022). Fetlock Joint Angle Pattern and Range of Motion Quantification Using Two Synchronized Wearable Inertial Sensors per Limb in Sound Horses and Horses with Single Limb Naturally Occurring Lameness. *Veterinary Sciences*, *9*(9), 456.

2.Pagliara, E., Pasinato, A., Valazza, A., Riccio, B., Cantatore, F., Terzini, M., ... & Bertuglia, A. (2022). Multibody Computer Model of the Entire Equine Forelimb Simulates Forces Causing Catastrophic Fractures of the Carpus during a Traditional Race. *Animals*, *12*(6), 737.

Articles not related to the PhD project

1.Bertuglia,A., Basano, I., Pagliara, E., Brkljaca Bottegaro, N., Spinella, G. and Bullone M (2021) Effect of intravenous tiludronate disodium administration on the radiographic progression of osteoarthritis of the fetlock joint in Standardbred racehorses. Journal of the American Veterinary Medical Association, Sept 15, Vol.259, No.6, pp 651-661

2.Pagliara E., Nicolo A., Rossi C., Cammaresi C., Donadio G., Bertuglia A. (2021) Transdermal application of anesthetic preparations is effective in increasing mechanical nociceptive threshold at perineural injection sites in horses, Journal of Equine Veterinary Science, Vol.103

3.Pagliara, E., Cantatore, F., Pallante, M., Valazza, A., Riccio, B. and Bertuglia A. (2020) Lateral Patellar instability in Standardbred horses at the weanling age: clinical and morphological features in four cases (2017-2019). Equine Veterinary Education.

4.Bertuglia, A., Pagliara, E., Manca, F., Pozzolo, P., & Mannelli, A. (2020). Prognostic indicators after musculoskeletal injuries in Standardbred racehorses in Italy. Journal of Equine Veterinary Science. Vol 92 https://doi.org/10.1016/j.jevs.2020.103180

5.Cantatore F., Marcatili M., Pagliara E., Bertuglia A., Withers J. (2020) Diffusion of radiodense contrast medium following perineural injection of the deep branch of the lateral plantar nerve using two different techniques in horses- an in vivo study. Vet Comp Orthop Traumatol. Jul; 33(4), pp 235-242 DOI: 10.1055/s-0040-1701655

Abstracts on international congress related to the PhD project

1. Pagliara E. (2022) Recording fetlock joint range of motion using wearable inertial sensors in sound and lame horses. 11th International Congress Equine Exercise Physiology-27 June-01 July, Uppsala, Sweden- Comparative exercise physiology 22 vol.18, Suppl 1 pag 49

2. Pagliara E. (2022) Multibody modelling of internal forces causing catastrophic carpal fracture during traditional race.11th International Congress Equine Exercise Physiology-27 June-01 July, Uppsala, Sweden- Comparative exercise physiology 22 vol.18, Suppl 1 pag 46

Abstracts on international congress not related to the PhD project

1.Cavallini D., Pagliara E., Raspa F., Valle E., 2019. Cases of stomatitis induced by Setaria glauca and Echinochloa crus-galli in horses. 23th Congress of the European Society of Veterinary and Comparative Nutrition, Torino, 18-20 settembre, 171 p.

2.Pagliara E, Cantatore F, Bertuglia A and Marcatili M. Negative pressure wound therapy (NPWT) for the treatment of surgical site infection (SSI) following ventral midline laparotomy in three horses. Sive international Congress, Bologna, Italy 22-23 January 2022

3.Penazzi L. , Valle E., Pagliara E., Ala U., Prola L. (2022). Foal neonatal diarrhea: can free dietary nucleotides be a help in the management? EWEN Conference, 23 August 2022, Cirenchester, UK

4.Penazzi L. , Valle E., Pagliara E., Ala U., Nervo T., Prola L. (2022). Free dietary nucleotides in newborn foals positively affect fecal volatile fatty acids production and microbiota. ECEIM international congress, 29 October 2022, Rome, Italy

Stays abroad

12/07/2021-1/10/2021 Pool house Equine Clinic, Lichfield, UK

Donnington Grove Equine Vets, Newbury, Uk

Rossdales Veterinary Surgeons, Newmarket, Uk

21/06/2022-3/07/2022 Swedish University of Agricultural Sciences, Uppsala, Sweden

18/10/2022-27/11/2022 Pool House Equine Clinic, Lichfield, UK